

UCSF

UC San Francisco Electronic Theses and Dissertations

Title

Dact1 functions in the planar cell polarity pathway during vertebrate gastrulation

Permalink

<https://escholarship.org/uc/item/2vx7x76p>

Author

Suriben, Rowena

Publication Date

2009

Peer reviewed|Thesis/dissertation

Dact1 functions in the planar cell polarity pathway during vertebrate gastrulation

by

Rowena Mae Obiña Suriben

DISSERTATION

Submitted in partial satisfaction of the requirements for the degree of

DOCTOR OF PHILOSOPHY

in

Developmental Biology

in the

GRADUATE DIVISION

of the

UNIVERSITY OF CALIFORNIA, SAN FRANCISCO

Acknowledgements

I would first like to thank my graduate advisor, Dr. Benjamin Cheyette for welcoming me into his lab and taking me on as his first graduate student. Coming from a small research university and coming to UCSF was a difficult and daunting transition. I had the privilege of receiving guidance and moral support from Ben, beginning in my first quarter in graduate school as a rotation student and continuing through the years. Thank you Ben for not only your scientific mentorship, but the constant support and guidance you have provided throughout numerous professional and personal obstacles that I've faced in the last five years. Most importantly thank you for nourishing my growth as a scientist and person; I am more confident in my skills and abilities. I hope my thesis seminar will reflect my personal growth as a scientist and professional.

Thank you to Dr. Gail Martin and Dr. Jeremy Reiter for providing insightful feedback on the progression of this thesis project during and outside thesis committee meetings. Your input on the embryonic analysis was instrumental in pushing this project forward in the right direction. Thank you, Gail, for connecting me with Dr. Patrick Tamm during his short visit in San Francisco. The opportunity to present the project and our hypothesis to a leading expert of early mouse development was refreshing and encouraging. Thank you Dr. Tamm for taking the time to learn about our work, share your ideas and provide essential feedback on the project.

This work would not have been possible without the guidance from members of the Cheyette lab; especially Daniel Fisher. Dan's daring dive into mouse embryology provided the foothold needed to initiate the far climb in understanding the *Dact1* mutant phenotype. It was also Dan's finding that the *Vangl2 Looptail* allele rescues *Dact1*

homozygous mutants that guided our findings of the primary tissue and signaling defects concluding this thesis and opening up doors for future progress in the lab. I am grateful to have overlapped with Dan during my years in the lab and am indebted for his work in this project and scientific advice. To all of the other members of the lab who I have overlapped with, thank for your critical thoughts and discussion, constant support, and tolerance of science related mood-swings.

Last but not least I would like to thank the coordinators of the Tetrad graduate program who I have overlapped with over the past 5 years. Thank you Claire Manneh, Danny Dam, Sue Adams and Billy Luh for all the administrative help you have provided during my years at UCSF.

Abstract

Dact1 functions in the Planar Cell Polarity pathway during vertebrate gastrulation

Rowena Suriben

The Dact family (also known as Dapper/Frodo) of cytoplasmic scaffold proteins are expressed during embryonic development and have been shown to modulate developmentally important signaling pathways such as the Wnt pathway. To gain a better understanding of the developmental stages and tissues in which *Dacts* function, the embryonic expression pattern of the mouse *Dact* family was characterized. *Dact1* is expressed in mesoderm derived tissue (i.e. presomitic mesoderm and somites) and in the primitive streak, where gastrulation occurs. To determine if *Dact1* is required for gastrulation, mouse mutants in the *Dact1* gene were analyzed during gastrulation stages (e7.0-e8.5). These data indicate that at the 6 somite stage, *Dact1* mutants have posterior morphological defects in the region of the primitive streak reminiscent of phenotypes associated with abnormalities in convergent extension movements necessary to elongate the embryo. These posterior defects are associated with disruptions in downstream readouts of the Planar Cell Polarity Pathway and not the Wnt/ β -catenin pathway. The morphological differences seen in *Dact1* mutants arise due to the abnormal upregulation of membrane Vangl2 and E-cadherin protein levels in primitive streak cells undergoing epithelial-mesenchymal transition (EMT) preceding cell migration. *Vangl2 Loop-tail* mutants show the opposite effect with a reduction in Vangl2 membrane localization in these cells. Importantly, crossing these two mutations (i.e. making *Dact1* mutants also heterozygous for the *Vangl2 Loop-tail* mutation) restored Vangl2 membrane levels at the primitive streak and rescued *Dact1* embryological phenotypes. These data identify a role

for Dact1 in regulating appropriate levels of the Planar Cell Polarity protein Vangl2
necessary for EMT and cell migration during mouse gastrulation.

Table of Contents

Chapter 1	Introduction	p.1
Chapter 2	Three Dact Gene Family Members are Expressed During Embryonic Development and in the Adult Brains of Mice	p.17
Chapter 3	<i>Dact1</i> Presomitic Mesoderm Expression Oscillates in phase with <i>Axin2</i> in the Somitogenesis Clock of Mice	p.46
Chapter 4	Posterior Malformations in <i>Dact1</i> mutant mice arise through misregulated <i>Vangl2</i> at the Primitive Streak	p.69

List of Tables

Table 3.1	Dact1 PSM Expression at E9.5	p. 65
Tables 4.1a-d	Breakdown of <i>Dact1</i> mutant phenotypes at birth	p.110
Table 4.2	Somitogenesis cycling abnormalities in <i>Dact1</i> mutants at E10.5	p.111
Tables 4.3a-b	<i>Dact1</i> and <i>Vangl2</i> mutations mutually rescue	p.112
Table 4.4	Primer sequences	p.113

List of Figures

Figure 2.1	Dact gene family molecular data	p.39
Figure 2.2	Developmental expression of Dact genes	p.41
Figure 2.3	Expression of Dact genes at E14.5 and in adult brain	p.42
Figure 2.S1	Predicted human DACT3 sequence compared to translation of cloned mouse Dact3 cDNA	p.43
Figure 2.S2	Ethidium bromide stained gels corresponding to all Northern blots shown in Figure 2.1D-E	p.44
Figure 2.S3	In situ hybridization controls using reverse complementary (sense) probes	p.45
Figure 3.1	Dact1 expression patterns in the PSM at E9.5	p.66
Figure 3.2	Dact1 cycles in phase with Axin2 but out of phase with Lfng	p.67
Figure 3.S1	TCF/LEF binding site consensus map of the mouse Dact1 promoter region plus intron 1	p.68
Figure 4.1	Birth phenotypes in Dact1 mutants compared to wild type	p.97
Figure 4.2	Dact1 mutant embryonic phenotypes	p.98
Figure 4.3	Biochemical correlates of PCP signaling are specifically affected at early phenotypic stages	p.99
Figure 4.4	Mutations in Dact1 and Vangl2 mutually rescue	p.100
Figure 4.5	The Dact1 and Vangl2 proteins associate independently of Dvl	p.101
Figure 4.6	Dact1 and Vangl2 functionally interact at the PS	p.102
Figure 4.S1	Gene targeting of the <i>Dact1</i> locus in mice	p.103
Figure 4.S2	Cell proliferation and apoptosis in the primitive streak region are not significantly different in <i>Dact1</i> mutants compared to wild type	p.104
Figure 4.S3	Brachyury expression and Dvl and Ctnnd1 (p120catenin) levels are not altered in <i>Dact1</i> ^{-/-} embryos	p.105

Figure 4.S4	<i>Dact1</i> ^{-/-} does not rescue the <i>Vangl2</i> ^{Lp/Lp} homozygous phenotype	p.106
Figure 4.S5	Quantitation of cell surface Vangl2 and E-cadherin protein signals in the PS ectoderm	p.107
Figure 4.S6	Vangl2, E-cadherin, and Wnt/β-catenin levels in <i>Dact1</i> mutants	p.108
Figure 4.S7	Allele specific genotyping of the <i>Vangl2</i> ^{Lp-m1Jus} point mutation	p.109

CHAPTER 1

Introduction

A key question in developmental biology is how multiple tissue layers are formed in an organism. The formation of a multilayered body plan is achieved through a process called gastrulation. It is through gastrulation that the primary embryonic layers which give rise to all the tissue in an adult organism are formed. During this process, cells are instructed to migrate internally and differentiate into the three primary germ layers.

In metazoans, the initial embryonic layer consists of a single epithelial sheet of cells derived from the inner cell mass of the blastocyst termed the epiblast. To initiate gastrulation, a small region of the epiblast is specified to undergo dramatic cellular rearrangement and form the primitive streak, a transient structure where the three germ layers arise. The primitive streak is first distinguishable morphologically by the thickening of the epiblast and molecularly by the transcriptional activation of region-specific genes such as *T* (encoding brachyury) and *Fgf8* (Tam and Behringer 1997; Robb and Tam 2004). These cells become more globular in shape and begin a series of cellular processes allowing them to delaminate from the epithelium and migrate ventrally. The delamination and migration of these cells away from the epithelium is the first step in forming a multilayered body plan.

The process of gastrulation at the site of the primitive streak gives rise to the three germ layers: mesoderm, ectoderm and endoderm. Endoderm cells are the first to ingress through the primitive streak followed by a heterogeneous population of endoderm and

mesoderm continually delaminating from the epithelium. Endoderm cells position ventrally and give rise to the digestive tube and associated organs (i.e. liver, pancreas and lungs). Mesoderm cells situate dorsal to the endoderm and mature into tissue such as cartilage, muscle and bone. Cells that remain in the epiblast epithelia after gastrulation mature into the ectoderm, giving rise to the nervous system and skin.

Formation of the germ layers from the epithelial epiblast is achieved through coordination of a series of events in a set of cells competent to form the primitive streak. These events include (1) the formation of the primitive streak, (2) the process of epithelial-mesenchymal transition necessary for cell ingression, (3) the migration of cells allowing for extension of the body in the anterior-posterior axis, and (4) the differentiation of structures from the germ layers. These cellular processes must be controlled precisely in time and space. The precise synchronization of these processes is achieved by modulating multiple signaling pathways during development, including the Wnt signaling pathway.

The formation of the primitive streak

A small region of the epiblast epithelium is specified to form the primitive streak. Wnts, a family of secreted signaling ligands, have been shown to be necessary and sufficient for primitive streak formation. The first indication that Wnts are necessary for primitive streak formation came from the analysis of *Wnt3* knockout mice. *Wnt3* mutants fail to express primitive streak markers such as *T* and *Fgf8* and arrest during early gastrulation (embryonic day 7.5). Tissue histology of *Wnt3* mutants shows a thicker

ectoderm and absence of a mesoderm layer, supporting a requirement for *Wnt3* in germ layer development associated with formation or maintenance of the primitive streak (Liu et al. 1999). Consistent with the idea that Wnts are involved in formation of the primitive streak, misexpression of chick *Wnt8c* in the mouse induces a secondary primitive streak structure. The ectopic structure expresses primitive streak markers and causes duplication of the embryonic axis (Popperl et al. 1997). To prevent such abnormalities during normal development, secreted Wnt inhibitors may be expressed to limit the field of cells competent to receive specification signals. Indeed, secreted Wnt antagonists Crescent and Dkk-1 are able to block the ability of misexpressed Wnt ligands to induce formation of ectopic primitive streak structures (Skromne and Stern 2001).

The ability of Wnts to induce a secondary primitive streak and axial duplication is due to activation of the Wnt/ β -catenin pathway. In this pathway, binding of Wnt ligands to Frizzled receptors inhibits degradation of cytoplasmic β -catenin. β -catenin accumulation in the cytoplasm results in its translocation to the nucleus, where it co-activates genes by binding to the Lef/Tcf family of transcription factors (Chien et al. 2009). Consistent with the hypothesis that Wnt induced axial duplication is due to activation of this pathway, overexpression of β -catenin in *Xenopus* induces the formation of a secondary axis (Guger and Gumbiner 1995), similar to the behaviors seen in *Wnt8c* overexpression studies. Further evidence that these effects are due to the transcriptional activation of the Wnt/ β -catenin pathway comes from dominant negative Tcf-3 N-terminal deletion constructs, which abrogate β -catenin binding and transcriptional activity. Overexpression of Tcf dominant negative constructs suppresses β -catenin induced

transcription and axis duplication (Molenaar et al. 1996), indicating that the inductive function of β -catenin lies upstream of Tcf. These studies support a major role for the Wnt/ β -catenin pathway in the formation of primitive streak to initiate gastrulation.

The process of epithelial-mesenchymal transition necessary for cell ingression

Once the primitive streak is formed, cells giving rise to endoderm and mesoderm must leave the epithelium and migrate ventrolaterally away from the dorsal midline. To do this, cells undergo a process called epithelial-mesenchymal transition (EMT) in which they lose their epithelial properties and assume a more mesenchymal morphology. The first step in this process requires removal of polarized adherence junction proteins at the membrane, including the cadherin and catenin family of adhesion proteins. During EMT, these adhesion molecules are targeted for degradation and their transcription is repressed. Once neighboring cell contacts are broken down, the cells then undergo apical constriction and dramatic cytoskeletal rearrangement and remodeling to favor epithelial delamination. The basement membrane must also be broken down in order for delaminating cells to leave the epithelial layer (Acloque et al. 2009).

The transcription factor family *Mesoderm posterior* (*Mesp*) is required for mesodermal EMT at the primitive streak. Mutations in the mouse *Mesp1* and *Mesp2* genes result in the lack of a mesodermal cell layer between the ectoderm and endoderm. These mutants are initially able to generate axial mesoderm (indicated by *brachyury* expression) but mesoderm formation is halted by e8.5. An abnormal accumulation of cells in the primitive streak at this stage suggests a failure in mesoderm ingression

(Kitajima et al. 2000). Studies in differentiating embryonic stem cells show that *Mesp1* inhibits expression of epithelial genes such as *E-cadherin* and members of the *Claudin* family of tight-junction proteins and activates transcription factors necessary for EMT such as *Snail1* and *Twist* (Lindsley et al. 2008). These same studies found that *Mesp1* expression is activated by Wnt/ β -catenin signaling, which suggests a role for Wnts in modulating downstream events necessary for EMT during gastrulation.

Mouse mutations in Fgf receptor 1 (*Fgfr1*) have defects in EMT in the primitive streak due to a failure in downregulating the adhesion proteins β -catenin and E-cadherin necessary for epithelial cell delamination. The inability of cells to ingress from the primitive streak in *Fgfr1* mutants results in an abnormal mass of cells arrested in the primitive streak ectoderm (Ciruna and Rossant 2001). It has been suggested that the abnormal accumulation of membrane β -catenin in *Fgfr1* mutants leads to a decrease in the cytoplasmic β -catenin pool, causing attenuation of Wnt/ β -catenin signaling levels in these cells. The reduced levels of Wnt/ β -catenin signaling in *Fgfr1* mutants may directly affect EMT in the primitive streak since the EMT inducer *Mesp1* is a direct target of the Wnt/ β -catenin signaling pathway.

During EMT, cells leaving the primitive streak epithelium lose their characteristic cuboidal shape and undergo apical constriction allowing for delamination. Proteins involved in regulating the cell cytoarchitecture like the Rho family of GTPases play important roles in the cell shape changes crucial for delamination and cell migration. In the chick epiblast, overexpression of RhoA GTPase results in the deficient delamination

of cells from the primitive streak associated with abnormal basement membrane breakdown (Nakaya and Sheng 2008). Although it has not been directly shown that Wnt pathways function in modulating Rho GTPase activity necessary during gastrulation, Wnt/ β -catenin independent pathways (discussed later) have been shown to regulate RhoA and Rac activity in other contexts affecting morphological changes in cell behavior (Schlessinger et al. 2009).

Convergent extension movements to elongate the embryo

The process of convergent extension involves intercalating cellular movements such that lateral cells converge toward the midline and extend the anterior-posterior axis. Groups of cells coordinating their movements in this manner result in narrowing and lengthening of the primitive streak as well as the whole anterior-posterior axis of the developing embryo. Intercalating cells undergo a series of cell shape changes; initiating with the development of a laterally polarized protrusion (lamellipodium) which allows for directionality, attachment, crawling, and insertion between neighboring cells (Keller et al. 2000). Mutations in genes required for this process cause a characteristic embryonic phenotype: having shorter anterior-posterior and wider medial-lateral axes. Along with abnormalities in length to width embryonic proportions, these phenotypes are also often accompanied by neural tube defects (e.g. spina bifida), which is linked to a failure in neural plate cells to meet at the dorsal midline during neural tube folding (Kibar et al. 2007).

Convergent extension phenotypes have been linked to defects in a β -catenin independent Wnt pathway termed Planar Cell Polarity (PCP). This pathway was first identified in the *Drosophila* eye and wing, where cells receive positional information necessary to generate polarized structures. Mutations in PCP components disrupt the symmetric distribution of these structures, such that wing hairs are misoriented in swirls and waves, and clusters of photoreceptors in the eye called ommatidia become disorganized relative to each other (Seifert and Mlodzik 2007). In contrast to the Wnt/ β -catenin pathway which modulates signaling levels through transcriptional regulation, downstream effects of the PCP pathway are achieved through asymmetric cytoplasmic and membrane localization of different molecular components of the pathway (Simons and Mlodzik 2008). It has been hypothesized that during convergent extension, the PCP pathway functions to asymmetrically localize protein complexes allowing for polarization of the cell and for region-specific activation of downstream effectors, such as the Rho family of GTPases, known to regulate cytoskeletal changes associated with morphogenesis (Seifert and Mlodzik 2007).

Mutations in vertebrate homologues of *Drosophila* PCP proteins have been shown to cause neural tube defects in the mouse. Among these proteins are the membrane components Frizzled, Celsr1 and Vangl2, and the cytoplasmic protein Dishevelled (Kibar et al. 2007). While mutations in all of these components cause neural tube defects associated with PCP, further work has demonstrated an additional requirement for Vangl2 and Dishevelled in the migration of cells necessary for convergent extension movements that elongate the embryo. Mice heterozygous for *Looptail*, a point mutation

in the mouse *Vangl2* gene, have a cell-autonomous failure of primitive streak cells to intercalate medially and to migrate anteriorly, resulting in a wider and shorter embryo (Ybot-Gonzalez et al. 2007). Histological analyses suggest that the *Looptail* mutation acts by destabilizing *Vangl2* protein from the membrane of these migrating cells (Torban et al. 2007). Dishevelled proteins have also been shown to function in convergent extension since compound mutations in the mouse *Dishevelled* genes phenocopy the *Vangl2 Looptail* embryonic defect including a failure in narrowing and lengthening the embryonic axis (Wang et al. 2006). The wider and shorter embryonic phenotypes seen in *Dishevelled* compound mutants can be exacerbated by crossing to the *Vangl2 Looptail* mutation (Etheridge et al. 2008), suggesting that these PCP components regulate similar cellular processes involved in convergent extension movements.

Differentiation of the three germ layers

The final step in the formation of adult tissue layers is the differentiation of the embryonic layers to form more mature structures. Once the germ layers are situated within the embryo, the cells are specified to give rise to differentiated tissue types. Endoderm, the ventral-most tissue layer, gives rise to the digestive tube and associated organs. To do this, the epithelial endodermal sheet formed during gastrulation closes ventrally to form the gut of the embryo, a process that initiates at the anterior foregut and the posterior hindgut. Besides forming the digestive lining, the endoderm also gives rise to liver, pancreas, and lung progenitors. The restricted specification of the liver and pancreas to the region of the foregut is due to the localized repression of Wnt/ β -catenin signaling in this region. Inhibiting β -catenin activity in more posterior regions of the gut

(i.e. posterior to the foregut) results in the promotion of ectopic structures which express kidney and pancreas specific markers (McLin et al. 2007). Conversely, activation of Wnt/ β -catenin signaling, via Wnt2/2b, is necessary and sufficient to promote lung development in specific regions of the foregut endoderm (Goss et al. 2009), further emphasizing the importance of region- and time-specific activation of this pathway.

At the same time that the endoderm is folding ventrally, the overlying dorsal ectoderm folds dorsally, connects at the lateral edges, and forms the neural tube. The neural tube mostly gives rise to the central nervous system, although a small proportion of dorsal cells, the neural crest, delaminate to form the peripheral nervous system, melanocytes and facial cartilage. Wnt pathways function in both the differentiation program and tissue morphogenesis necessary for maturation of the ectoderm. Components of the pathway have been shown to modulate cell differentiation into the ectoderm or mesoderm cell lineages. For example, mutation in *Wnt3a* which primarily functions in the Wnt/ β -catenin pathway, results in the promotion of ectodermal structures (neural tube) at the expense of the mesodermal germ layer (Yoshikawa et al. 1997). These results suggest that *Wnt3a* is necessary to turn off the ectodermal program in mesodermal progenitors ingressing through the streak. Mutations in other components of the pathway phenocopy the differentiation defects seen in *Wnt3a* mutants (Galceran et al. 1999; Pinson et al. 2000), confirming a role for Wnt/ β -catenin signaling in the differentiation program necessary to form mesoderm versus endoderm.

The mesoderm gives rise to multiple cell types, dependent on their location. Lateral mesoderm gives rise to red blood cells while the axial mesoderm gives rise to the notochord, a flexible rod-like structure which physically shapes the embryo and also secretes inducing factors essential for tissue patterning. Paraxial mesoderm (between the lateral and axial mesoderm) gives rise to the segments of the animal through a process called somitogenesis.

During somitogenesis, spherical blocks of mesodermal cells, called somites, are laid down along the medial axis in an anterior to posterior manner. It has been proposed that the formation of somites is coordinated through a regulated cyclic expression of genes in the paraxial mesoderm termed the segmentation clock. According to this model, during somitogenesis the clock generates periodic pulses of Notch, Wnt and FGF signals which are converted to positional information necessary to specify somite boundaries (Ozbudak and Pourquie 2008). The signaling levels of these pathways leads to the timed development of each somite segment. Once laid down, each somite matures and gives rise to the dermis, muscle and bone corresponding to its segmental position.

Dact genes as modulators of Wnt signaling

The involvement of Wnt signaling in multiple steps necessary for the development of adult tissue layers, from inducing the formation of the primitive streak to the differentiation of adult structures, requires that the pathway be tightly controlled temporally and regionally. Wnt signal regulation is achieved through the tissue specific expression and function of multiple activators and inhibitors of the pathway. Signal

modulation can be attained extracellularly, by facilitating or blocking the interactions between the ligand and receptor, in the cytoplasm, by modulating the activity of proteins involved in signal transduction, or in the nucleus, by regulating levels of gene transcription.

One intracellular regulator of Wnt signaling is the Dact (Dpr/Frodo) family of scaffold proteins. Dacts were initially identified via yeast-two hybrid screens for Dishevelled interacting proteins. Initial studies to determine Dact function in Wnt pathway regulation highlighted the ability of Dact proteins to modulate both Wnt/ β -catenin dependent and independent pathways. Overexpression of *Xenopus* Dpr in animal caps leads to a decrease in soluble β -catenin and the Wnt responsive gene *siamois*, suggesting an inhibitory role in the Wnt/ β -catenin pathway (Cheyette et al. 2002). However, in another set of studies, overexpression of the closely related Frodo gene on the ventral side of early *Xenopus* embryos synergized with Disheveled in axis induction and increased *siamois* reporter gene activation (Gloy et al. 2002), suggesting Frodo is an activator of Wnt/ β -catenin signaling. Further studies attempting to resolve these conflicting results have revealed that in some cellular contexts Dact proteins can behave as inhibitors (Cheyette et al. 2002; Yau et al. 2005; Zhang et al. 2006) whereas in other contexts they behave as activators (Gloy et al. 2002; Waxman et al. 2004) of the Wnt/ β -catenin pathway. Initial studies also characterized a function of Dacts in Wnt/ β -catenin independent pathways, since Dpr overexpression in HeLa cells inhibited the phosphorylation of Jun by the PCP associated kinase JNK (c-Jun NH₂-terminal kinase) (Cheyette et al. 2002).

Dact proteins have also been implicated in modulating gene transcription downstream of β -catenin. Frodo has been shown to bind TCF directly to modulate Wnt target gene transcription independent of β -catenin (Hikasa and Sokol 2004). Furthermore, *Xenopus* Frodo can activate genes downstream of the transcriptional repressor Kaiso through its interaction with p120-catenin. Frodo is able to bind and stabilize cytoplasmic levels of p120-catenin which in turn results in the sequestration of Kaiso in the cytoplasm, allowing derepression of Kaiso target genes (Park et al. 2006). There is evidence from other studies that Dact proteins can bind catenin family members more generally (Cheyette et al. 2002; Gao et al. 2008). The Dact protein family may also function in inhibiting gene transcription downstream of TGF β signaling since zebrafish and mammalian Dpr2 are able to bind TGF β receptors ALK4 and ALK5 and accelerate their lysosomal degradation (Zhang et al. 2004; Su et al. 2007).

The ability of Dacts to modulate signaling pathways and gene transcriptional networks that are activated during gastrulation suggests a function for Dact1 in this process. Previous findings that *Dact* family members are expressed during embryonic development in multiple organisms further support a role for *Dact* genes in embryogenesis (Gillhouse et al. 2004; Waxman 2005; Hunter et al. 2006).

The goal of this work was to better understand the cellular and signaling mechanisms driving gastrulation. More specifically a significant part of this thesis has focused on identifying a role for *Dact1* in regulating the events necessary for germ layer

development. The first two chapters describe the embryonic expression pattern of the mouse *Dact* genes. Chapter 1 identifies the *Dact* family members in the mouse and characterizes their mRNA expression pattern during early embryonic and brain development. Chapter 2 dissects the oscillating expression pattern of mouse *Dact1* in the paraxial mesoderm and compares its expression to components of the Notch and Wnt pathway involved in the segmentation clock. In Chapter 3, the cellular and signaling function of *Dact1* during embryonic development are characterized utilizing a mouse knockout for the *Dact1* gene. Analysis of *Dact1* mutant embryos identifies an early function for *Dact1* in regulating membrane protein levels in the primitive streak. These studies link DACT1 to the PCP pathway and not the Wnt/ β -catenin pathway during gastrulation. The results of these studies reveal a requirement for *Dact1* in the primitive streak and have contributed to a better understanding of the molecular mechanisms underlying vertebrate gastrulation.

References

- Acloque, H., Adams, M.S., Fishwick, K., Bronner-Fraser, M., and Nieto, M.A. 2009. Epithelial-mesenchymal transitions: the importance of changing cell state in development and disease. *J Clin Invest* **119**(6): 1438-1449.
- Cheyette, B.N., Waxman, J.S., Miller, J.R., Takemaru, K., Sheldahl, L.C., Khlebtsova, N., Fox, E.P., Earnest, T., and Moon, R.T. 2002. Dapper, a Dishevelled-associated antagonist of beta-catenin and JNK signaling, is required for notochord formation. *Dev Cell* **2**(4): 449-461.
- Chien, A.J., Conrad, W.H., and Moon, R.T. 2009. A Wnt survival guide: from flies to human disease. *J Invest Dermatol* **129**(7): 1614-1627.
- Ciruna, B. and Rossant, J. 2001. FGF signaling regulates mesoderm cell fate specification and morphogenetic movement at the primitive streak. *Dev Cell* **1**(1): 37-49.
- Etheridge, S.L., Ray, S., Li, S., Hamblet, N.S., Lijam, N., Tsang, M., Greer, J., Kardos, N., Wang, J., Sussman, D.J. et al. 2008. Murine dishevelled 3 functions in redundant pathways with dishevelled 1 and 2 in normal cardiac outflow tract, cochlea, and neural tube development. *PLoS Genet* **4**(11): e1000259.
- Galceran, J., Farinas, I., Depew, M.J., Clevers, H., and Grosschedl, R. 1999. Wnt3a^{-/-} like phenotype and limb deficiency in Lef1^(-/-)Tcf1^(-/-) mice. *Genes Dev* **13**(6): 709-717.
- Gao, X., Wen, J., Zhang, L., Li, X., Ning, Y., Meng, A., and Chen, Y.G. 2008. Dapper1 is a nucleocytoplasmic shuttling protein that negatively modulates Wnt signaling in the nucleus. *J Biol Chem* **283**(51): 35679-35688.
- Gillhouse, M., Wagner Nyholm, M., Hikasa, H., Sokol, S.Y., and Grinblat, Y. 2004. Two Frodo/Dapper homologs are expressed in the developing brain and mesoderm of zebrafish. *Dev Dyn* **230**(3): 403-409.
- Gloy, J., Hikasa, H., and Sokol, S.Y. 2002. Frodo interacts with Dishevelled to transduce Wnt signals. *Nat Cell Biol* **4**(5): 351-357.
- Goss, A.M., Tian, Y., Tsukiyama, T., Cohen, E.D., Zhou, D., Lu, M.M., Yamaguchi, T.P., and Morrisey, E.E. 2009. Wnt2/2b and beta-catenin signaling are necessary and sufficient to specify lung progenitors in the foregut. *Dev Cell* **17**(2): 290-298.
- Guger, K.A. and Gumbiner, B.M. 1995. beta-Catenin has Wnt-like activity and mimics the Nieuwkoop signaling center in *Xenopus* dorsal-ventral patterning. *Dev Biol* **172**(1): 115-125.
- Hikasa, H. and Sokol, S.Y. 2004. The involvement of Frodo in TCF-dependent signaling and neural tissue development. *Development* **131**(19): 4725-4734.
- Hunter, N.L., Hikasa, H., Dymecki, S.M., and Sokol, S.Y. 2006. Vertebrate homologues of Frodo are dynamically expressed during embryonic development in tissues undergoing extensive morphogenetic movements. *Dev Dyn* **235**(1): 279-284.
- Keller, R., Davidson, L., Edlund, A., Elul, T., Ezin, M., Shook, D., and Skoglund, P. 2000. Mechanisms of convergence and extension by cell intercalation. *Philos Trans R Soc Lond B Biol Sci* **355**(1399): 897-922.
- Kibar, Z., Capra, V., and Gros, P. 2007. Toward understanding the genetic basis of neural tube defects. *Clin Genet* **71**(4): 295-310.
- Kitajima, S., Takagi, A., Inoue, T., and Saga, Y. 2000. MesP1 and MesP2 are essential for the development of cardiac mesoderm. *Development* **127**(15): 3215-3226.

- Lindsley, R.C., Gill, J.G., Murphy, T.L., Langer, E.M., Cai, M., Mashayekhi, M., Wang, W., Niwa, N., Nerbonne, J.M., Kyba, M. et al. 2008. *Mesp1* coordinately regulates cardiovascular fate restriction and epithelial-mesenchymal transition in differentiating ESCs. *Cell Stem Cell* **3**(1): 55-68.
- Liu, P., Wakamiya, M., Shea, M.J., Albrecht, U., Behringer, R.R., and Bradley, A. 1999. Requirement for *Wnt3* in vertebrate axis formation. *Nat Genet* **22**(4): 361-365.
- McLin, V.A., Rankin, S.A., and Zorn, A.M. 2007. Repression of *Wnt/beta-catenin* signaling in the anterior endoderm is essential for liver and pancreas development. *Development* **134**(12): 2207-2217.
- Molenaar, M., van de Wetering, M., Oosterwegel, M., Peterson-Maduro, J., Godsave, S., Korinek, V., Roose, J., Destree, O., and Clevers, H. 1996. *XTcf-3* transcription factor mediates *beta-catenin*-induced axis formation in *Xenopus* embryos. *Cell* **86**(3): 391-399.
- Nakaya, Y. and Sheng, G. 2008. Epithelial to mesenchymal transition during gastrulation: an embryological view. *Dev Growth Differ* **50**(9): 755-766.
- Ozbudak, E.M. and Pourquie, O. 2008. The vertebrate segmentation clock: the tip of the iceberg. *Curr Opin Genet Dev* **18**(4): 317-323.
- Park, J.I., Ji, H., Jun, S., Gu, D., Hikasa, H., Li, L., Sokol, S.Y., and McCrea, P.D. 2006. *Frodo* links *Dishevelled* to the *p120-catenin/Kaiso* pathway: distinct *catenin* subfamilies promote *Wnt* signals. *Dev Cell* **11**(5): 683-695.
- Pinson, K.I., Brennan, J., Monkley, S., Avery, B.J., and Skarnes, W.C. 2000. An *LDL-receptor-related* protein mediates *Wnt* signalling in mice. *Nature* **407**(6803): 535-538.
- Popperl, H., Schmidt, C., Wilson, V., Hume, C.R., Dodd, J., Krumlauf, R., and Beddington, R.S. 1997. Misexpression of *Cwnt8C* in the mouse induces an ectopic embryonic axis and causes a truncation of the anterior neuroectoderm. *Development* **124**(15): 2997-3005.
- Robb, L. and Tam, P.P. 2004. *Gastrula* organiser and embryonic patterning in the mouse. *Semin Cell Dev Biol* **15**(5): 543-554.
- Schlessinger, K., Hall, A., and Tolwinski, N. 2009. *Wnt* signaling pathways meet *Rho GTPases*. *Genes Dev* **23**(3): 265-277.
- Seifert, J.R. and Mlodzik, M. 2007. *Frizzled/PCP* signalling: a conserved mechanism regulating cell polarity and directed motility. *Nat Rev Genet* **8**(2): 126-138.
- Simons, M. and Mlodzik, M. 2008. Planar cell polarity signaling: from fly development to human disease. *Annu Rev Genet* **42**: 517-540.
- Skromne, I. and Stern, C.D. 2001. Interactions between *Wnt* and *Vg1* signalling pathways initiate primitive streak formation in the chick embryo. *Development* **128**(15): 2915-2927.
- Su, Y., Zhang, L., Gao, X., Meng, F., Wen, J., Zhou, H., Meng, A., and Chen, Y.G. 2007. The evolutionally conserved activity of *Dapper2* in antagonizing *TGF-beta* signaling. *FASEB J* **21**(3): 682-690.
- Tam, P.P. and Behringer, R.R. 1997. Mouse gastrulation: the formation of a mammalian body plan. *Mech Dev* **68**(1-2): 3-25.
- Torban, E., Wang, H.J., Patenaude, A.M., Riccomagno, M., Daniels, E., Epstein, D., and Gros, P. 2007. Tissue, cellular and sub-cellular localization of the *Vangl2* protein

- during embryonic development: effect of the Lp mutation. *Gene Expr Patterns* **7**(3): 346-354.
- Wang, J., Hamblet, N.S., Mark, S., Dickinson, M.E., Brinkman, B.C., Segil, N., Fraser, S.E., Chen, P., Wallingford, J.B., and Wynshaw-Boris, A. 2006. Dishevelled genes mediate a conserved mammalian PCP pathway to regulate convergent extension during neurulation. *Development* **133**(9): 1767-1778.
- Waxman, J.S. 2005. Regulation of the early expression patterns of the zebrafish Dishevelled-interacting proteins Dapper1 and Dapper2. *Dev Dyn* **233**(1): 194-200.
- Waxman, J.S., Hocking, A.M., Stoick, C.L., and Moon, R.T. 2004. Zebrafish Dapper1 and Dapper2 play distinct roles in Wnt-mediated developmental processes. *Development* **131**(23): 5909-5921.
- Yau, T.O., Chan, C.Y., Chan, K.L., Lee, M.F., Wong, C.M., Fan, S.T., and Ng, I.O. 2005. HDPR1, a novel inhibitor of the WNT/beta-catenin signaling, is frequently downregulated in hepatocellular carcinoma: involvement of methylation-mediated gene silencing. *Oncogene* **24**(9): 1607-1614.
- Ybot-Gonzalez, P., Savery, D., Gerrelli, D., Signore, M., Mitchell, C.E., Faux, C.H., Greene, N.D., and Copp, A.J. 2007. Convergent extension, planar-cell-polarity signalling and initiation of mouse neural tube closure. *Development* **134**(4): 789-799.
- Yoshikawa, Y., Fujimori, T., McMahon, A.P., and Takada, S. 1997. Evidence that absence of Wnt-3a signaling promotes neuralization instead of paraxial mesoderm development in the mouse. *Dev Biol* **183**(2): 234-242.
- Zhang, L., Gao, X., Wen, J., Ning, Y., and Chen, Y.G. 2006. Dapper 1 antagonizes Wnt signaling by promoting dishevelled degradation. *J Biol Chem* **281**(13): 8607-8612.
- Zhang, L., Zhou, H., Su, Y., Sun, Z., Zhang, H., Zhang, Y., Ning, Y., Chen, Y.G., and Meng, A. 2004. Zebrafish Dpr2 inhibits mesoderm induction by promoting degradation of nodal receptors. *Science* **306**(5693): 114-117.

CHAPTER 2

Three Dact Gene Family Members are Expressed During Embryonic Development and in the Adult Brains of Mice

Daniel A Fisher, Saul Kivimäe, Jun Hoshino, Rowena Suriben, Pierre-Marie Martin,
Nichol Baxter, Benjamin NR Cheyette

Department of Psychiatry & Graduate Programs in Developmental Biology and
Neuroscience, University of California, San Francisco, 94143-2611

Abstract

Members of the Dact protein family were initially identified through binding to Dishevelled (Dvl), a cytoplasmic protein central to Wnt signaling. During mouse development, *Dact1* is detected in the presomitic mesoderm and somites during segmentation, in the limb bud mesenchyme and other mesoderm-derived tissues, and in the central nervous system (CNS). *Dact2* expression is most prominent during organogenesis of the thymus, kidneys, and salivary glands, with much lower levels in the somites and in the developing CNS. *Dact3*, not previously described in any organism, is expressed in the ventral region of maturing somites, limb bud and branchial arch mesenchyme, and in the embryonic CNS; of the three paralogs it is the most highly expressed in the adult cerebral cortex. These data are consistent with studies in other vertebrates showing that *Dact* paralogs have distinct signaling and developmental roles, and suggest they may differentially contribute to postnatal brain physiology.

Introduction

Signaling downstream of secreted Wnt ligands is a conserved process in multicellular animals that plays important roles during development and, when misregulated, contributes to cancer and other diseases (Polakis, 2000; Moon et al., 2002). In mammals many Wnt signaling components are expressed in the postnatal brain, where manipulations of their activity can lead to effects on behavior (Madsen et al., 2003; Beaulieu et al., 2004; Kaidanovich-Beilin et al., 2004; O'Brien et al., 2004; Shimogori et al., 2004). Although more than one molecular cascade has been identified downstream of Wnt receptors, all such cascades involve a cytoplasmic scaffold protein called

Dishevelled (Dvl in mammals) (Veeman et al., 2003; Wharton, Jr., 2003). Because of its central role in Wnt signal transduction, efforts have been made to identify the direct binding partners of Dvl. One such protein, which binds to the Dvl PDZ domain via a conserved C-terminal PDZ-binding motif (Cheyette et al., 2002), has alternately been named Dapper (Dpr), Frodo/Frd, THYEX3, HNG3, MTNG3, and Dact in various organisms (Cheyette et al., 2002; Gloy et al., 2002; Gillhouse et al., 2004; Yau et al., 2004; Zhang et al., 2004; Hunter et al., 2005; Katoh, 2005). For simplicity, hereafter we use the symbol “*Dact*” assigned by the Human Genome Organization Nomenclature Committee and the Mouse Genome Informatics website for all members of this gene family. Interestingly, despite the importance of Wnt signaling during invertebrate development, we have been unable to identify *Dact* orthologs in the completely sequenced genomes of the invertebrates *Drosophila melanogaster* and *Caenorhabditis elegans*, nor in that of the simple chordate, *Ciona intestinalis* (data not shown).

The function of Dact proteins in signal regulation remains ambiguous, with some studies indicating they act positively in Wnt signal transduction (Gloy et al., 2002; Waxman et al., 2004), and others indicating an inhibitory function (Cheyette et al., 2002; Wong et al., 2003; Yau et al., 2004; Brott and Sokol, 2005a; Zhang et al., 2006). Previous research in zebrafish has shown that two members of the Dact family have distinct effects on Wnt signaling, with Dact1 having a greater impact on β -catenin-dependent signaling, and Dact2 having a greater impact on a β -catenin-independent process called planar cell polarity/convergent-extension signaling (Waxman et al., 2004). Furthermore, in zebrafish and when overexpressed in mammalian cells, Dact2 but not Dact1 can inhibit Nodal signaling by promoting the endocytic degradation of Type I

TGF β receptors (Zhang et al., 2004). Taken together, the evidence suggests that different Dact paralogs have distinct signaling activities, and that even a single Dact protein may have more than one role that can vary under changing cellular conditions (Hikasa and Sokol, 2004; Brott and Sokol, 2005b).

Because of this gene family's manifold yet conserved functions in vertebrate signal transduction, we have cloned cDNAs corresponding to the full-length coding regions of all three mouse *Dact* homologs, and have characterized their developmental and adult expression patterns.

Results and Discussion

Identification of a Three-Member *Dact* Gene Family

Using the previously described *Dact* sequences from frogs and fish, we scanned the mouse genome and expressed sequence tag (EST) databases for similar sequences, and then cloned full-length cDNAs by RT-PCR (Fig. 2.1A). Based on sequence similarity, *Dact1*, which maps to mouse chromosome 12D1, is the closest mammalian homolog to the *Dpr* and *Frodo* sequences identified in *Xenopus*, and corresponds to the mammalian *Dpr1* and *Frd1* genes reported in the literature (Cheyette et al., 2002; Katoh and Katoh, 2003; Yau et al., 2004; Zhang et al., 2004; Brott and Sokol, 2005; Hunter et al., 2005). *Dact2*, which is most closely related to the *frd2/dpr2* sequences identified in zebrafish (Gillhouse et al., 2004; Waxman et al., 2004), maps to mouse chromosome 17A2. *Dact3*, which has not previously been described, maps to mouse chromosome 7A2.

Dact3 is a bone fide member of the *Dact* gene family (Fig.2.1A-C). Upon alignment at the amino acid sequence level, mouse *Dact3* is approximately 27% similar to *Dact1* and 24% similar to *Dact2* (compared to 26% similarity between *Dact1* and *Dact2*, Fig. 2.1B). In and around a conserved leucine zipper domain, *Dact1* and *Dact2* are more closely similar to each other than to *Dact3*. However, at the C-terminus *Dact1* and *Dact3* are more closely related (compare PDZ-binding domains in Fig. 2.1A).

The predicted amino acid sequence for the *Dact3* protein is approximately 20% shorter than either *Dact1* or *Dact2* (610 amino acids for *Dact3* vs. 778 amino acids for *Dact1* and 757 amino acids for *Dact2*). There is an open reading frame that continues upstream to an ATG located at position -156 in the genomic locus of *Dact3*, which if transcribed and translated could therefore theoretically add 52 amino acids to the amino terminus of the *Dact3* polypeptide. We have excluded this upstream sequence as a part of the *Dact3* transcript produced in newborn forebrain by using 5' RACE to determine the start of transcription (see Methods for details). A highly conserved ortholog of *Dact3* is identifiable in the human genome and EST databases. The human *DACT3* gene maps to chromosome 19q13.32 and is predicted to encode a protein 85% identical to mouse *Dact3* (Fig.2.1C, Fig.2.S1). A similar *Dact3* gene distinct from *Dact1* and *Dact2* is also identifiable in the zebrafish and pufferfish genomic and EST public sequence databases (data not shown).

The 5' region of each of the mouse *Dact* genes is extremely GC-rich, and the intron-exon structure is also conserved, consisting of three small 5' coding exons which together encode a short 5' UTR and the amino-terminus of the polypeptide, and a larger fourth exon containing approximately 2/3 of the translated sequence plus a longer 3'

UTR (data not shown). To summarize, we have identified three paralogous *Dact* genes in mouse, one of which (*Dact3*) is entirely novel. Overall homology relationships between the principal members of the proposed *Dact* gene family are diagrammed schematically in Fig. 2.1C.

Developmental and Tissue-Specific Expression

Using Northern blots we have profiled the expression of each *Dact* gene across embryonic stages and adult tissues. This has been complemented by Quantitative PCR (Q-PCR) to more accurately compare relative mRNA levels between the three genes. Over the course of embryogenesis, the *Dact* genes have quite different temporal patterns of expression. From embryonic day (E) 4.5-8.5 there is only weak expression of these genes, some of which may occur in maternal and extra-embryonic tissues (Fig. 2.1D). In the embryo proper, *Dact1* expression increases dramatically from E9.5-10.5, peaks between E11.5-13.5, then diminishes slowly thereafter. In contrast, *Dact2* expression is very low overall for most of embryogenesis (Fig. 2.1D middle blot). *Dact3* expression is initially low, peaks at E10.5, then declines again (Fig. 2.1D bottom blot). Because both *Dact1* and *Dact3* levels decline while *Dact2* remains relatively constant overall, all three genes are expressed at roughly comparable levels at E18.5, three days prior to birth (Fig. 2.1D, G).

Using similar methodology, the three *Dact* genes show quite different adult tissue expression patterns. In the adult, *Dact1* is present primarily in the brain, lung, and uterus, with significantly weaker expression in other tissues (Fig. 2.1E). *Dact2* is present in the brain and uterus, but is also quite notable in the kidneys, small intestines, thymus, and

testes (Fig. 2.1E, H, I). The adult distribution of *Dact3* is most restricted: it is present in the uterus (Fig. 2.1E, I), and is the principally-expressed Dact family member in the adult brain (Fig. 2.1E, H).

In summary, the three *Dact* genes are broadly expressed during mouse embryogenesis and in adult tissues, and yet have distinct temporal and tissue-specific signatures. This is consistent with these molecules playing separable roles during development and in adult tissue physiology. To further clarify these differences, we have performed mRNA in situ hybridization analysis in whole mounts (WISH) and sections (ISH) during embryonic development and in the adult brain.

Embryonic Expression of the *Dact* gene family through Segmentation Stages

As expression of all three family members is low at early embryonic stages, and as the expression of *Dact1* has been described up to E8.5-9, we have focused our attention primarily on later developmental stages. Consistent with a prior report (Hunter et al., 2005), at E7.5 our *Dact1*-specific probe detects expression primarily in the mesoderm and at very low levels in the neurectoderm (Dr. Uta Grieshammer and BNRC, data not shown). In the E9.0 embryo, *Dact1* expression is highest in the septum transversum, cranial mesenchyme, the caudal presomitic mesoderm (PSM), and in the somites that derive from it (Hunter et al., 2005), as well as in the wall of Rathke's pouch, the dorsal aorta, the aortic sac, and the branchial arch arteries (Fig. 2.2A). Within the PSM, a band of low *Dact1* is apparent between high expressing zones in the caudal PSM and the newly forming somite at the rostral edge (Fig. 2.2A). *Dact1* exhibits a strong caudal to rostral gradient that inversely correlates with the developmental age of somites:

highest expression in the most recently formed (*i.e.* caudal) somite, and diminishing expression in more mature (*i.e.* rostral) somites. Within individual somites *Dact1* shows a progressively restricted spatial pattern. In younger (caudal) somites, *Dact1* is preferentially expressed ventromedially along the rostral-caudal extent and along both the rostral and caudal somite walls (Fig. 2.2A, I). As the somite matures, *Dact1* expression decreases rostrally, such that its localization becomes progressively restricted to the ventromedial and caudal domains (Fig. 2.2A inset). By section ISH, *Dact1* expression is also prominent in the nephrogenic cords, the ventral mesentery and the mesenchymal outer walls of the foregut, the dorsal aorta, and its main branches (Fig. 2.2G).

Dact2 is detectable only at very low levels in the E9.0 embryo by mRNA in situ techniques (Fig. 2.2B), though it is fairly widely distributed. At this stage, low *Dact2* expression is appreciable in the retina, otic vesicle, ventral mesentery of the foregut, the umbilical veins, dorsal neural tube, and in a gradient in the somites with highest levels in the caudal (youngest) somites much like *Dact1* (Figure 2.2B and insets). Unlike *Dact1*, *Dact2* is not detected within the caudal PSM at this stage (Fig. 2.2B). Compared to *Dact1*, *Dact2* also shows a significantly different domain of expression within each somite. Whereas *Dact1* is most highly expressed ventromedially, *Dact2* is more highly expressed dorsolaterally. Furthermore, unlike *Dact1* which becomes more *caudally* restricted, *Dact2* becomes progressively more *rostrally* restricted (Fig. 2.2B left inset). As a consequence, the two paralogs occupy complementary intrasomitic distributions as somites mature.

At E9.0, *Dact3* mRNA is found in a tissue distribution distinct from the other two *Dact* genes (Fig. 2.2C). Like *Dact1*, *Dact3* is expressed in craniofacial mesenchyme, but

it is more prominent in the branchial arch mesenchyme, the aortic sac, and the aortic arches (Fig. 2.2C, P) where *Dact1* expression is comparatively lower. Also different from *Dact1*, *Dact3* is not expressed in the PSM, nor is it present in a caudal-rostral gradient among developing somites like both *Dact1* and *Dact2*. Instead, *Dact3* is expressed in the ventral domain of more mature somites, located centrally along the rostral-caudal axis (Fig. 2.2C, Q).

At E10.5, high *Dact1* expression continues in the PSM and caudal somites (Fig. 2.2D, L, compare to 2.2A). *Dact1* is also present at low levels in other tailbud tissues, such as the ventral mesoderm of the tail bud (Fig. 2.2D). More anteriorly, *Dact1* at this stage is present in the forelimb and hindlimb buds, where it is expressed in mesoderm in a proximal (low)-apical (high) gradient (Fig. 2.2D, J). It continues to be expressed significantly in mesenchyme surrounding foregut derivatives such as the left and right main bronchi, as well as in the sclerotome derived from the ventral somite (Fig. 2.2J), but comparatively is only weakly detectable in the branchial arch mesenchyme (data not shown). At this stage, it first starts to be expressed in post-mitotic neurons, chiefly evident in the differentiating motor pools of the ventral spinal cord (Fig. 2.2J).

Consistent with the Northern and Q-PCR data, at E10.5 *Dact2* is only weakly detectable by mRNA in situ hybridization and appears to be more restricted in its tissue distribution than at E9.0. The main loci of expression at this time are in the otic vesicle and in the caudal-most somites where the strongest signal is in the most-recently formed somite and a diminishing signal is in the next two youngest somites (Fig. 2.2E, inset E). In contrast, *Dact3* at this stage is very prominent throughout the branchial arch

mesenchyme, limb bud mesenchyme, as well as continued expression in maturing somites (Fig. 2.2F, Q, R, S).

Taken together, the expression of *Dact* family members at embryonic stages through E10.5 suggests overlapping roles especially during mesoderm and neural crest development. At E9.0 *Dact1* and *Dact3* overlap in the facial mesoderm and septum transversum, where they may play either complementary or redundant roles. The exclusive expression of *Dact1* in the PSM suggests a more unique function in that tissue during segmentation. The robust expression of *Dact3* in the branchial arches, facial mesenchyme, and ventral somites is consistent with this gene being important in the migration or differentiation of neural crest cells and of mesoderm-derived mesenchyme. The expression pattern of *Dact1* at early stages has been proposed to indicate a role in mesenchymal to epithelial transitions (Hunter et al., 2005). A comprehensive view based on the embryonic expression patterns of all three *Dact* genes suggests involvement in a subset of signaling events, including those that control morphogenesis but extending to the regulation of cellular differentiation and tissue patterning.

The distinct domains of *Dact* gene expression within developing somites correlates with domains of signaling activity that pattern this tissue. Sonic hedgehog (Shh) secreted from the notochord and floor plate is an important ventromedial somite patterning signal, whereas TGF β s and Wnts play a similar role dorsolaterally (Lee et al., 2000; Christ et al., 2004). Given that *Dact1* and *Dact3* are primarily restricted to the ventromedial domain, and that *Dact2* is concentrated dorsally and laterally, these signaling cascades could differentially regulate *Dact* expression. Simultaneously, based on their known functions *Dact* proteins are likely to be involved in the intracellular

modulation of the signaling cascades that pattern these tissues. The ventromedial expression of *Dact1* and *Dact3* is consistent with a role in signaling within the presumptive sclerotome, which produces the cartilage and vertebral bodies making up the axial skeleton (Christ et al., 2004). The complementary expression of *Dact2* dorsolaterally is consistent with a signaling role in the presumptive dermomyotome, which at later stages gives rise to the dermis as well as the deep back and intercostal musculature (Borycki et al., 1999; Wagner et al., 2000).

Prenatal Expression of Dact genes in the Developing Central Nervous System

After E10.5, expression of *Dact1* and *Dact3* becomes concentrated in the developing CNS. In situ hybridization of sagittally-sectioned embryos at E14.5 shows that *Dact1* and *Dact3* RNA are broadly expressed in the brain and spinal cord, (Fig. 2.3A, C). By contrast, *Dact2*, although also expressed in the developing CNS, is clearly present at higher levels in several non-neuronal tissues, particularly the developing kidneys, salivary glands, and thymus (Fig. 2.3B, K-N).

In the developing brain, *Dact1* is expressed in some progenitor zones. In the ventricular zone of the cerebral cortex at E14.5, it is expressed in a ventral (high)-dorsal (low) gradient (Fig. 2.3D). There is high expression in the ventricular zone of the basal ganglia anlagen (lateral and medial ganglionic eminences) (Fig. 2.3D); here, *Dact1* expression labels radially aligned clusters of cells (Fig. 2.3D, G). *Dact1* also shows differential regional expression in postmitotic neurons. For instance, within the cerebral cortex (Fig. 2.3D), *Dact1* is expressed in the cortical plate in a rostroventral (low)-caudodorsal (high) gradient, which is complementary to the gradient in the underlying

ventricular zone. *Dact3* is also concentrated in the cortical plate zone at this stage (Fig. 2.3F). By contrast, using a carefully-validated probe to avoid cross-detection of the two more heavily expressed paralogs (see Methods), *Dact2* message is detectable only very weakly in either the proliferative zones or post-mitotic domains of the forebrain (Fig. 2.3E).

Since *Dact1* is regionally expressed in the CNS at this stage of development, we have conducted a more thorough analysis of its distribution in developing nervous tissue. At the level of the developing midbrain (Fig. 2.3H), *Dact1* message is notable dorsally in the tectum, in postmitotic neurons of the ventral midbrain, as well as in some nuclei of the developing hypothalamus. Moving more caudally within the CNS, *Dact1* is also found in cerebellar precursors near the midbrain-hindbrain junction, as well as in the rhombic lip region and in the pons (Fig. 2.3A, I). In the spinal cord, *Dact1* is detected in primary sensory neurons of the developing dorsal horns, and in neurons of the motor pools located ventrally (Fig. 2.3J).

Postnatal Expression of the *Dact* genes in the Central Nervous System

In sharp contrast to the embryonic period, *Dact1* is the most weakly expressed of the gene family in the adult brain (*cf.* Fig. 2.1E, H). Nonetheless, *Dact1* message can be detected in many postnatal neuronal populations, and it is differentially expressed in neuronal sub-types (Fig. 2.3O). For example in the adult cerebellum, although *Dact1* is present at relatively high levels in the granule cell layer, it is not detectable in most Purkinje cells (Fig. 2.3O, inset). This pattern of expression in the adult cerebellum is complementary to *Dact2* and *Dact3*, both of which are detected more strongly in the

Purkinje cell layer (Fig. 2.3P, Q insets). Elsewhere in the brain, all three *Dact* genes are co-expressed in the hippocampus. In the dorsal forebrain *Dact1* and *Dact3* are expressed throughout all layers of the cerebral cortex, *Dact2* is preferentially expressed in more superficial layers (Fig. 2.3P, compare to Fig. 2.3O, Q). Given prior studies showing that changes in Wnt signaling components can alter complex behaviors (Madsen et al., 2003; Beaulieu et al., 2004; Long et al., 2004; Kaidanovich-Beilin et al., 2004; O'Brien et al., 2004), the regional adult brain expression patterns of *Dact* family members suggest different roles in brain function.

Implications for signaling

Sequence similarities and differences among the three mouse *Dact* genes, together with prior studies focused on *Dact1* and *Dact2* in other organisms (Waxman et al., 2004; Zhang et al., 2004; Zhang et al., 2006), suggest that each *Dact* paralog has both conserved and divergent functions in signal transduction. The tissue distribution of the three murine genes during embryogenesis is consistent with roles in a subset of developmental events downstream of Wnt signaling, as well as perhaps in other types of signaling as has been suggested for *Dact2* in modulating TGF β receptors (Zhang et al., 2004). The postnatal expression of the mouse *Dact* genes points to important functions in several adult organs including the CNS, uterus, testes, thymus, and kidneys. Ongoing work in our lab will explore the molecular and cellular roles of these signal scaffold molecules during development, and especially in the postnatal CNS.

Methods

5' RACE to determine transcriptional start of *Dact3*.

5'RACE was carried out using an RNA ligation-mediated protocol to ensure capture of the 5' end of the mRNA. FirstChoice RLM-RACE kit (Ambion, Austin TX) was used according to the manufacturer's protocol with the addition of Thermo-X RT polymerase (Invitrogen, Carlsbad, CA). The RT reaction was performed at 62°C for 2 h with reverse primer: 5'CAGGCGTCCATAGGAGCCAGATCCGGAG3' on total RNA extracted from mouse strain C57Bl/6 neonatal forebrain. Dissected brain was frozen on dry ice and RNA isolated with RNeasy kit (Invitrogen) using the manufacturer's animal tissue protocol. RT products were amplified with the 5'RACE outer primer provided by the manufacturer and gene-specific reverse primer:

5'GTGGTGAATCTGGGCCTCCAGTAGAACTG3' using Pfx DNA polymerase (Invitrogen, Carlsbad, CA). Purified PCR products were treated with Taq polymerase in the presence of 2mM dATP and cloned into pCR-4 TOPO vector (Invitrogen Carlsbad, CA). 12 RACE clones were sequenced to determine the mRNA start site. Relative to the proposed translational start, the distribution of transcriptional start sites was: 1 clone of each: positions -120, -111, -104, -77, -47, +11; 2 clones of each: -115, -110, -56.

Consistent with the proposed translational start site for *Dact3* based on 5'RACE, the sequence surrounding this codon corresponds to the Kozak consensus site (Kozak, 1987) at 8 out of 10 residues (gccgcagccATGa). This methionine is also conserved in the predicted sequence of human *DACT3*, and aligns well with the starts of the two other *Dact* family members (Fig. 2.1A).

Cloning of Mouse *Dact* Genes

The cloning of mouse *Dact1* (*Dpr1*) has previously been described (Cheyette et al., 2002). The full-length clones of mouse *Dact2* and *Dact3* were obtained by RT-PCR from adult cerebral cortex and neonatal forebrain respectively (see above for mRNA extraction). RT reactions were performed using ThermoScript (*Dact2*) and Thermo-X RT (*Dact3*) polymerases (Invitrogen, Carlsbad, CA) according to the manufacturer's instructions for GC-rich templates, and the following gene-specific primers:

gene	RT primer
<i>Dact2</i>	5'AGCGCAATAGCAAGGTTGATAC3'
<i>Dact3</i>	5'ATTAAGTGCAGTGAAGTTCAAGCCCATCCCGCCCCAAC3'

RT product was amplified by PCR with Pfu (Stratagene, La Jolla, CA) and Pfx (Invitrogen, Carlsbad, CA) polymerases for *Dact2* and *Dact3* respectively, using a forward primer specific for the 5'UTR of each gene and a reverse primer specific for the 3'UTR internal to the first-strand synthesis primer. Amplified cDNAs were isolated and subcloned using standard molecular biology techniques, and confirmed by sequencing with both vector-based and gene-specific primers.

Accession Numbers and Sequence Comparisons

The GenBank accession number for mouse *Dact1* (*Dpr1*) has previously been reported (Cheyette et al., 2002) and is AF488775. For the mouse *Dact2* (*Dpr2*) and *Dact3* sequences whose cloning is described here, accession numbers are AY297430 and DQ832319 respectively. Chromosomal positions were determined using the June 2006 update of the Ensembl Genome Browser (v 39).

Protein sequences were compared with VectorNTI Advance v. 9.1 (Invitrogen, Carlsbad, CA) AlignX software using an amino acid identity matrix. In the phylogenetic

tree shown (Fig. 2.1C), distance from a node along the horizontal axis indicates sequence divergence. Distance from a node along the vertical axis is arbitrary and has been manually enhanced to emphasize family subgroupings (*i.e. Dact1 vs. Dact2 vs. Dact3* subfamilies).

Northern Blotting

DNA probes were labeled by incorporation of ³²P-labeled dCTP. Mouse embryonic multi-stage and postnatal multi-tissue Northern blots (Seegene, Seoul S. Korea) containing 20 µg total RNA per lane were hybridized according to the manufacturer's instructions and the following stringencies and times: hybridization overnight at 55°C in Ultrahyb buffer (Ambion, Austin TX), wash 3 X 15 minutes in 0.2x SSC, 0.5% SDS at 60°C. Exposure to film was overnight (15 hours) at -80°C with two intensification screens. Two different probes were used to validate each gene pattern, and a pair of fresh blots (1 embryonic and 1 adult multi-tissue) was used for the initial characterization of each gene. Probes used for data shown (numbers relative to translational start): *Dact1* 613-1377; *Dact2* 586-1769; *Dact3* 853-1673.

Quantitative Reverse-Transcriptase PCR (Q-PCR)

For preparation of template, 2 µg total RNA was isolated from the experimental tissue indicated, taken from CD1 outbred mice (Charles River Laboratories, Wilmington MA), DNaseI-treated (Roche, Indianapolis IN), and reverse-transcribed (25°C x 10 min, 42°C x 50 min, 72°C x 10 min) using random primers and Superscript II (Invitrogen, Carlsbad, CA). Q-PCR primers for *Dact1*, *Dact2*, and *Dact3* have been designed using

PrimerExpress (Applied Biosystems, Foster City, CA) and validated to ensure: 1) amplification of a single product and 2) appropriate efficiency of amplification. The linear plot of cycle number determined at threshold (C_T) vs. cDNA concentration (log ng) gives a linear slope of -3.3 ± 0.1 for the housekeeping gene (mouse cyclophilin) and for *Dact1*, *Dact2*, and *Dact3*. Furthermore, a no-template control was conducted in each trial to ensure that the primers did not dimerize, and that amplified DNA is not the result of contamination. Steady-state mRNA was measured using an ABI 7300 quantitative real time PCR thermal cycler and standard conditions [1 cycle x (2 min @ 50°C, 10 min @ 95°C), then 40 cycles x (15 sec @ 95°C, 1 min @ 60°C)]. Sybr green (Applied Biosystems, Foster City, CA) was utilized to detect the PCR product in real-time, and a standard dissociation curve was generated. Mouse cyclophilin (NM 011149) was employed as an internal control for standardizing the measurements between reactions. Experimental PCR products were subcloned and sequenced to verify their identity. Data from each experiment (n=3 for 2 independent tissue samples in each case) was calculated using the $\Delta\Delta C_t$ method (Livak and Schmittgen, 2001). The following primer pairs were used:

<i>gene</i>	<i>forward</i>	<i>reverse</i>
<i>Cyclophilin</i>	5'TGGAGAGCACCAAGACAGACA3'	5'TGCCGGAGTCGACAATGAT3'
<i>Dact1</i>	5'TCAGGGTTTTATGAGCTGAGT3'	5'GAACACGGAGTTGGAGGAGTTA3'
<i>Dact2</i>	5'GGCTGACGGGCATGTTC3'	5'CCCCACGTCAGCTGGAA3'
<i>Dact3</i>	5'AGGCTTCTATGAAGACCCAGT3'	5'AGATCCGGAGAAGCCACTGT3'

Probes for mRNA in situ Hybridization

Riboprobes were labeled by incorporation of digoxigenin-labeled UTP (DIG RNA Labeling Mix, Roche Applied Science, Indianapolis IN). Sense controls were

performed in parallel and compared in each case to confirm the specificity of the expression patterns shown (Fig. 2.S3). The validity of tissue expression observed for each gene was further confirmed by the observation of identical expression patterns using multiple non-overlapping antisense probes derived from the same cDNA. Probes used (nt numbers relative to translational start):

gene	probe for data shown (nt)	pattern validated with probe (nt)
<i>Dact1</i>	1250-1601	316-692
<i>Dact2</i>	1639-1963	610-1080
<i>Dact3</i>	239-607	813-1153, 1162-1641, 1643-1910

mRNA in situ Hybridization: Tissue Preparation

Embryos were fixed by immersion, neonatal and postnatal animals by perfusion, with 4% paraformaldehyde in PBS. Embryos or tissue (*e.g.* brains) were dehydrated in sequential concentrations of ethanol and stored in 100% ethanol at -20°C. Prior to experimental use, tissue was rehydrated sequentially from ethanol into PBS containing 0.1% Tween-20.

mRNA in situ Hybridization: Thick sections

Embryos/tissues were embedded in gelatin/albumin gel polymerized with glutaraldehyde. Gel solution was 30% ovalbumin (w/v), 0.5% gelatin in 0.1M sodium acetate, pH 6.5, filtered. Gel was polymerized by addition of 2.5% glutaraldehyde, and solidified by storing overnight with embedded tissue at 4°C. Embedded tissue was sectioned to 100 µm thickness on a Leica VT1000S fluid immersion vibratome.

mRNA in situ Hybridization: Hybridization and Development

Embryos or thick sections were collected in PBT (PBS containing 0.1% Tween-20), and treated with 3% H₂O₂ (for whole mounts) or 6% H₂O₂ (for sections, including adult brain sections) in PBT for 1 h. Embryos/sections were washed sequentially in 3 X 5 min PBT, 5 min 10ug/mL proteinase K in PBT, 5 min 2mg/mL glycine in PBT, 2 X 5 min PBT, 20 min 4% paraformaldehyde, 0.2% glutaraldehyde in PBT, 3 X 5 min PBT. Tissue was prehybridized for 2 h in hybridization solution at 70°C, followed by hybridization overnight in fresh hybridization solution containing 0.5 µg/ml digoxigenin labeled RNA probe. Hybridization solution was 50% formamide, 5X SSC pH4.5 (pH 7.0 for adult brain sections), 1% SDS, 50ug/mL yeast tRNA, 50ug/mL heparin. Stringency washes were used to remove unbound probe. These consisted of 2 X 30 min in 50% formamide, 4X SSC, 1% SDS at 70°C, followed by 2 X 30 min in 50% formamide, 2X SSC, 1% SDS at 70°C.

Following hybridization, tissue was washed with MABT (0.1M maleic acid buffer pH 7.5 with 0.1% Tween-20) for 2 X 10 min at room temperature. Tissue was labeled with 1:4000 anti-digoxigenin (Roche, Indianapolis, IN) overnight at 4°C. Blocking for 2 h and immunolabeling were performed in 10% heat inactivated sheep serum, 2% BM blocking reagent (Roche, Indianapolis, IN), in MABT. Following antibody incubation, tissues were washed 5 X 30 min with MABT at room temperature.

For development reactions, tissue was washed 3 X 10 min in NTMT (0.1 M Tris pH 9.5, 0.1 M NaCl, 0.05 M MgCl₂, 0.1% Tween-20), and incubated in dark in NBT/BCIP (Bio-Rad) in NTMT. Incubation times were variable depending on when clear development was visible, but usually 4-6 h at room temperature for embryos, and 10-14 h for adult brain sections.

References

- Beaulieu, J.M., Sotnikova, T.D., Yao, W.D., Kockeritz, L., Woodgett, J.R., Gainetdinov, R.R., and Caron, M.G. 2004. Lithium antagonizes dopamine-dependent behaviors mediated by an AKT/glycogen synthase kinase 3 signaling cascade. *Proc. Natl. Acad. Sci. U. S. A* 101: 5099-5104.
- Borycki, A.G., Brunk, B., Tajbakhsh, S., Buckingham, M., Chiang, C., and Emerson, C.P., Jr. 1999. Sonic hedgehog controls epaxial muscle determination through Myf5 activation. *Development* 126: 4053-4063.
- Brott, B.K. and Sokol, S.Y. 2005a. A vertebrate homolog of the cell cycle regulator Dbf4 is an inhibitor of Wnt signaling required for heart development. *Dev. Cell* 8: 703-715.
- Brott, B.K. and Sokol, S.Y. 2005b. Frodo proteins: modulators of Wnt signaling in vertebrate development. *Differentiation* 73: 323-329.
- Cheyette, B.N.R., Waxman, J.S., Miller, J.R., Takemaru, K., Sheldahl, L.C., Khlebtsova, N., Fox, E.P., Earnest, T., and Moon, R.T. 2002. Dapper, a Dishevelled-associated antagonist of beta-catenin and JNK signaling, is required for notochord formation. *Dev. Cell* 2: 449-461.
- Christ, B., Huang, R., and Scaal, M. 2004. Formation and differentiation of the avian sclerotome. *Anatomy and Embryology* 208: 333-350.
- Gillhouse, M., Nyholm, M.W., Hikasa, H., Sokol, S.Y., and Grinblat, Y. 2004. Two Frodo/Dapper homologs are expressed in the developing brain and mesoderm of zebrafish. *Developmental Dynamics* 230: 403-409.
- Gloy, J., Hikasa, H., and Sokol, S.Y. 2002. Frodo interacts with Dishevelled to transduce Wnt signals. *Nat. Cell Biol.* 4: 351-357.
- Hikasa, H. and Sokol, S.Y. 2004. The involvement of Frodo in TCF-dependent signaling and neural tissue development. *Development* 131: 4725-4734.
- Hunter, N.L., Hikasa, H., Dymecki, S.M., and Sokol, S.Y. 2005. Vertebrate homologues of Frodo are dynamically expressed during embryonic development in tissues undergoing extensive morphogenetic movements. *Dev. Dyn.* 235: 279-284.
- Kaidanovich-Beilin, O., Milman, A., Weizman, A., Pick, C.G., and Eldar-Finkelman, H. 2004. Rapid antidepressive-like activity of specific glycogen synthase kinase-3 inhibitor and its effect on beta-catenin in mouse hippocampus. *Biological Psychiatry* 55: 781-784.
- Katoh, M. and Katoh, M. 2003. Identification and characterization of human DAPPER1 and DAPPER2 genes in silico. *Int. J. Oncol.* 22: 907-913.
- Katoh, M. 2005. Identification and characterization of rat Dact1 and Dact2 genes in silico. *International Journal of Molecular Medicine* 15: 1045-1049.

- Kozak, M. 1987. At least six nucleotides preceding the AUG initiator codon enhance translation in mammalian cells. *J. Mol. Biol.* 196: 947-950.
- Lee, C.S., Buttitta, L.A., May, N.R., Kispert, A., and Fan, C.M. 2000. SHH-N upregulates *Sfrp2* to mediate its competitive interaction with WNT1 and WNT4 in the somitic mesoderm. *Development* 127: 109-118.
- Livak, K.J. and Schmittgen, T.D. 2001. Analysis of relative gene expression data using real-time quantitative PCR and the $2^{-(\Delta\Delta C(T))}$ Method. *Methods* 25: 402-408.
- Long, J.M., LaPorte, P., Paylor, R., and Wynshaw-Boris, A. 2004. Expanded characterization of the social interaction abnormalities in mice lacking *Dvl1*. *Genes Brain Behav.* 3: 51-62.
- Madsen, T.M., Newton, S.S., Eaton, M.E., Russell, D.S., and Duman, R.S. 2003. Chronic electroconvulsive seizure up-regulates beta-catenin expression in rat hippocampus: Role in adult neurogenesis. *Biological Psychiatry* 54: 1006-1014.
- Moon, R.T., Bowerman, B., Boutros, M., and Perrimon, N. 2002. The promise and perils of Wnt signaling through beta-catenin. *Science* 296: 1644-1646.
- O'Brien, W.T., Harper, A.D., Jove, F., Woodgett, J.R., Maretto, S., Piccolo, S., and Klein, P.S. 2004. Glycogen synthase kinase-3beta haploinsufficiency mimics the behavioral and molecular effects of lithium. *J. Neurosci.* 24: 6791-6798.
- Polakis, P. 2000. Wnt signaling and cancer. *Genes Dev.* 14: 1837-1851.
- Shimogori, T., VanSant, J., Paik, E., and Grove, E.A. 2004. Members of the Wnt, Fz, and Frp gene families expressed in postnatal mouse cerebral cortex. *Journal of Comparative Neurology* 473: 496-510.
- Veeman, M.T., Axelrod, J.D., and Moon, R.T. 2003. A second canon: Functions and mechanisms of beta-catenin-independent wnt signaling. *Developmental Cell* 5: 367-377.
- Wagner, J., Schmidt, C., Nikowits, W., and Christ, B. 2000. Compartmentalization of the somite and myogenesis in chick embryos are influenced by Wnt expression. *Developmental Biology* 228: 86-94.
- Waxman, J.S., Hocking, A.M., Stoick, C.L., and Moon, R.T. 2004. Zebrafish *Dapper1* and *Dapper2* play distinct roles in Wnt-mediated developmental processes. *Development* 131: 5909-5921.
- Wharton, K.A., Jr. 2003. Runnin' with the Dvl: proteins that associate with Dsh/Dvl and their significance to Wnt signal transduction. *Dev. Biol.* 253: 1-17.
- Wong, H.C., Bourdelas, A., Krauss, A., Lee, H.J., Shao, Y., Wu, D., Mlodzik, M., Shi, D.L., and Zheng, J. 2003. Direct binding of the PDZ domain of Dishevelled to a

conserved internal sequence in the C-terminal region of Frizzled. *Mol. Cell* 12: 1251-1260.

Yau, T.O., Chan, C.Y., Chan, K.L., Lee, M.F., Wong, C.M., Fan, S.T., and Ng, I.O. 2004. HDPR1, a novel inhibitor of the WNT/beta-catenin signaling, is frequently downregulated in hepatocellular carcinoma: involvement of methylation-mediated gene silencing. *Oncogene* 24: 1607-1614.

Zhang, L., Gao, X., Wen, J., Ning, Y., and Chen, Y.G. 2006. Dapper 1 antagonizes Wnt signaling by promoting dishevelled degradation. *J. Biol. Chem.* 281: 8607-8612.

Zhang, L., Zhou, H., Su, Y., Sun, Z., Zhang, H., Zhang, L., Zhang, Y., Ning, Y., Chen, Y.G., and Meng, A. 2004. Zebrafish Dpr2 inhibits mesoderm induction by promoting degradation of nodal receptors. *Science* 306: 114-117.

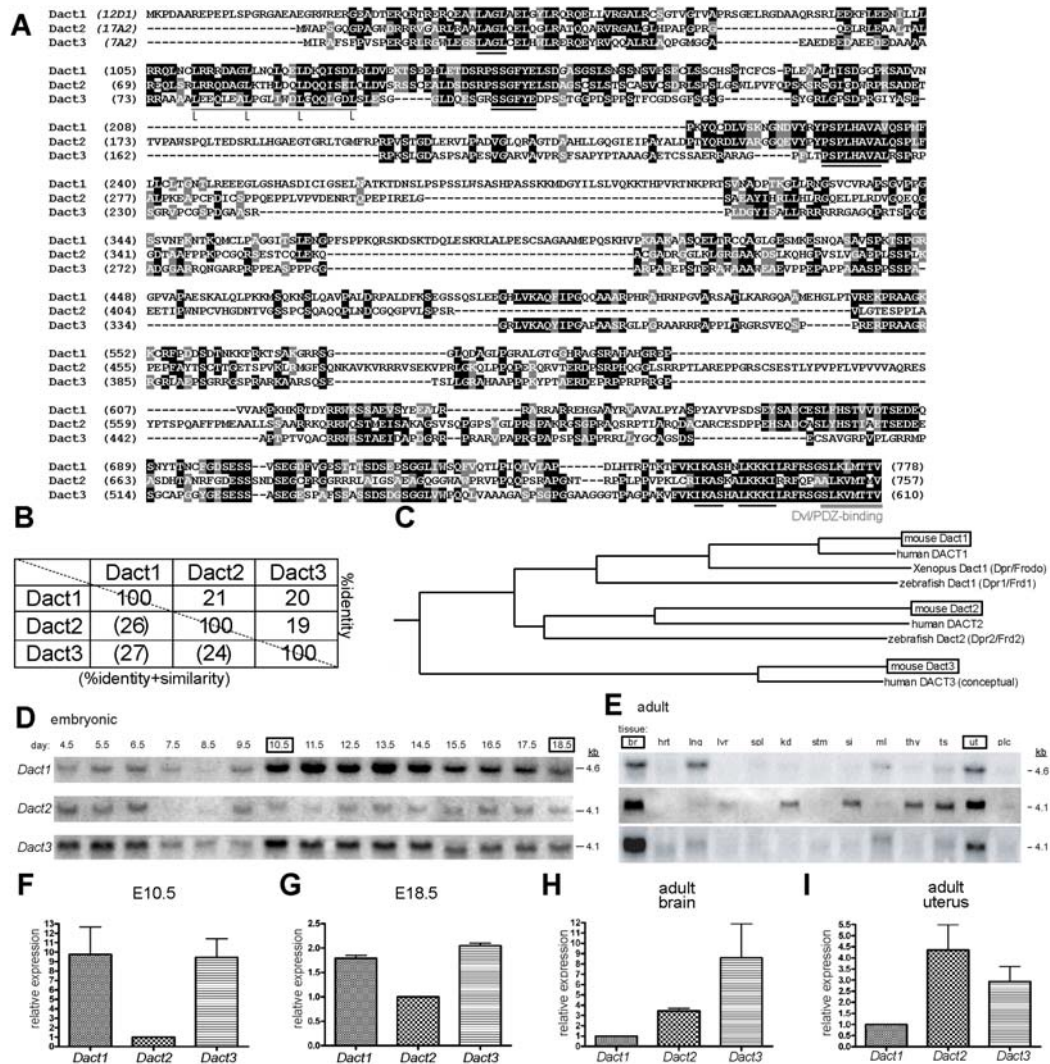


Figure 2.1 Dact gene family molecular data

A. Alignment of primary protein sequences, mouse Dact1, Dact2, Dact3. Chromosomal positions are shown in the first line. Black blocks indicate identity; grey indicates similarity. Blocks of four or more amino acids conserved in all three paralogs are underlined in black. The coiled-coil domain (with four absolutely conserved leucines indicated) and the Dvl/PDZ-binding domain (Cheyette et al, 2002) are underlined in grey. **B.** Table showing percentage conservation in the primary protein sequences, aligned as in **A.** Numbers to the top right indicate % identity; numbers (in parentheses) to the bottom left indicate % identity plus highly similar residues. **C.** Deduced phylogenetic relationships between the Dact proteins described in this paper and those previously described. The three mouse cDNAs whose coding sequences have been cloned in their entirety are boxed. The originally-described Dpr and Frodo genes are both homologs of Dact1, corresponding to a recent duplication event in the Xenopus lineage (not shown). The human DACT3 sequence is a predicted cDNA based on public database information (see text and also Fig. S1). **D, E.** Northern blots. Note: Different blots were probed for each gene, loading controls are provided in Fig. S2. **D.** Embryonic stages. Samples from the first three days post-coitus (E4.5-6.5) include both extra-embryonic and maternal uterine tissue, while the next three (E7.5-9.5) are the embryo plus extra-embryonic membranes. E10.5-18.5 correspond to embryonic tissues only. **E.** Adult tissues: (br) brain, (hrt) heart, (lng) lung, (lvr) liver, (spl) spleen, (kd) kidney, (stm) stomach, (si) small intestine, (ml) striated muscle, (thv) thymus, (ts) testis, (ut) non-pregnant uterus, (plc) placenta. **F-I.** Q-PCR showing relative expression of Dact1 vs. Dact 2 vs. Dact3 at selected developmental stages and adult tissues. **F.** E10.5 **G.** E18.5 **H.** adult (8 week postnatal) brain, **I.** adult (8 week postnatal; non-pregnant) uterus. Note: Y-axis scale changes from **F-I**; units denote relative expression within each sample, absolute levels are not measured by this technique.

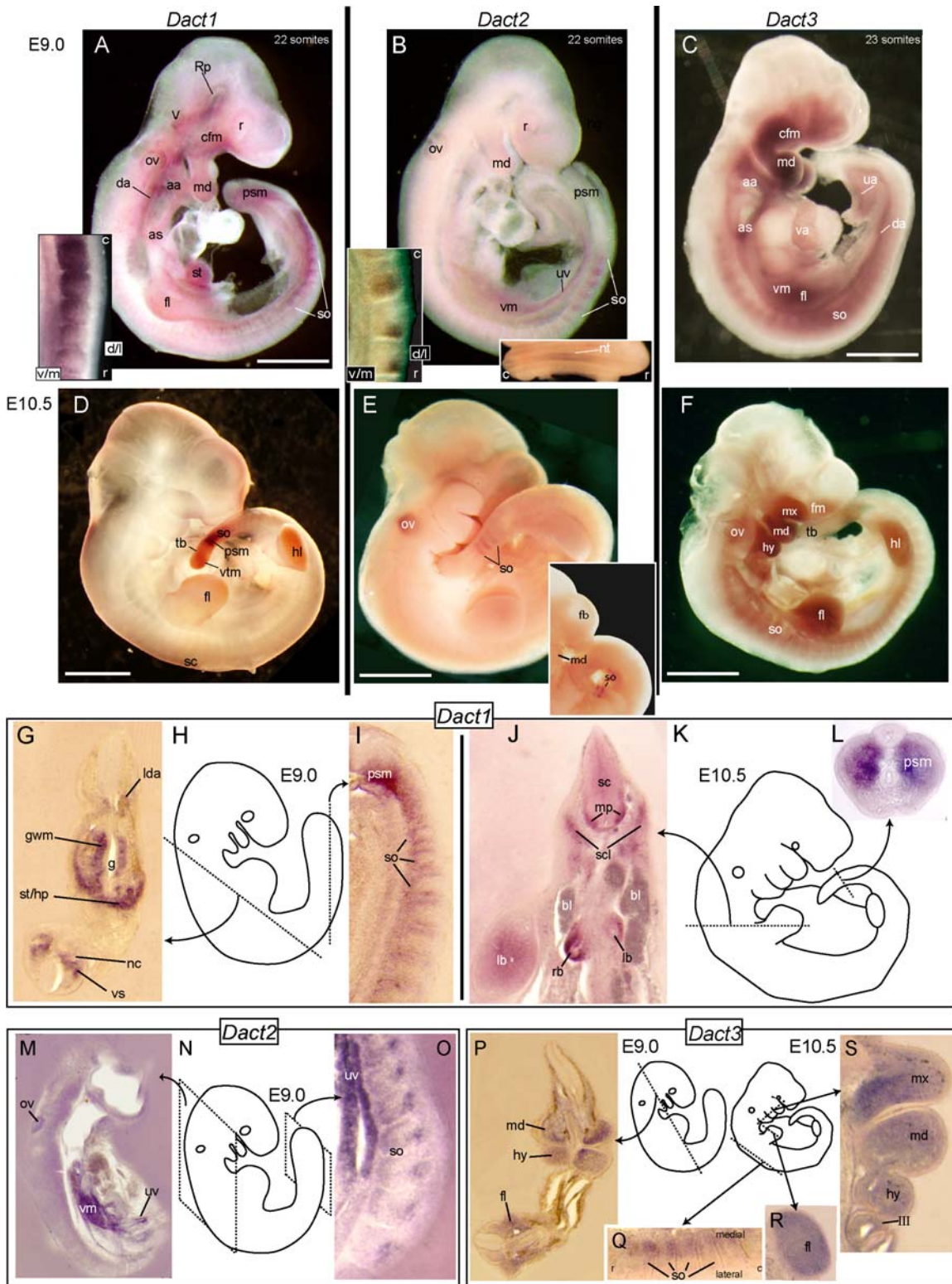


Figure 2.2 Developmental expression of Dact genes

A-C. WISH at E9.0. A. Dact1-specific probe. Expression is most prominent in presomitic mesoderm (psm), somites (so), septum transversum (st), craniofacial mesenchyme (cfm), and the ganglion of cranial nerve V (V), and is also present in the retina (r), around Rathke's pouch (Rp), the otic vesicle epithelium (ov), the mandibular arch (md), aortic sac (as), aortic arches (aa), and dorsal aorta (da), and in the forelimb bud (fl). Inset (lateral aspect): Dact1 becomes polarized ventromedially (v/m) and caudally (c) as somites mature. B. Dact2-specific probe. Only weak expression is detectable: in caudal somites (so), umbilical veins (uv), ventral mesentery of the foregut (vm), otic vesicle (ov), mandibular arch (md), and retina (r). Left inset (lateral aspect): Dact2 becomes polarized dorsolaterally (d/l) and rostrally (r) in the caudal somites. Right inset (dorsal aspect): Dact2 is expressed in the dorsal neural tube caudally. C. Dact3-specific probe. Expression in the craniofacial mesenchyme (cfm), mandibular arch mesenchyme (md), aortic sac (as), aortic arches (aa), and dorsal aorta (especially caudally; da), umbilical artery (ua), vitelline artery (va), ventral mesentery of the foregut (vm), forelimb bud (fl), and ventrally in mature somites (so). D-F. WISH at E10.5. D. Dact1-specific probe. Expression in the presomitic mesoderm (PSM), caudal somites (so), more weakly in the ventral mesoderm of the tail bud (tb; vtm), limb buds (fl, hl), as well as the ventral spinal cord (sc). E. Dact2-specific probe. Expression is detected in the otic vesicle plus the rostral portion of the most recently formed somites (so). Inset: another example of caudal somite expression plus no expression detected in the forebrain (fb) or mandibular arch (md; obscured in E). F. Dact3-specific probe. Expression in facial mesenchyme (fm), branchial arch mesenchyme: (mx) maxillary, (md) mandibular, (hy) hyoid, limb buds (fl, hl), as well as ventral somites (so). G-S. Dact family member ISH on representative sections from E9-E10.5. G. At E9.0 Dact1 is detected in the ventral somite (vs), nephrogenic cords (nc), septum transversum and hepatic primordium (st/hp), and the gut wall mesenchyme (gwm). H. Schematic showing approximate level and orientation of sections in G, I. I. At E9.0 Dact1 is expressed in the PSM, in the ventral domains of somites, and along the rostral and caudal somite walls. J. At E10.5 Dact1 is detected in the limb bud mesoderm (lb), outer walls of the right and left main bronchi (rb, lb), sclerotome (scl), and the motor pools of the spinal cord (mp, sc). K. Schematic showing approximate level and orientation of sections in J, L. L. At E10.5 and earlier Dact1 is highly expressed in the PSM and caudal somites. M. At E9.0 Dact2 is detected in the otic vesicle (ov), ventral mesentery of the foregut (vm), and umbilical veins (uv). N. Schematic showing approximate levels and orientation of sections in M and O. O. Dact2 is detected in the umbilical veins (uv) and within somites (so) rostrally and dorsally. P. At E9.0 Dact3 is detected throughout mesenchyme, including that of the limb buds such as the forelimb (fl), as well as the hyoid (hy) and mandibular (md) branchial arches, in a section corresponding to the plane shown in the schema at right. Q-S. E10.5 ISH on sections corresponding to the planes shown in the accompanying diagram. Q. Expression ventrally in maturing somites. R. Expression in forelimb mesoderm (fl). S. Expression in branchial arch mesenchyme: (mx) maxillary, (md) mandibular, (hy) hyoid, (III) third. Other abbreviations: (lda) left dorsal aorta, (bl) blood. Scale bars: A-C 0.5 mm; D-F 1.0 mm.

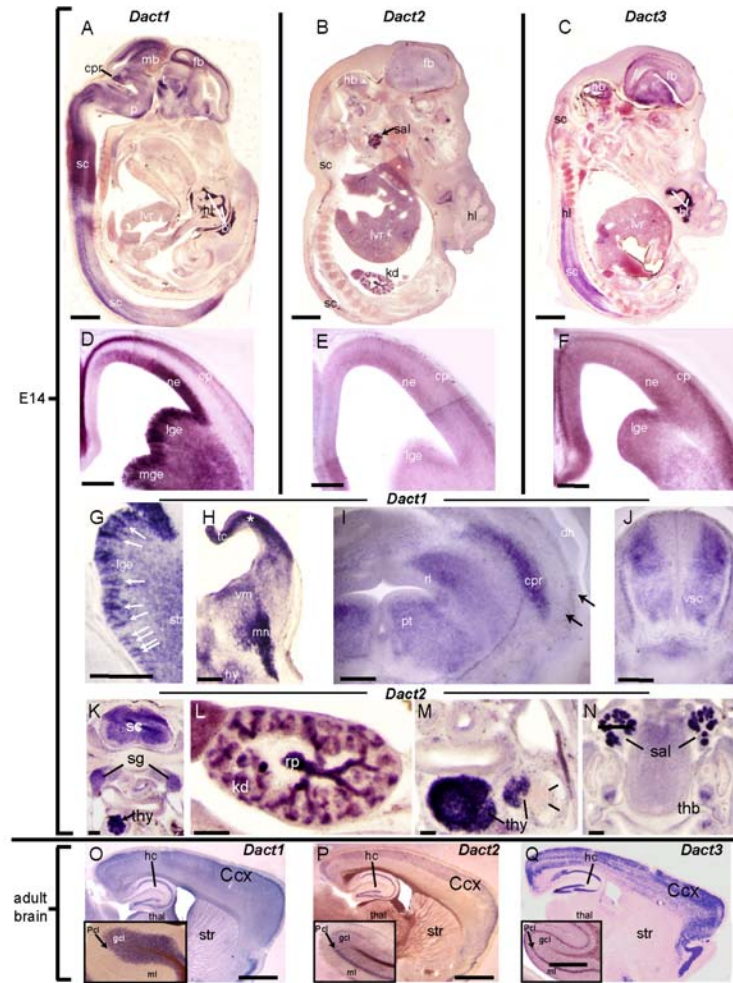


Figure 2.3 Expression of Dact genes at E14.5 and in adult brain

A-C. Sagittal sections of whole embryos at E14.5 stained by in situ hybridization with probes for Dact1 (A), Dact2 (B), and Dact3 (C). Dact1 and Dact3 are most prominent in the developing CNS, Dact2 has domains of higher expression in the developing salivary glands (sal) and kidneys (kd). D-F. Horizontal sections of forebrain at E14.5 stained with probes for Dact1 (D), Dact2 (E), and Dact3 (F). G. Close-up of horizontal section through the ventricular proliferative zone at the level of the lateral ganglionic eminence, showing Dact1 expression in radially-arranged cell clusters (arrows). H-J. Horizontal sections at progressively more caudal planes of the E14.5 CNS showing Dact1 expression in many populations of differentiating neurons. H. Midbrain. I. Midbrain-hindbrain junction and pons. J. Spinal cord. Abbreviations: (tc) tectum/dorsal midbrain, (vm) ventral midbrain, (mn) migrating neurons of the ventral midbrain, (hy) hypothalamic nuclei, (pt) pontine tegmentum, (rl) rhombic lip of the fourth ventricle, (cpr) cerebellar precursors, (dh) developing dorsal horn of the spinal cord. Arrows: neurons in the motor pools of the ventral spinal cord (vsc). K-N. Sections showing Dact2 expression in E14.5 tissues. K. Horizontal section through spinal cord (sc) and sympathetic ganglia (sg). Compare to higher level of expression in the nearby edge of the developing thymus (thy). L. Section of developing kidney showing high levels of expression in the collecting system and renal pelvis (rp). M. Section through the main lobe of the thymus (thy). N. Section of the oral cavity showing expression in the developing salivary glands (sal) as well as weaker expression in the toothbuds (thb). O-Q. Sagittal sections of adult brains stained with in situ hybridization probes for Dact1 (O), Dact2 (P), and Dact3 (Q). All three genes are expressed in the hippocampus (hc), in different patterns in the cerebral cortex (Ccx) and other structures of the forebrain (see text). Insets: Expression in the adult cerebellum. Dact1 (inset O) is specifically expressed in the granule cell layer (gcl), whereas both Dact2 (inset P) and Dact3 (inset Q) are expressed significantly in the Purkinje cell layer (Pcl). Sense and no probe controls provided in Fig. S3. Other abbreviations: (fb) forebrain, (mb) midbrain, (hb) hindbrain, (thal) adult thalamus, (str) striatum, (t) thalamic eminence, (p) pons, (lvr) liver, (hl) hindlimb, (cp) cortical plate zone, (ne) neuroepithelium, (lge) lateral ganglionic eminence, (mge) medial ganglionic eminence, (ml) molecular layer of the cerebellum, (bl) extravasated blood, (*) folded tissue. Scale bars: A-C 1 mm; D-N 0.2 mm; O-Q 2 mm.

```

H.s. DACT3 (19q13) MIRAFFPVSPEGRRLRGWLEGLAGLCELHWLRERQYRVOQALRLAOPMGGAEDDEDAEDEDAAAARRAAAALEEQLEALPGLWDLGQQLGDLSESGGL
M.m. Dact3 (7A2) MIRAFFPVSPEGRRLRGWLEGLAGLCELHWLRERQYRVOQALRLAOPMGGAEDDEDAEDEDAAAARRAAAALEEQLEALPGLWDLGQQLGDLSESGGL

H.s. DACT3 (108) EOESGRSSGFYEDPSTTGGPDSPPSTFCGDSGFSGSSYGRLGPSVPRGIYASERPKSLGDASPSAPEVVGARNAVPRFSAPYPTAGSAGPACSSAERRARAGE
M.m. Dact3 (108) EOESGRSSGFYEDPSTTGGPDSPPSTFCGDSGFSGSSYGRLGPSVPRGIYASERPKSLGDASPSAPEVVGARNAVPRFSAPYPTA--AGAPACSSAERRARAGE

H.s. DACT3 (215) FLTSPPLHAVAMRSPRCGRFPDSDPAQEAQRPLDGYISALLRRRRRRGAGQPRTSPGGADGCPRRONSVPORPPHASPFGSARPAPEPSLVRVGGHPTSPAALS
M.m. Dact3 (213) FLTSPPLHAVAMRSPRCGRVPCGSDPAQEAQRPLDGYISALLRRRRRRGAGQPRTSPGGADGCPRRONGARPRPPHASPFGSARPAPEPSL-----

H.s. DACT3 (322) RAWASWEEDANFEPAPFPAAPSPFSSPAEGRLVKAQYIPGAQAARGLPGRAARRKPPPLTRGRSVEQSPPRERPRRAGRRGRMAEASGRRGSPRARKARSQSET
M.m. Dact3 (306) RAWAAWEAEVPEPAPFAAASPFSSPAEGRLVKAQYIPGAQAARGLPGRAARRKPPPLTRGRSVEQSPPRERPRRAGRRGRMAEASGRRGSPRARKARSQSET

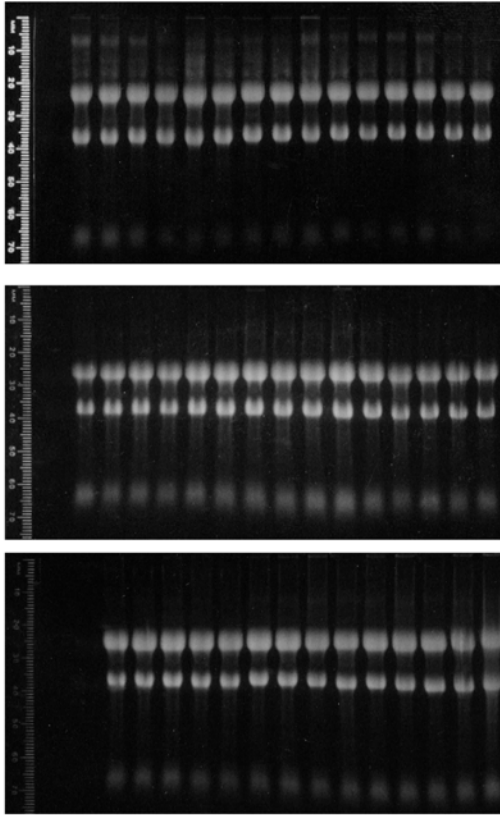
H.s. DACT3 (429) SILGRSAWVSGPPKYPTAERDEPRPPRRRGPAPLAAQAAGCRRWRSTAEIDADGRRVRRPAPAAVPEEGFSPSAPORRLLYCCAGSDSECSAGRLCPLGR
M.m. Dact3 (412) SILGRSAWVSGPPKYPTAERDEPRPPRRRGPAPLPTVQ---CRRWRSTAEIDADGRRVRRPAPAAVPEEGFSPSAPORRLLYCCAGSDSECSAVGRPVPVLR

H.s. DACT3 (535) RFPVGGVGGYGESESSASEGESPAFSSASSSDSGSGLVWPQQLVAAMAS---GGAGCAGPAGPAKVFVKIKASHALKKKILRFRSGSLKVMTTV (629)
M.m. Dact3 (512) RFPVGGVGGYGESESSASEGESPAFSSASSSDSGSGLVWPQQLVAAMASPSGFGCAGCAGPAGPAKVFVKIKASHALKKKILRFRSGSLKVMTTV (610)

```

Figure 2.S1 Predicted human DACT3 sequence (H.s. Dact3) compared to translation of cloned mouse Dact3 cDNA (M.m. Dact3) Chromosomal positions are shown in the first line. Black blocks indicate identity; grey indicates similarity. The human sequence is based on publicly-available human cDNA fragments (e.g. GenBank CV029753, BG715516, BF515069, BF115250, BM468105, etc), previously identified 5'truncated cDNAs (e.g. BC016161), and human genomic sequence corresponding to chromosome 19q13.32. Genscan also identifies this as a transcribed locus based on genomic sequence-level criteria.

A embryonic stage blots



B adult multi-tissue blots

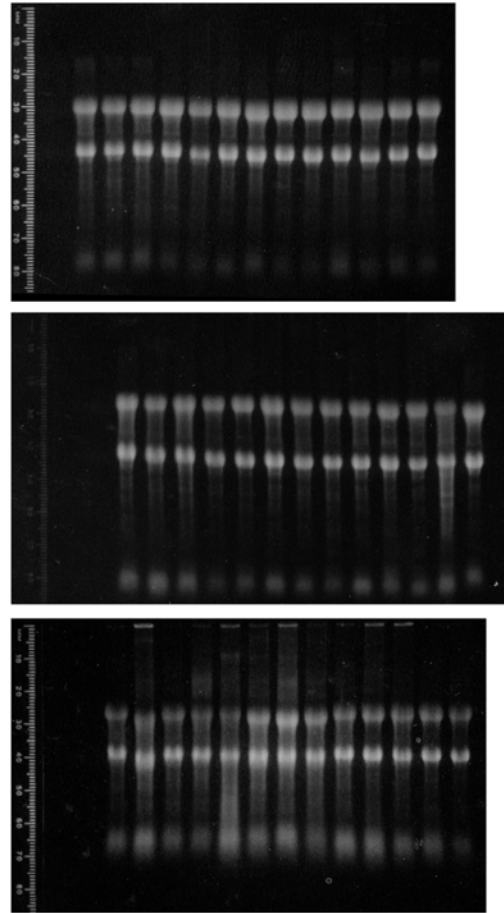


Figure 2.S2 Ethidium bromide stained gels corresponding to all Northern blots shown in Figure 2.1D-E. Northern blots demonstrating similar levels of 18S and 28S ribosomal RNA in each lane as a loading control. A total of 6 (3 pairs of embryonic (A) and adult (B) blots) were used to generate data in Fig 2.1: one pair of fresh blots for each Dact gene. Expression data was cross-validated by sequentially stripping and re-testing each blot pair with the other 2 probes.

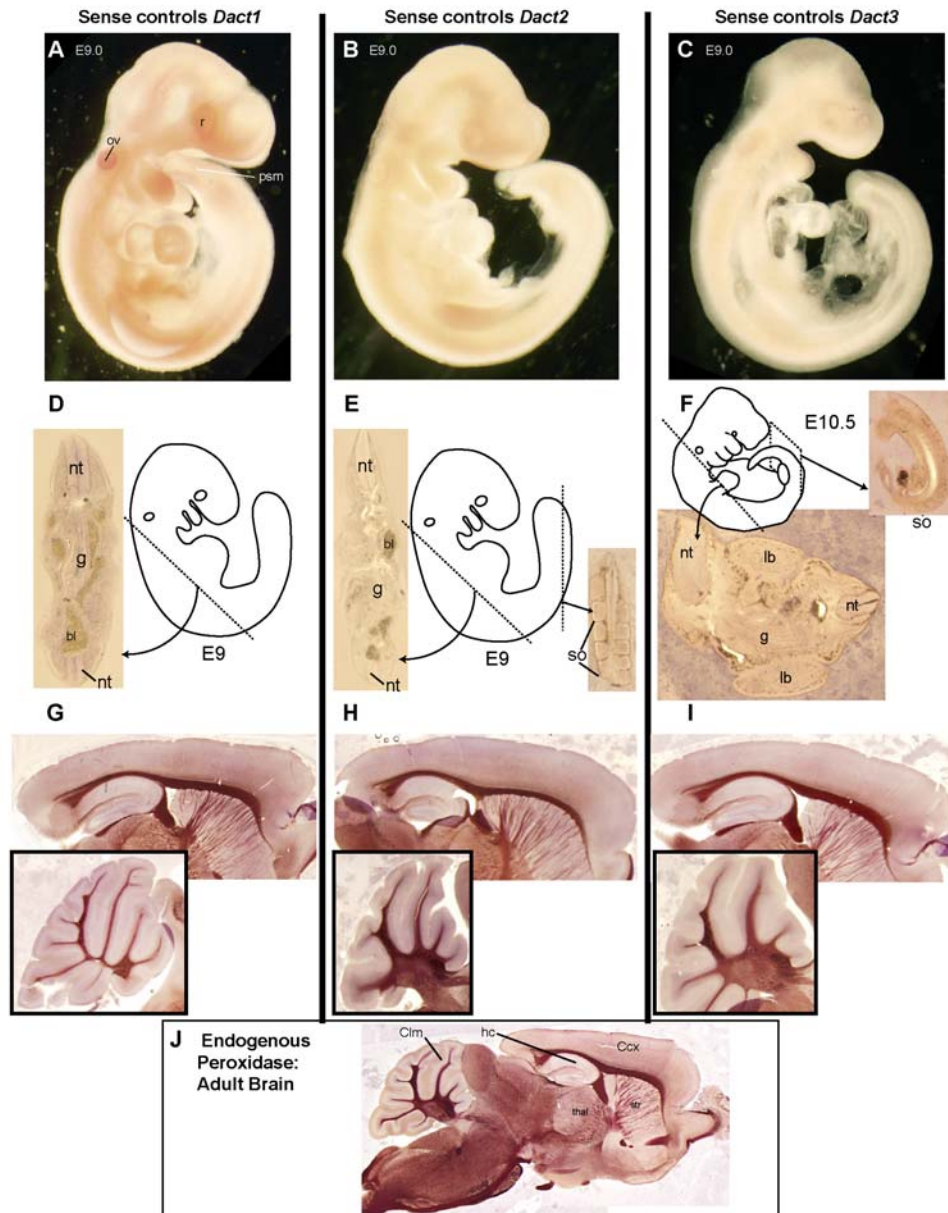


Figure 2.S3 In situ hybridization controls using reverse complementary (sense) probes. Controls corresponding to the cDNAs, hybridization, and development conditions used in Figs. 2.2 and 2.3. A-C. WISH at E 9.0: (A) Dact1. (B) Dact2. (C) Dact3. Aside from very weak staining of the retina and otic vesicle with the sense probe for Dact1, essentially no signal comparable to the antisense staining is seen with any of the sense controls. Note the absence of PSM, somite, septum transversum, and major arterial staining with the Dact1 sense probe. Abbreviations: (r) retina, (ov) otic vesicle, (psm) presomitic mesoderm. D-F. ISH on representative sections at E9.0 and E10.5 using sense probes: (D) Dact1. (E) Dact2. (F) Dact3. No specific signal is detected. G-I. ISH on adult brain sections, forebrain and cerebellum (insets): (G) Dact1. (H) Dact2. (I) Dact3. No signals comparable to the cortical, hippocampal, or cerebellar staining in Fig. 2.3O-Q is observed. J. No-probe control for adult brain section ISH, showing background levels of endogenous peroxidase activity under conditions used to generate adult brain expression data shown in Fig. 2.3O-Q and Fig. 2.S3G-I. Note absence of staining in cortical structures including the cerebellum (Cim), hippocampus (hc) and cerebral cortex (Ccx). Brownish peroxidase stain is apparent in the striatum (str) and thalamus (thal).

CHAPTER 3

***Dact1* Presomitic Mesoderm Expression Oscillates in phase with *Axin2* in the Somitogenesis Clock of Mice**

Rowena Suriben,* Daniel A Fisher,* Benjamin NR Cheyette

Department of Psychiatry & Graduate Program in Developmental Biology, University of
California, San Francisco, 94143-2611

*Contributed equally

Abstract

During segmentation (somitogenesis) in vertebrate embryos, somites form in a rostral to caudal sequence according to a species-specific rhythm, called the somitogenesis clock. The expression of genes participating in somitogenesis oscillates in the presomitic mesoderm (PSM) in time with this clock. We previously reported that the *Dact1* gene, which encodes a cytoplasmic regulator of Wnt signaling, is prominently expressed in the PSM as well as in a caudal-rostral gradient across the somites of mouse embryos. This observation led us to examine whether *Dact1* expression oscillates in the PSM. We have found that *Dact1* PSM expression does indeed oscillate in time with the somitogenesis clock. Consistent with its known signaling functions and with the “clock and wavefront” model of signal regulation during somitogenesis, the oscillation of *Dact1* occurs in phase with the Wnt signaling component *Axin2*, and out of phase with the Notch signaling component *Lfng*.

Introduction

Vertebrates are segmented organisms whose vertebrae, ribs, muscles, and dermis innervated by each spinal nerve are embryonically derived from packets of mesoderm called somites. Bilateral pairs of somites bud in a rostral to caudal sequence from the presomitic mesoderm (PSM), which is formed from mesoderm arising initially by gastrulation at the primitive streak, and at late stages in the tail bud. The time interval between the budding of each new pair of somites varies according to the animal species and has been termed the somitogenesis clock. For example, in mouse embryos the somitogenesis clock takes approximately 2 hours to complete a full cycle, that is the time

between the generation of successive somites (Forsberg et al., 1998; Iulianella et al., 2003; Giudicelli and Lewis, 2004).

The ligand *Wnt3a* plays an important role in both the formation and the identity of somites (Takada et al., 1994; Greco et al., 1996; Ikeya and Takada, 2001; Aulehla et al., 2003). Mice with allelic combinations of a *Wnt3a null* mutation and the partial loss-of-function mutation *Wnt3a^{vt}* (“*vestigial tail*”) show varying degrees of caudal truncation plus homeotic transformations in a subset of more anterior segments (Greco et al., 1996; Ikeya and Takada, 2001). Similarly, mutation of the cytoplasmic Wnt signal transduction molecule *Dvl2* leads to defects in somite development including abnormal segmental bifurcations, deletions, and fusions (Hamblet et al., 2002). This is reminiscent of phenotypes resulting from mutations in the Notch inhibitor *Lunatic fringe (Lfng)*, which cause truncation of tail segments similar to *vestigial tail*, accompanied by abnormal patterning of more anterior somite derivatives similar to *Dvl2* (Evrard et al., 1998; Zhang and Gridley, 1998). The expression of *Lfng* as well as that of several other Notch signaling molecules and target genes cycles rhythmically in the PSM (McGrew et al., 1998; Forsberg et al., 1998; Aulehla and Johnson, 1999; Bessho et al., 2001; Pourquié, 2003a). Levels of *Axin2*, a cytoplasmic inhibitor of the Wnt/ β -catenin pathway, also cycle in the PSM, but out of phase with *Lfng* (Aulehla et al., 2003). In contrast, another cytoplasmic Wnt/ β -catenin pathway inhibitor, *Nkd1*, cycles out of phase with *Axin2* and in phase with *Lfng* (Ishikawa et al., 2004).

The observation of reciprocal expression cycling between *Lfng* and *Axin2*, in combination with phenotypes in Notch and Wnt loss and gain of function experiments (Evrard et al., 1998; Zhang and Gridley, 1998; Serth et al., 2003; Aulehla et al., 2003;

Dale et al., 2003) supports a “clock and wavefront” model of somitogenesis (Cooke and Zeeman, 1976) in which Notch and Wnt signaling alternate in the PSM via delayed negative feedback (Pourquié, 2003a; Aulehla and Herrmann, 2004). According to this model, as presomitic cells mature and migrate rostrally within the PSM they experience alternating cycles of high Notch and Wnt signal transduction, while a gradient of Wnt3a originating caudally from the tail bud determines the “determination front”: the point at which the most anterior “presomite” pinches off from the PSM to form a new somite (Aulehla et al., 2003; Pourquié, 2003a). The reciprocal oscillation between inhibitors of Wnt signaling (*i.e.* Axin2) and of Notch signaling (*i.e.* Lfng) have led to the proposal that oscillations in the levels of such inhibitors critically contributes to the offset between the Wnt and Notch signaling cycles in the PSM, via a delayed negative feedback loop mechanism (Aulehla et al., 2003).

We previously compared embryonic expression levels and patterns of the three murine members of the Dact gene family, which encode conserved Dvl-binding regulators of Wnt signaling (Fisher et al., 2006). Compared to its paralogs, *Dact1* is uniquely expressed at high levels in the PSM. This led us to examine whether *Dact1* exhibits cycles of expression in the PSM, and if so, whether such cycles of *Dact1* occur in phase with the somitogenesis cycling of the Wnt signaling inhibitor *Axin2*, or instead with the Notch signaling inhibitor, *Lfng*.

Results and Discussion

Dact1 expression in the PSM is dynamic and consistent with somitogenesis cycling

We performed whole-mount in situ hybridization (WISH) using a *Dact1* specific probe on embryonic day (E) 9.0-9.5 mouse embryos and examined the distribution of *Dact1* in the PSM to determine whether patterns observed were consistent with cyclical gene expression. In over 100 embryos examined by this technique, we have observed a range of *Dact1* expression in the caudal PSM that can be organized into 3 apparent phases by analogy with the phase patterns of *Axin2* which the *Dact1* patterns most closely resemble (Pourquié and Tam, 2001, Aulehla et al., 2003). In a representative sample taken from 4 complete litters in the CD1 outbred mouse strain (38 embryos) numbers observed in each of these phases correspond with expected ratios based on previous descriptions of genes undergoing somitogenesis cycling (Aulehla et al., 2003; Dale et al., 2003) (Table 3.1).

The phases of *Dact1* expression that we observe in the PSM can be arranged into a cyclical pattern that coincides with the formation of new somites (Fig 3.1). In all phases, expression is pronounced in the s0 presomite (those cells at the rostral tip of the PSM that will pinch off to form the next somite). In Phase 1, *Dact1* expression also extends from the caudal tip of the PSM rostrally up to the position of the s-1 presomite (the next somite to form after s0), where its expression is low (Fig 3.1A, B). In Phase 2, expression of *Dact1* commences in the s-1 presomite, and the caudal expression of *Dact1* recedes caudally, such that the band of low expression moves to the s-2 somite (Fig 3.1C, D). At the juncture between Phase 2 and Phase 3, the s0 presomite pinches off from the rostral PSM to become the new s1 somite. At this point the former s-3 becomes the new

s-2, the former s-2 becomes s-1, and the former s-1 becomes s0 (Fig 3.1E, H). In Phase 3, expression is strong in s0 but weak throughout the rest of the PSM (Fig 3.1F). Expression in the caudal PSM then resumes, bringing the PSM back into Phase 1 and completing the cycle (Fig 3.1H).

To summarize this experiment, we have observed a range of *Dact1* expression patterns in the embryonic mouse PSM that can be subdivided into 3 phases depending on the extent of staining caudally and the position of the somite-presomite boundary rostrally. Embryos fall into these phases in a ratio that is consistent with phases observed for genes such as *Axin2* or *Lfng*, suggesting that the patterns observed for *Dact1* correspond to transitions in the somitogenesis cycle previously identified with these other somitogenesis genes. The phases of *Dact1* expression can be arranged cyclically in a manner consistent with the timing between the formation of new somites. These results show that *Dact1* expression within the PSM during segmentation stages is dynamic, and suggest that *Dact1* cycles in the PSM according to the somitogenesis clock.

Dact1 cycling in the PSM occurs in phase with *Axin2* and out of phase with *Lfng*

To establish that *Dact1* is indeed cycling in the PSM with the somitogenesis clock, as well as to compare its pattern of cycling to that of previously described cycling genes in the Notch and Wnt signaling pathways, we performed Double-WISH for *Dact1* and either *Lfng* or *Axin2* on E9.5 embryos (Fig 3.2A, B). As expected, the expression patterns of all three genes varied from embryo to embryo depending on the phase of the somitogenesis clock. The spatial domains of *Dact1* and *Axin2* expression in the PSM overlap and always correspond to the same phase, suggesting that these genes cycle

together in PSM cells. The degree of spatial overlap in the caudal PSM is especially evident when both genes are in Phase 1 (Fig 3.2A). In contrast, in any given embryo the *Dact1* and *Lfng* patterns correspond to different phases of their cycle, such that their spatial distribution in the caudal PSM is most frequently complementary (e.g. Fig 3.2B, compare with Aulehla et al Fig 3.2G and Dale et al., 2003; by convention, *Lfng* phases are written in Roman numerals; *Axin2* and *Dact1* phases in Arabic numerals.) These results are entirely consistent with a prior study demonstrating that *Lfng* and *Axin2* have reciprocal cycles of expression in the PSM (Aulehla et al., 2003), and show that the cycling of *Dact1* in the caudal PSM coincides with that of *Axin2*.

To confirm this result, we also performed WISH for *Dact1* versus either *Lfng* or *Axin2* on paired (L-R) sagittal hemisections from single E9.5 embryos. This is informative because maturation of both sides of a normal vertebrate embryo is tightly coordinated; the PSM on each side proceeds through the somitogenesis cycle in synchrony with its bilaterally-symmetrical partner (Aulehla et al., 2003; Pourquié, 2003b; Vermot and Pourquié, 2005; Saude et al., 2005). Each embryo was scored for its phase of the somitogenesis cycle based on the *Axin2* or *Lfng* WISH pattern from the PSM on one side, and this was compared to the phase of *Dact1* WISH observed on its other side. Consistent with the Double-WISH data, *Lfng* and *Dact1* expression from left and right halves of the same embryo correspond to different phases (e.g. Fig 3.2C vs. C'). Taken together and with previously reported results, our data indicate that when *Dact1* expression in the caudal PSM peaks (Phase 1), *Lfng* expression in the caudal PSM is lowest (Phase III), and that when *Dact1* expression is regressing in the caudal PSM (Phase 2), *Lfng* expression is increasing and moving rostrally (Phase I) (Dale et al, 2003).

In contrast, although the spatial patterns of *Dact1* and *Axin2* are distinct in many locations including the neural tube (where *Axin2* is far more prominent) and newly formed somites (where *Dact1* is far more prominent), these genes are expressed in overlapping domains in the rostral presomites and in the caudal PSM. Using the hemisection technique, a range of E9.5 embryos spanning the somitogenesis clock show similar patterns of expression for *Dact1* and *Axin2* in their left and right PSM, especially caudally (Fig 3.2D). Taken together and with previously reported results, these data indicate that *Axin2* expression and *Dact1* expression wax and wane together in the caudal PSM throughout the somitogenesis cycle.

Implications for the Clock and Wavefront model of Somitogenesis

We have discovered that *Dact1* expression cycles in the PSM during segmentation stages in the mouse. Furthermore, we have shown that unlike *Nkd1* (Ishikawa et al., 2004), which encodes another cytoplasmic protein that binds to Dvl (Rousset et al., 2001), *Dact1* gene expression in the PSM cycles in phase with *Axin2*, which itself is transcribed downstream of Wnt/ β -catenin signaling (Jho et al., 2002). These results suggest that like *Axin2*, the expression of *Dact1* in PSM cells is positively regulated by cyclical waves of Wnt/ β -catenin signaling. β -catenin-dependent *Axin2* expression in the PSM is regulated via conserved TCF/LEF sites located within its promoter and first intron (Jho et al., 2002), as is the expression of the Notch ligand *Dll1* (Galceran et al., 2004). Similarly, we have identified twelve consensus TCF/LEF binding sites in the 5 kb promoter region and the first intron of the mouse *Dact1* gene, many of which are conserved in the human *DACT1* locus (Fig 3.S1). The presence of these

conserved TCF/LEF binding sites in the *Dact1* and *Axin2* genomic regions, together with the synchronous oscillation of these genes in the PSM, suggests that other Wnt/ β -catenin-responsive genes regulated by TCF/LEF transcription factors may undergo somitogenesis cycling in phase with *Dact1* and *Axin2*.

Observations that the Wnt inhibitor *Axin2* cycles out of phase with Notch signaling molecules in the PSM, combined with prior evidence that the Wnt signal transducer Dvl can inhibit Notch signaling in some contexts (Axelrod et al., 1996), has led to a model for the somitogenesis clock involving molecular feedback between these two signaling pathways in PSM cells (Aulehla et al., 2003; Pourquié, 2003a; Aulehla and Herrmann, 2004). This model proposes that when Wnt signaling is high in PSM cells, one activity of the Dvl protein is to repress simultaneous Notch signaling.

Transcriptional activation of *Axin2* downstream of Wnt/ β -catenin signaling leads to increases in *Axin2* protein levels. As its levels rise, *Axin2* inhibits ongoing Wnt signal transduction, and consequently Dvl ceases to repress Notch signaling. With Notch signaling ascendant, lack of Wnt/ β -catenin signal transduction reduces *Axin2* transcription. Once the previously synthesized *Axin2* protein degrades, Wnt signal transduction resumes, to complete the cycle (Figure 3.2E).

In the context of this molecular model, we propose that *Dact1*, which has been characterized as a Wnt/ β -catenin antagonist (Cheyette et al., 2002; Wong et al., 2003; Kakinuma et al., 2004; Brott and Sokol, 2005a; Zhang et al., 2006) may cooperate with *Axin2* in this delayed feedback loop as both a target and an inhibitor of Wnt/ β -catenin signaling (Fig 3.2E). Such functional redundancy between the *Dact1* and *Axin2* proteins

in the PSM could explain why mutations in *Axin2* alone do not cause defects in somitogenesis (Yu et al., 2005).

However, insertion of *Dact1* alongside *Axin2* as part of the clock and wavefront model of somitogenesis is qualified because the function of Dact proteins in Wnt/ β -catenin signal regulation is not securely established: some studies have indicated that Dact proteins act positively in Wnt/ β -catenin signaling (Gloy et al., 2002; Hikasa and Sokol, 2004; Waxman et al., 2004). Moreover, Dact proteins also regulate non- β -catenin-dependent forms of Wnt signaling (Cheyette et al., 2002; Waxman et al., 2004), which may contribute to morphogenetic movements necessary for PSM cell migration and to the mesenchymal-epithelial transition in the s0 presomite as it becomes the new s1 somite (Fig 3.2F) (Duband et al., 1987; Nakaya et al., 2004). Given the context-dependent signaling roles reported for Dact proteins (Hikasa and Sokol, 2004; Waxman et al., 2004; Brott and Sokol, 2005b), a plausible model is that the *Dact1* protein coordinates β -catenin-dependent and non- β -catenin-dependent signaling important for different aspects of PSM cell maturation and somitogenesis (Figure 3.2E, F). *Dact1* is also expressed at earlier and later stages of mesoderm development (Hunter et al., 2005; Fisher et al., 2006) where both types of signaling and extensive morphogenesis occur (Yoshikawa et al., 1997; Yamaguchi et al., 1999; Chen et al., 2005; Dale et al., 2006; Schmidt et al., 2006; Satoh et al., 2006). Further elucidation of the role of *Dact1* in these crucial embryonic processes will be aided by phenotypic analysis and signaling assays in targeted mutant mouse lines.

Methods

Probes for Whole mount mRNA in situ Hybridization (WISH)

Riboprobes were labeled by incorporation of digoxigenin-labeled UTP (DIG RNA Labeling Mix, Roche Applied Science, Indianapolis IN). Sense controls (for *Dact1*) were the same as previously reported (Fisher et al., 2006). Multiple antisense probes were used to validate expression of *Dact1*, and phasic patterns of expression in the PSM were observed with all of them:

gene	probe	nt (numbered from translation start)
<i>Dact1</i>	“A”	316-692 (Fisher et al., 2006)
<i>Dact1</i>	“B”	1250-1473 (not previously reported)
<i>Dact1</i>	“C”	1250-1601 (Fisher et al., 2006)
<i>Axin2</i>	-	1-2397 (Jho et al., 2002)
<i>Lfng</i>	-	273-1030 (Cohen et al., 1997)

WISH Tissue Preparation and Hybridization

Embryos were fixed by immersion in 4% paraformaldehyde in PBS, then dehydrated in sequential concentrations of ethanol and stored in 100% ethanol at -20°C. Prior to experimental use, tissue was rehydrated sequentially from ethanol into PBS containing 0.1% Tween-20. Embryos were treated with 3% H₂O₂ in PBT for 1 hour, then washed sequentially in: 3 X 5 min PBT, 5 min 10µg/ml proteinase K in PBT, 5 min 2mg/ml glycine in PBT, 2 X 5 min PBT, 20 min 4% paraformaldehyde + 0.2% glutaraldehyde in PBT, 3 X 5 min PBT. Tissue was prehybridized for 2 hrs in hybridization solution at 70°C, followed by hybridization overnight in fresh hybridization solution containing 0.5 µg/ml digoxigenin labeled RNA probe. Hybridization solution was 50% formamide, 5X SSC pH4.5, 1% SDS, 50µg/ml yeast tRNA, 50µg/ml heparin. Stringency washes were used to remove unbound probe. These consisted of 2 X 30 min in 50% formamide, 4X

SSC, 1% SDS at 70°C, followed by 2 X 30 min in 50% formamide, 2X SSC, 1% SDS at 70°C.

Antibody labeling and Colorimetric Development (Single-WISH)

Following hybridization, tissue was washed with MABT (0.1M maleic acid buffer pH 7.5 with 0.1% Tween-20) for 2 X 10 min at room temperature. Tissue was labeled with alkaline phosphatase (AP) conjugated 1:4000 anti-digoxigenin (Roche Applied Science) overnight at 4°C. Blocking for 2 hours and immunolabeling were performed in 10% heat inactivated sheep serum, 2% BM blocking reagent (Roche Applied Science), in MABT. Following antibody incubation, tissues were washed 5 X 30 min with MABT at room temperature.

For development reactions, tissue was washed 3 X 10 min in NTMT (0.1 M Tris pH 9.5, 0.1 M NaCl, 0.05 M MgCl₂, 0.1% Tween-20), and incubated in the dark in NBT/BCIP (Bio-Rad) in NTMT. Incubation times were variable depending on when clear development was visible, but usually 4-6 hrs at room temperature (RT).

Hemisection WISH

For hemisection experiments, embryos were collected and fixed as for single WISH. Following rehydration individual embryos were bisected sagittally in PBS using etched tungsten micro-needles (Fine Science Tools Inc, North Vancouver, Canada). The halves of each embryo were moved to histology baskets (15mm Netwell Insert, Corning Co., Corning NY) and were fixed overnight in 4% paraformaldehyde, then washed 3 X 10 min PBS. Baskets were kept in adjacent wells and treated as a pair for all subsequent

hybridization, incubation, and development steps. Antibody labeling and colorimetric development were as described for single-WISH and double-WISH.

Double-WISH

Dact1/Axin2: Initial stages of double-WISH were identical to single-WISH until the hybridization step. For double-WISH hybridization, embryos were incubated in hybridization solution (as in single WISH) containing two probes: digoxigenin-labeled *Dact1* and fluorescein-labeled *Axin2*. Fluorescein labeling of RNA used the same procedure as digoxigenin labeling, but with fluorescein RNA labeling mix (Roche Applied Science) instead of digoxigenin labeling mix. Following hybridization, embryos underwent stringency washes, blocking, and immunolabeling with anti-digoxigenin Fab fragments (Roche Applied Science) at 1:4000 dilution (as in single WISH). After 5 x 30 min washes in MABT, double labeled embryos were incubated for development in 0.1M Tris pH8.2, 0.1% Tween-20 for 3 x 10 min, followed by incubation in the same buffer containing 6 µl/ml each of Vector Blue reagents 1, 2 and 3 (Vector Laboratories, Burlingame CA) to detect *Dact1* signal. *Dact1* signal incubation proceeded for approximately 4 hrs in the dark at RT. Once a desired intensity of color development was achieved, embryos were post-fixed for 1 hr at RT in 4% paraformaldehyde in PBS. Following post-fixing, residual AP was inactivated by incubation for 1 hr at 65°C in PBS, followed by 15 min in 0.1M glycine pH2.2, 0.1% Tween-20 at RT. Following AP inactivation, blocking and immunostaining steps were repeated using 1:4000 AP-conjugated anti-fluorescein Fab (Roche Applied Science). MABT washes and development proceeded as previously, but using Vector Red reagents 1, 2 and 3 at 6µl/ml

(Vector Laboratories) for detection of fluorescein-labeled *Axin2*. Development times was approximately 5 hrs at RT for *Axin2*. Embryos were post-fixed for 1 hr at RT in 4% paraformaldehyde in PBS prior to photography.

Dact1/Lfng: Double-WISH was identical to *Dact1/Axin2* except for the following changes and substitutions. *Lfng* probe was digoxigenin-labeled and *Dact1* probe was fluorescein-labeled. *Lfng* signal was developed first, by washing 3 X 10 min in NTMT and then incubation in the dark in 75ul INT/BCIP (Roche Applied Sciences)/10 ml NTMT. First post-fixing, AP inactivation, *Dact1* signal development, and second post-fixing were as described above.

Imaging

Samples were photographed at 5.6x magnification on an Olympus SZX7 microscope equipped with an Olympus DP70 digital camera.

References

Aulehla, A. and Herrmann, B.G. (2004). Segmentation in vertebrates: clock and gradient finally joined. *Genes Dev.* *18*, 2060-2067.

Aulehla, A. and Johnson, R.L. (1999). Dynamic expression of lunatic fringe suggests a link between notch signaling and an autonomous cellular oscillator driving somite segmentation. *Dev. Biol.* *207*, 49-61.

Aulehla, A., Wehrle, C., Brand-Saberi, B., Kemler, R., Gossler, A., Kanzler, B., and Herrmann, B.G. (2003). Wnt3a plays a major role in the segmentation clock controlling somitogenesis. *Dev. Cell* *4*, 395-406.

Axelrod, J.D., Matsuno, K., Artavaris-Tsakonas, S., and Perrimon, N. (1996). Interaction between Wingless and Notch signaling pathways mediated by dishevelled. *Science* *271*, 1826-1832.

Bessho, Y., Sakata, R., Komatsu, S., Shiota, K., Yamada, S., and Kageyama, R. (2001). Dynamic expression and essential functions of Hes7 in somite segmentation. *Genes Dev.* *15*, 2642-2647.

Brott, B.K. and Sokol, S.Y. (2005a). A vertebrate homolog of the cell cycle regulator Dbf4 is an inhibitor of Wnt signaling required for heart development. *Dev. Cell* *8*, 703-715.

Brott, B.K. and Sokol, S.Y. (2005b). Frondo proteins: modulators of Wnt signaling in vertebrate development. *Differentiation* *73*, 323-329.

Chen, A.E., Ginty, D.D., and Fan, C.M. (2005). Protein kinase A signalling via CREB controls myogenesis induced by Wnt proteins. *Nature* *433*, 317-22.

Cheyette, B.N.R., Waxman, J.S., Miller, J.R., Takemaru, K., Sheldahl, L.C., Khlebtsova, N., Fox, E.P., Earnest, T., and Moon, R.T. (2002). Dapper, a Dishevelled-associated antagonist of beta-catenin and JNK signaling, is required for notochord formation. *Dev. Cell* *2*, 449-461.

Cohen, B., Bashirullah, A., Dagnino, L., Campbell, C., Fisher, W.W., Leow, C.C., Whiting, E., Ryan, D., Zinyk, D., Boulianne, G., Hui, C.C., Gallie, B., Phillips, R.A., Lipshitz, H.D., and Egan, S.E. (1997). Fringe boundaries coincide with Notch-dependent patterning centres in mammals and alter Notch-dependent development in *Drosophila*. *Nat. Genet.* *16*, 283-288.

Cooke, J. and Zeeman, E.C. (1976). A clock and wavefront model for control of the number of repeated structures during animal morphogenesis. *J. Theor. Biol.* *58*, 455-476.

Dale, J.K., Malapert, P., Chal, J., Vilhais-Neto, G., Maroto, M., Johnson, T., Jayasinghe, S., Trainor, P., Herrmann, B., and Pourquié, O. (2006). Oscillations of the snail genes in

- the presomitic mesoderm coordinate segmental patterning and morphogenesis in vertebrate somitogenesis. *Dev. Cell* *10*, 355-366.
- Dale, J.K., Maroto, M., Dequeant, M.L., Malapert, P., McGrew, M., and Pourquié, O. (2003). Periodic notch inhibition by lunatic fringe underlies the chick segmentation clock. *Nature* *421*, 275-278.
- Duband, J.L., Dufour, S., Hatta, K., Takeichi, M., Edelman, G.M., and Thiery, J.P. (1987). Adhesion molecules during somitogenesis in the avian embryo. *J. Cell Biol.* *104*, 1361-1374.
- Evrard, Y.A., Lun, Y., Aulehla, A., Gan, L., and Johnson, R.L. (1998). lunatic fringe is an essential mediator of somite segmentation and patterning. *Nature* *394*, 377-381.
- Fisher, D.A., Kivimae, S., Hoshino, J., Suriben, R., Martin, P.-M., Baxter, N., and Cheyette, B.N.R. (2006). Three Dact Gene Family Members are Expressed During Embryonic Development and in the Adult Brains of Mice. *Dev. Dyn*, *in press*; *Epub ahead of print*.
- Forsberg, H., Crozet, F., and Brown, N.A. (1998). Waves of mouse Lunatic fringe expression, in four-hour cycles at two-hour intervals, precede somite boundary formation. *Curr. Biol.* *8*, 1027-1030.
- Galceran, J., Sustmann, C., Hsu, S.C., Folberth, S., and Grosschedl, R. (2004). LEF1-mediated regulation of Delta-like1 links Wnt and Notch signaling in somitogenesis. *Genes Dev.* *18*, 2718-2723.
- Giudicelli, F. and Lewis, J. (2004). The vertebrate segmentation clock. *Current Opinion in Genetics & Development* *14*, 407-414.
- Gloy, J., Hikasa, H., and Sokol, S.Y. (2002). Frodo interacts with Dishevelled to transduce Wnt signals. *Nat. Cell Biol.* *4*, 351-357.
- Greco, T.L., Takada, S., Newhouse, M.M., McMahon, T.A., McMahon, A.P., and Camper, S.A. (1996). Analysis of the vestigial tail mutation demonstrates that Wnt-3a gene dosage regulates mouse axial development. *Genes & Development* *10*, 313-324.
- Hamblet, N.S., Lijam, N., Ruiz-Lozano, P., Wang, J., Yang, Y., Luo, Z., Mei, L., Chien, K.R., Sussman, D.J., and Wynshaw-Boris, A. (2002). Dishevelled 2 is essential for cardiac outflow tract development, somite segmentation and neural tube closure. *Development* *129*, 5827-5838.
- Hikasa, H. and Sokol, S.Y. (2004). The involvement of Frodo in TCF-dependent signaling and neural tissue development. *Development* *131*, 4725-4734.
- Hunter, N.L., Hikasa, H., Dymecki, S.M., and Sokol, S.Y. (2005). Vertebrate homologues of Frodo are dynamically expressed during embryonic development in tissues undergoing extensive morphogenetic movements. *Dev. Dyn.* *235*, 279-284.

- Ikeya, M. and Takada, S. (2001). Wnt-3a is required for somite specification along the anteroposterior axis of the mouse embryo and for regulation of cdx-1 expression. *Mechanisms of Development* 103, 27-33.
- Ishikawa, A., Kitajima, S., Takahashi, Y., Kokubo, H., Kanno, J., Inoue, T., and Saga, Y. (2004). Mouse Nkd1, a Wnt antagonist, exhibits oscillatory gene expression in the PSM under the control of Notch signaling. *Mech. Dev.* 121, 1443-1453.
- Iulianella, A., Melton, K.R., and Trainor, P.A. (2003). Somitogenesis: breaking new boundaries. *Neuron* 40, 11-14.
- Jho, E.H., Zhang, T., Domon, C., Joo, C.K., Freund, J.N., and Costantini, F. (2002). Wnt/beta-catenin/Tcf signaling induces the transcription of Axin2, a negative regulator of the signaling pathway. *Molecular and Cellular Biology* 22, 1172-1183.
- Kakinuma, Y., Saito, F., Osawa, S., Miura, M. (2004). A mechanism of impaired mobility of oligodendrocyte progenitor cells by tenascin C through modification of wnt signaling. *FEBS letters* 568, 60-64.
- McGrew, M.J., Dale, J.K., Fraboulet, S., and Pourquié, O. (1998). The lunatic fringe gene is a target of the molecular clock linked to somite segmentation in avian embryos. *Curr. Biol.* 8, 979-982.
- Nakaya, Y., Kuroda, S., Katagiri, Y.T., Kaibuchi, K., and Takahashi, Y. (2004). Mesenchymal-epithelial transition during somitic segmentation is regulated by differential roles of Cdc42 and Rac1. *Dev. Cell* 7, 425-438.
- Pourquié, O. (2003a). The segmentation clock: converting embryonic time into spatial pattern. *Science* 301, 328-330.
- Pourquié, O. (2003b). Vertebrate somitogenesis: a novel paradigm for animal segmentation? *Int J Dev Biol.* 47, 597-603.
- Pourquié, O. and Tam, P.P. (2001). A nomenclature for prospective somites and phases of cyclic gene expression in the presomitic mesoderm. *Dev. Cell* 1, 619-620.
- Roose, J. and Clevers, H. (1999). TCF transcription factors: molecular switches in carcinogenesis. *Biochimica et Biophysica Acta-Reviews on Cancer* 1424, M23-M37.
- Rousset, R., Mack, J.A., Wharton, K.A., Axelrod, J.D., Cadigan, K.M., Fish, M.P., Nusse, R., and Scott, M.P. (2001). Naked cuticle targets dishevelled to antagonize Wnt signal transduction. *Genes Dev.* 15, 658-671.
- Satoh, W., Gotoh, T., Tsunematsu, Y., Aizawa, S., and Shimono, A. (2006). Sfrp1 and Sfrp2 regulate anteroposterior axis elongation and somite segmentation during mouse embryogenesis. *Development* 133, 989-999.

- Saude, L., Lourenco, R., Goncalves, A., and Palmeirim, I. (2005). *terra* is a left-right asymmetry gene required for left-right synchronization of the segmentation clock. *Nat. Cell Biol.* 7, 918-920.
- Schmidt, C., Otto, A., Luke, G., Valasek, P., Otto, W.R., and Patel, K. (2006). Expression and regulation of Nkd-1, an intracellular component of Wnt signalling pathway in the chick embryo. *Anat. Embryol. (Berl)*. *Epub ahead of print*.
- Serth, K., Schuster-Gossler, K., Cordes, R., and Gossler, A. (2003). Transcriptional oscillation of lunatic fringe is essential for somitogenesis. *Genes Dev.* 17, 912-925.
- Takada, S., Stark, K.L., Shea, M.J., Vassileva, G., McMahon, J.A., and McMahon, A.P. (1994). Wnt-3a regulates somite and tailbud formation in the mouse embryo. *Genes Dev* 8, 174-89.
- van de Wetering, M., Cavallo, R., Dooijes, D., van Beest, M., van Es, J., Loureiro, J., Ypma, A., Hursh, D., Jones, T., Bejsovec, A., Peifer, M., Mortin, M., and Clevers, H. (1997). Armadillo coactivates transcription driven by the product of the *Drosophila* segment polarity gene dTCF. *Cell* 88, 789-799.
- Vermot, J. and Pourquié, O. (2005). Retinoic acid coordinates somitogenesis and left-right patterning in vertebrate embryos. *Nature* 435, 215-220.
- Waxman, J.S., Hocking, A.M., Stoick, C.L., and Moon, R.T. (2004). Zebrafish Dapper1 and Dapper2 play distinct roles in Wnt-mediated developmental processes. *Development* 131, 5909-5921.
- Wong, H.C., Bourdelas, A., Krauss, A., Lee, H.J., Shao, Y., Wu, D., Mlodzik, M., Shi, D.L., and Zheng, J. (2003). Direct binding of the PDZ domain of Dishevelled to a conserved internal sequence in the C-terminal region of Frizzled. *Mol. Cell* 12, 1251-1260.
- Yamaguchi, T.P., Bradley, A., McMahon, A.P., and Jones, S. (1999). A Wnt5a pathway underlies outgrowth of multiple structures in the vertebrate embryo. *Development* 126, 1211-1223.
- Yoshikawa, Y., Fujimori, T., McMahon, A.P., Takada, S. (1997). Evidence That Absence of *Wnt-3a* Signaling Promotes Neuralization Instead of Paraxial Mesoderm Development in the Mouse. *Developmental Biology* 183, 234-242.
- Yu, H.M., Jerchow, B., Sheu, T.J., Liu, B., Costantini, F., Puzas, J.E., Birchmeier, W., and Hsu, W. (2005). The role of Axin2 in calvarial morphogenesis and craniosynostosis. *Development* 132, 1995-2005.
- Zhang, L., Gao, X., Wen, J., Ning, Y., and Chen, Y.G. (2006). Dapper 1 antagonizes Wnt signaling by promoting dishevelled degradation. *J. Biol. Chem.* 281, 8607-8612.

Zhang, N.A. and Gridley, T. (1998). Defects in somite formation in lunatic fringe deficient mice. *Nature* 394, 374-377.

Table 3.1 Dact1 Presomitic Mesoderm Expression at E9.5

	Phase 1 pattern	Phase 2 pattern	Phase 3 pattern
number of embryos	20	9	9
approximate ratio	2	1	1

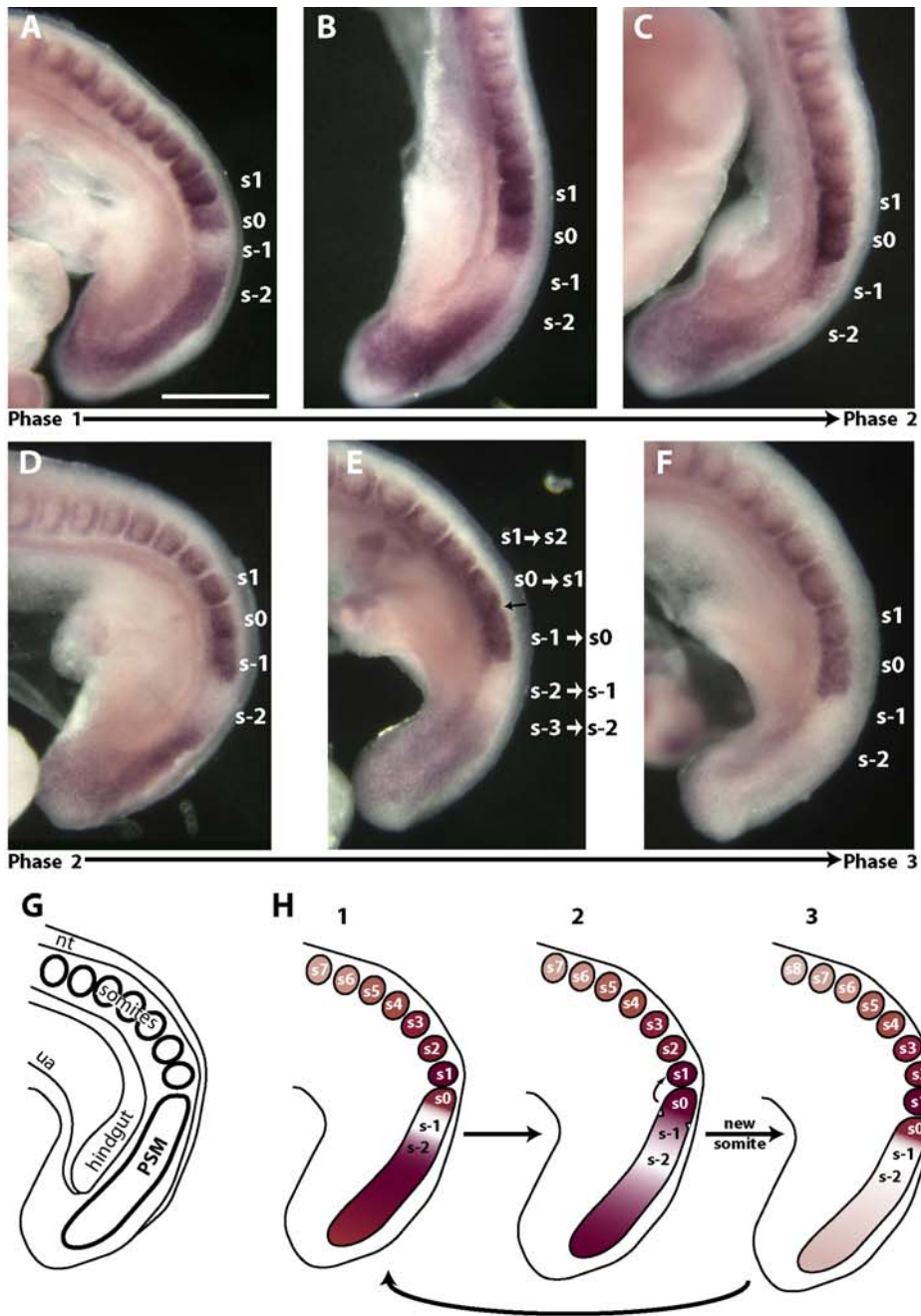


Figure 3.1 Dact1 expression patterns in the PSM at E9.5

A-B. Phase 1: Dact1 is prominent in the presomite s0 as well as caudally in the PSM up to the position of the s-1 presomite, where expression is low. **C-D.** Phase 2: Dact1 begins to be expressed in s-1, and the band of low expression shifts caudally to s-2. **E.** Transition Phase2-Phase 3: As a new somite boundary forms (black arrow) to separate the former s0 from the PSM, the next Dact1 expressing presomite (former s-1) becomes the new s0 presomite. Similarly, the former s-2 presomite becomes the new s-1 presomite, and the former s-3 presomite becomes s-2. **F.** Phase 3: Dact1 expression diminishes throughout the PSM except for in s0. **G.** Diagram of the lateral aspect of the E9.5 tail bud as shown in **A-G**, with orientation of the PSM and somites relative to other visible structures. Abbreviations: (nt) neural tube, (ua) umbilical artery. **H.** Cartoon of proposed PSM cycling of Dact1 expression and its relationship to new somite formation. Scale bar in **A** = 0.5 mm, magnification equivalent for all photomicrographs.

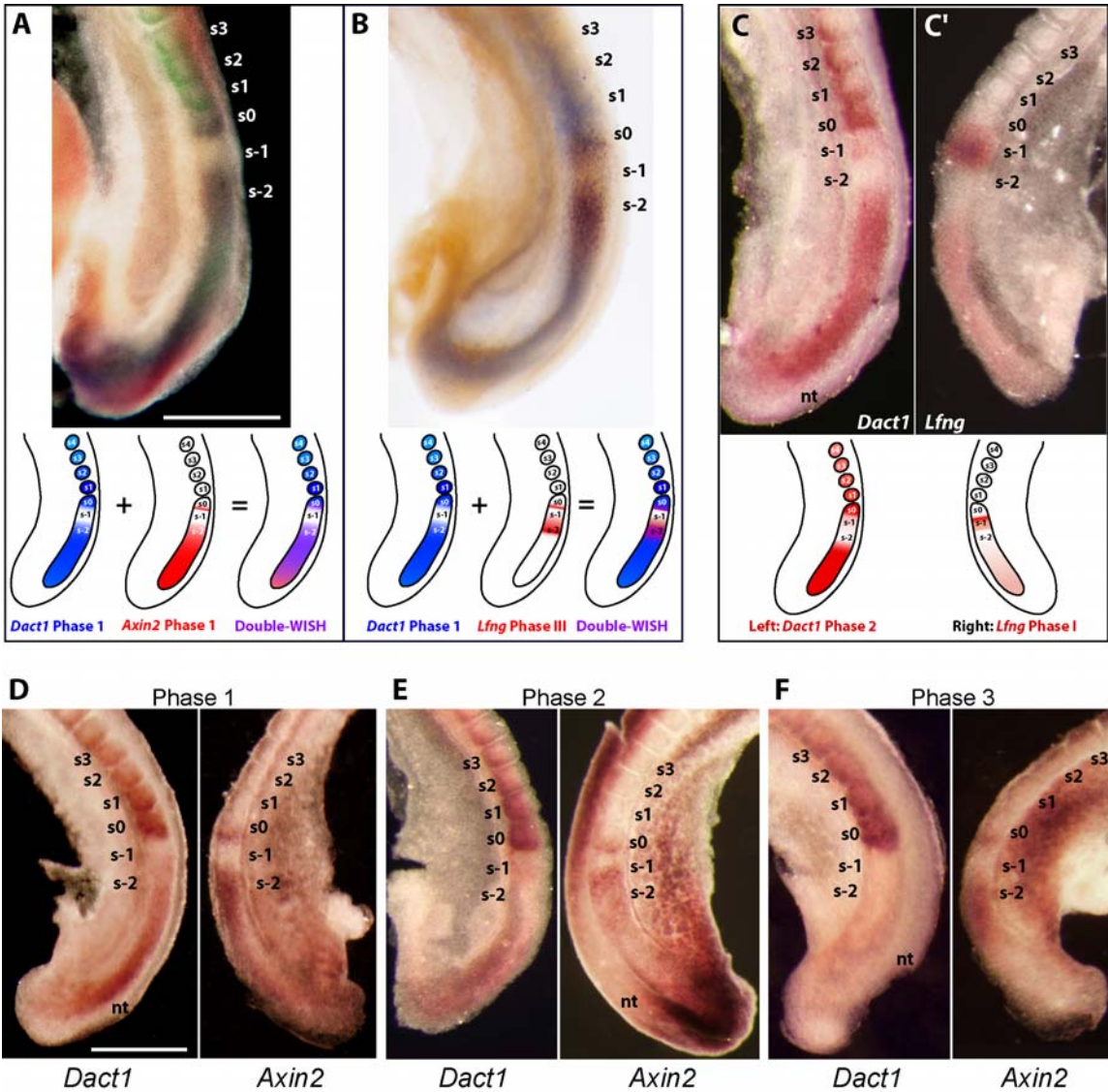


Figure 3.2 Dact1 cycles in phase with Axin2 but out of phase with Lfng

A,B: Double-WISH for *Dact1* and *Axin2* (**A**) or *Lfng* (**B**); top: photomicrograph; bottom: explanatory diagram. **A:** *Dact1* (blue) *Axin2* (red). Expression in the PSM closely coincides except in the rostral part of *s0* (where *Dact1* is exclusively expressed). Both are in a Phase 1 pattern. **B:** *Dact1* (blue) *Lfng* (red). Expression overlaps at the caudal boundaries of the *s0* and *s-1* presomites and in *s-2*. *Dact1* is strongly expressed in the caudal PSM, where *Lfng* is not detected. The *Dact1* pattern corresponds to Phase 1 whereas the *Lfng* pattern corresponds to Phase III. **C,C':** Hemisection WISH comparing *Dact1* to *Lfng* on left-right halves of a single embryo; top: photomicrograph; bottom: explanatory diagram. **C:** *Dact1* (left side). Phase 2, characterized by onset of weak expression in *s-1* and recession of caudal PSM staining such that expression is undetectable at the *s-2* position (see also Fig. 3.1C,H). **C':** *Lfng* (right side). Phase I, characterized by expression in *s-1* plus weak expression caudally in the PSM (Dale et al., 2003). n.b.: For hemisection experiments, only one side (the left side in this case) includes the neural tube (nt) which does not express *Dact1*, but does express *Axin2* (below). **D-F:** Hemisection WISH series comparing *Dact1* to *Axin2* on the left vs. right sides of single embryos. **D:** Phase 1; **E:** Phase 2; **F:** Phase 3. Although *Dact1* and *Axin2* have distinct presomitic distributions in each phase (see text), throughout the somitogenesis clock *Axin2* expression (right) overlaps with *Dact1* (left) caudally in the PSM and in the *s0* presomite. Scale bars 0.5 mm; magnification equivalent in **A-C'**, and in **D-F**

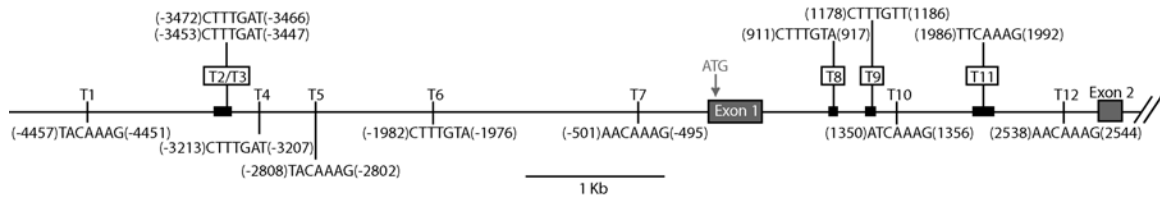


Figure 3.S1 TCF/LEF binding site consensus map of the mouse Dact1 promoter region plus intron 1

In the 5 kb region upstream of the transcriptional start (position 1: 62 bp 5' of ATG), there are 7 elements (T1-T7) matching the TCF/LEF binding site consensus [(A/T)(A/T)CAAAG or reverse complement] (van de Wetering et al., 1997; Roose and Clevers, 1999; Jho et al., 2002). Another 5 sites (T8-T12) are present in intron 1. Five of the sites (T2, T3, T8, T9, and T11; boxed) occur in the same position in the human DACT1 locus where they are 100% identical to the mouse sites. Each of these conserved sites is nested within longer stretches of conserved sequence (filled black boxes = mouse:human sequences >90% identical over >50 bp surrounding a TCF/LEF binding site). Other conserved regions are not shown.

CHAPTER 4

Posterior Malformations in *Dact1* mutant mice arise through misregulated Vangl2 at the Primitive Streak

Rowena Suriben^{1,2*}, Saul Kivimäe^{1*}, Daniel A. Fisher^{1*}, Randall T. Moon⁴,
Benjamin N.R. Cheyette^{1,2,3}

¹Department of Psychiatry, University of California San Francisco, 1550 4th St, San Francisco, CA, 94158, USA

²Graduate Program in Developmental Biology, University of California San Francisco, 1550 4th St, San Francisco, CA, 94158, USA

³Graduate Program in Neuroscience, University of California San Francisco, 1550 4th St, San Francisco, CA, 94158, USA

⁴Howard Hughes Medical Institute, Institute for Stem Cell and Regenerative Medicine, and Department of Pharmacology, University of Washington School of Medicine, Seattle WA, 95195, USA

*These authors contributed equally to this work.

Abstract

Mice homozygous for mutations in *Dact1* (*Dpr/Frodo*) phenocopy human malformations involving the spine, genitourinary system, and distal digestive tract. We trace this phenotype to disrupted germ layer morphogenesis at the primitive streak (PS). Remarkably, heterozygous mutation of *Vangl2*, a transmembrane component of the Planar Cell Polarity (PCP) pathway, rescues recessive *Dact1* phenotypes, whereas loss of *Dact1* reciprocally rescues semidominant *Vangl2* phenotypes. We show that Dact1, an intracellular protein, forms a complex with Vangl2. In *Dact1* mutants, Vangl2 is increased at the PS where cells ordinarily undergo an epithelial-mesenchymal transition. This is associated with abnormal E-cadherin distribution and changes in biochemical measures of the PCP pathway. We conclude that Dact1 contributes to morphogenesis at the PS by regulating Vangl2 upstream of cell adhesion and the PCP pathway.

Introduction

Multiple developmental events occur at or within close proximity to the primitive streak (PS) in the posterior embryo. These include epithelial-mesenchymal transition (EMT) associated with specification of primary germ layers, ventral closure of endoderm to form hindgut, medial-lateral division of mesoderm, posterior elongation of the notochord, segment formation, and dorsal closure of neuroectoderm to form the neural tube. Planar Cell Polarity (PCP) and Wnt/ β -catenin signaling are both involved in these processes (Yoshikawa et al. 1997; Wang et al. 2006; Ybot-Gonzalez et al. 2007; Torban et al. 2008).

Vangl2 (Van Gogh-like/Strabismus) is a four-pass-transmembrane protein that plays a major role in the PCP pathway. By establishing asymmetric localization of both membrane and cytoplasmic components, this pathway regulates cell polarity and movements, particularly convergent-extension (CE) movements that shape germ layer derivatives shortly after gastrulation at the PS (Veeman et al. 2003a). Vangl proteins directly interact with the intracellular protein Dishevelled (Dvl), a central component of both the PCP and Wnt/ β -catenin signaling pathways (Torban et al. 2004). The Wnt/ β -catenin pathway is mechanistically distinct from PCP; it determines cell decisions by regulating transcriptional activity of target genes downstream of post-translational stabilization of the β -catenin protein (Huang and He 2008).

Mice with mutations affecting each of these pathways have phenotypes linked to events in the PS region. For example, mutations in *Wnt3a*, a posterior patterning ligand that activates the Wnt/ β -catenin pathway, cause posterior truncation stemming from defective mesoderm specification (Yoshikawa et al. 1997). Mutations in *Vangl* family members that diminish PCP activity cause neural tube defects traced to defective cell movements in the neuroectoderm (Torban et al. 2008). Despite established roles in both these pathways in other systems, *Dvl* mutations have so far been linked only to PCP phenotypes in mice (Etheridge et al. 2008).

Dact (Dapper/Frodo) proteins bind Dvl and have been shown to modulate several signaling pathways, including Wnt/ β -catenin signaling (Cheyette et al. 2002; Gloy et al. 2002; Zhang et al. 2006; Jiang et al. 2008; Lagathu et al. 2009). By studying an engineered mutation in mouse *Dact1*, we have discovered strong and reciprocal genetic interactions with *Vangl2*. Biochemical and embryonic analyses reveal that this unusual

genetic relationship reflects a role for *Dact1* in post-translational regulation of Vangl2 at the PS, upstream of cell adhesion and PCP signaling.

RESULTS

A spectrum of posterior birth defects in *Dact1* mutant mice

We genetically engineered an allelic series at the mouse *Dact1* locus including two equally severe alleles deduced to be *nulls* on molecular and biochemical grounds (**Fig 4.S1**). One allele (*Dact1^{neoΔ}*) was backcrossed for more than ten generations to the C57BL/6 isogenic mouse strain for use in this study; these homozygotes are hereafter referred to as *Dact1* mutants.

Dact1 mutants are born at near Mendelian ratios (**Table 4.1a**), but with rare exceptions die within a day of birth. These neonates have a short tail, no anus, no urinary outlet, nor external genitalia (**Fig 4.1a-d**). Internally, the vast majority have blind-ended colons (**Fig 4.1e-f**) and no bladder (**Fig 4.1g-h, Table 4.1b**). Ureters are present but connect at the midline or fuse with the reproductive ducts, while the kidneys are invariably hydronephrotic (**Fig 4.1h**). The kidneys also display variable developmental malformations ranging from fusion at the midline to complete agenesis (**Fig 4.1h, Table 4.1c**). Rare mutants (<1%) that survive postnatally nonetheless have non-lethal genitourinary and digestive tract abnormalities evident upon laparotomy (**Fig 4.1i-k**). Gonads of mutants of both sexes are typically present and grossly normal (**Fig 4.1h**).

In addition to genitourinary and gastrointestinal phenotypes, most (~90%) *Dact1* mutants are immediately distinguishable from littermates by virtue of segmental truncation (**Fig 4.1a-b; Table 4.1d**). Skeletal analysis reveals segmental loss that is most

commonly (73%) restricted to the tail (**Fig 4.1l-m; o-p**). A smaller percentage (17%) has truncations extending into sacral and lumbar regions (**Fig 4.1n, q**); these are rarely accompanied by malformations of the pelvis and hindlimbs, including sirenomelia (**Fig 4.1r**). Most severely truncated mutants have spina bifida (13% of total; **Fig 4.1s**). Although there are usually a few smaller malformed vertebrae immediately anterior to the segmental truncation, all other vertebrae and ribs are of normal size, morphology, and identity (**Fig 4.1p-q**). Since segmentation in vertebrates proceeds from anterior to posterior (Tam 1986), the striking lack of anterior segment abnormalities in *Dact1* mutants suggests segmentation failure restricted to late developmental stages, as opposed to a more general disruption of this process (Zhang and Gridley 1998; Ikeya and Takada 2001).

Embryonic defects in *Dact1* mutants

The earliest developmental differences we detect in *Dact1* mutants occur at embryonic day (E) 8.25, shortly after segmentation begins when the embryo has 4-7 newly formed somites (Tam 1986). Unstained wild type and mutant embryos are indistinguishable anteriorly (**Fig 4.2a-b**), and whole mount mRNA in situ hybridization (WISH) using an *Uncx4.1* probe that marks the posterior compartment of each segment (Zhang and Gridley 1998), demonstrates that somites are normal (**Fig 4.2a-b insets**) at this stage. Nonetheless, *Dact1* mutants are misshapen posteriorly in the region of the PS. Viewed dorsally, the wild type embryo has a rounded posterior contour (**Fig 4.2a**) whereas *Dact1* mutants are slightly spade shaped: widening abnormally before tapering to a more pointed tip (**Fig 4.2b asterisk**). As morphological differences in *Dact1* mutants

are confined to the posterior, we quantified them by measuring Length-Width Ratio (LWR) specifically in this region (“Posterior LWR”; **Methods**). Posterior LWR at the 6-7 somite stage is significantly reduced in *Dact1* mutant embryos compared to wild type (1.57 ± 0.05 vs. 1.85 ± 0.04 , $p = 0.0008$) (**Fig 4.2c**). We also detected a significant reduction compared to wild type in the Posterior LWR of *Vangl2*^{Lp/+} embryos (1.67 ± 0.04 vs. 1.85 ± 0.04 , $p = 0.0096$) (**Fig 4.2c**), which are heterozygous for a semidominant allele in *Vangl2* (Montcouquiol et al. 2006). Consistent with a prior report (Wang et al. 2006), using LWR based on the whole embryo (“whole embryo LWR”; **Methods**), we detected no significant differences between wild type (9.42 ± 0.23) and *Vangl2*^{Lp/+} (9.05 ± 0.36 ; $p = 0.4$) at the 6-7 somite stage, nor between wild type and *Dact1* mutants (9.48 ± 0.43 ; $p = 0.9$) (**Fig 4.2d**). Since CE movements in the posterior embryo have been shown to be affected in *Vangl2*^{Lp/+} embryos at this stage (Ybot-Gonzalez et al. 2007), our findings suggest that Posterior LWR reflects cell movements within this embryonic region, and that these are disrupted in *Dact1* mutants.

We next used a panel of WISH markers to assess morphology of individual tissues in this region. Viewed from either the ventral or lateral aspect, WISH for Shh shows that the presumptive notochord domain (Echelard et al. 1993) is broader in *Dact1* mutants and does not extend as far posteriorly beyond the last-formed somite (labeled by *Uncx4.1* WISH) (**Fig 4.2e-h**). There are also differences in morphology of the posterior endoderm, which like the presumptive notochord domain does not extend as far posteriorly and is delayed in folding ventrally to form the hindgut diverticulum (**Fig 4.2g-h**). Presomitic mesoderm labeled with *Dll1* is normal in volume but is redistributed around the shortened axial and ventral structures (**Fig 4.2i-j**). Unlike the shortened axial

mesoderm and endoderm, the ectoderm in *Dact1* mutants extends to the posterior tip of the embryo, even in mutants where ventral defects are severe (**Fig 4.2i-j** arrows).

Consistent with these WISH data, cross section at the PS reveals that all three germ layers are present in the posterior *Dact1* mutant embryo at the 6 somite stage, but there is a notable divergence from wild type morphology. The endoderm is open ventrally and fails to form a tubular hindgut with columnar epithelium (**Fig 4.2k-l**). Ectoderm morphology is variable but is often 1 to 2 cells thicker apical-basally, and is more acutely folded (**Fig 4.2k-l** insets & asterisk). Rates of proliferation and cell death are not significantly different in this region even in mutants with severely affected morphology (**Fig 4.S2**).

To investigate how these early morphological defects progress, we examined the development of germ layer derivatives at later stages. At E9.5, presomitic mesoderm expressing *Dll1* continues to extend fully posteriorly in mutants, as does the overlying ectoderm (**Fig 4.2m-n**). However, axial structures that normally separate left from right presomitic (paraxial) mesoderm terminate more anteriorly, such that this tissue assumes an abnormal Y- instead of a U-shape when viewed dorsally (**Fig 4.2o-p**).

The posterior segments that are frequently missing in *Dact1* mutants are generated only after E9.5 from the presomitic mesoderm (PSM) located in the tail bud (Tam 1986). Concordantly, *Uncx4.1* WISH reveals segmental defects only after E9.5 and only in the most recently formed somites (**Fig 4.2q-r**). Segmentation is governed in part by the somitogenesis cycle, a regular oscillation of gene expression in the PSM, and some mutations that cause segmental loss disrupt this cycle throughout development (Aulehla et al. 2003). We tested whether *Dact1* mutants have disruptions in the somitogenesis

cycle at late stages by examining expression of well-established somitogenesis genes such as *Lfng* (Zhang and Gridley 1998; Aulehla et al. 2003). Expression of *Lfng* and other somitogenesis cycle markers was disrupted in *Dact1* mutants by E10.5 (**Fig 4.2s-t; Table 4.2**). However, these somitogenesis cycle defects never occurred before E10 and never in isolation: mutant tail buds by this stage invariably displayed extensive anatomical disorganization and evidence of histolysis including absence of the tail gut (posterior endoderm), severe shortening of the notochord, and pockets of pooled blood and serous fluid (**Fig 4.2u-x; Table 4.2**).

Taken together, these embryological data suggest that the *Dact1* mutant phenotype arises from a primary defect in germ layer morphogenesis at the PS; segmental truncations in these mutants are associated with failed somitogenesis occurring in the context of tail bud disorganization and deterioration at later stages.

PCP but not Wnt/ β -catenin signaling is affected in *Dact1* mutant embryos

Work in other systems has suggested that *Dact1* primarily modulates Wnt/ β -catenin signaling (Cheyette et al. 2002; Gloy et al. 2002; Zhang et al. 2006; Lagathu et al. 2009). We accordingly asked whether Wnt/ β -catenin pathway defects underlie the earliest observable *Dact1* mutant phenotypes in the posterior embryo. We measured Wnt/ β -catenin target mRNA levels by Quantitative Reverse Transcriptase PCR (QPCR) at the stage when morphological differences are first detected in *Dact1* mutants (5-7 somites). We validated this assay using previously studied signaling mutants (Ikeya and Takada 2001; Ybot-Gonzalez et al. 2007) and the established Wnt/ β -catenin targets, *Dll1* and *Axin2* (Lickert et al. 2005). Levels of both these targets were significantly reduced in

posterior tissues from *Wnt3a null* embryos compared to control littermates (% of average wild type for *Dll1*: 16 ± 2 vs. 100 ± 10 ; $p < 0.0001$, for *Axin2*: 42 ± 7 vs. 100 ± 14 ; $p = 0.004$) (**Fig 4.3a-b**). Moreover, levels of these targets were not significantly different in posterior tissues from heterozygotes for the semidominant PCP signaling mutant *Vangl2^{Lp}* (% of average wild type for *Dll1*: 121 ± 11 vs. 100 ± 9 ; $p = 0.2$, for *Axin2*: 77 ± 11 vs. 100 ± 20 ; $p = 0.3$) (**Fig 4.3c-d**). *Dact1* mutant posterior tissues showed no significant differences in these Wnt/ β -catenin target gene levels compared to controls (% of average wild type for *Dll1*: 95 ± 8 vs. 100 ± 7 ; $p = 0.6$, for *Axin2*: 85 ± 17 vs. 100 ± 15 ; $p = 0.5$) (**Fig 4.3e-f**). Similarly, we measured levels of activated β -catenin protein at E9 by immunoblot with dephospho-specific β -catenin antibody (mAb 8E7)(Staal et al. 2002); there were no significant differences compared to controls (% of average wild type = 81 ± 8 vs. 100 ± 10 ; $p = 0.2$) (**Fig 4.3g-h**). Finally, when assessed by WISH, expression of the posterior Wnt/ β -catenin signaling targets *Dll1* and *Brachyury (T)* were not significantly reduced in *Dact1* mutant embryos (**Fig 4.2i-j, m-p; Fig 4.S3a-b**). We also detected no differences in levels of the p120-catenin (*Ctnnd1*) or *Dvl* proteins (**Fig 4.S3c-d**), previously shown to be regulated by *Dact* family members in other contexts (Park et al. 2006b; Zhang et al. 2006; Lagathu et al. 2009).

Some of the phenotypes observed in *Dact1* mutants, such as neural tube defects, broadening of the presumptive notochord domain, and differences in posterior LWR, resemble those known to result from PCP pathway disruptions (Ybot-Gonzalez et al. 2007; Vandenberg and Sassooson 2009). Among several putative intracellular effectors, PCP signaling is linked to regulation of two kinases: Rho associated kinase (Ybot-Gonzalez et al. 2007) and c-Jun N-terminal Kinase (JNK) (Veeman et al. 2003a). We

tested whether activities of these kinases are altered in the *Dact1* mutant posterior embryo. To assess Rho kinase activity we used immunoblotting with a phospho-specific antibody to measure amounts of its phosphorylated substrate, Mypt1 (Feng et al. 1999). In E8 posterior embryo lysates from *Dact1* mutants, levels of phosphorylated Mypt1 were significantly reduced compared to controls (% of average wild type = 69 ± 9 vs. 100 ± 8 ; $p = 0.03$) (**Fig 4.3i-j**). We measured activated JNK in posterior embryo lysates at E9 through direct phosphorylation of a GST-Jun fusion protein normalized against total JNK recovered in a pull-down assay (Hibi et al. 1993). Endogenous JNK activity was unambiguously increased in *Dact1* mutant posterior embryos at this stage (% of average wild type = 258 ± 19 vs. 99 ± 13 ; $p = 0.0005$) (**Fig 4.3k-l**).

In summary, molecular, biochemical, and embryonic assays at early phenotypic stages do not support changes in Wnt/ β -catenin signaling in *Dact1* mutants; they instead indicate defects in the PCP pathway.

Mutations in *Dact1* and *Vangl2* exhibit reciprocal genetic rescue

In mice, synergy with one copy of *Vangl2*^{Lp} to cause neural tube defects is generally accepted as evidence that a genetic locus participates in the PCP pathway (Wang et al. 2006). Because *Dact1* mutants display a partially penetrant neural tube defect (spina bifida) and also have abnormalities in embryological and biochemical measures associated with PCP signaling, we predicted that mice homozygous for the *Dact1* mutation and heterozygous for *Vangl2*^{Lp} would display severe defects in neural tube closure.

Unexpectedly, mutations in *Dact1* and *Vangl2* mutually rescue each other, such that nearly all *Dact1* mutant mice heterozygous for *Vangl2*^{Lp} appear grossly normal and display neither *Vangl2*^{Lp} semidominant nor *Dact1* recessive phenotypes (**Fig 4.4a-d**). From a cross conducted in a 97% isogenic C57Bl/6 genetic background, approximately 80% (9/11) of *Dact1*^{-/-}; *Vangl2*^{Lp/+} mice had normal genitourinary (GU) systems, normal gastrointestinal (GI) systems, no segmental truncation, and no neural tube defects, compared to *Dact1*^{-/-}; *Vangl2*^{+/+} littermates of which 100% (11/11) had GU phenotypes, 90% (10/11) had GI phenotypes, >50% (6/11) had segmental truncation, and ~20% (2/11) had spina bifida (**Fig 4.4e** red vs. blue; **Table 4.3a**). *Vangl2* mutant-mediated rescue of the *Dact1* mutant phenotype is not due to a molecular peculiarity of the *Vangl2*^{Lp} allele because a very similar pattern of rescue is observed with an independently derived allele (Kibar et al. 2001a), *Vangl2*^{Lp-m1Jus} (**Fig 4.4e** green vs. yellow; **Table 4.3a**). Conversely, whereas more than 80% of animals heterozygous for either *Vangl2*^{Lp} or *Vangl2*^{Lp-m1Jus} (5/6 & 8/10 respectively) display the characteristic semidominant curly tail (*Loop-tail*) phenotype, penetrance of this phenotype drops to <65% (11/17 & 9/22 respectively) when animals are heterozygous, and to ≤20% (1/10 & 3/15 respectively) when homozygous, for the *Dact1* mutant allele (**Fig 4.4f**; **Table 4.3b**). Nevertheless, although *Dact1* loss rescues the semidominant *Loop-tail* phenotype, it does not rescue the recessive craniorachischesis phenotype of homozygous *Vangl2* mutant embryos (**Fig 4.S4**).

To summarize, genetic experiments demonstrate that recessive *Dact1* mutant phenotypes are abrogated by mutation of one *Vangl2* allele, and conversely that semidominant *Vangl2* mutant phenotypes are ameliorated by loss of *Dact1*. Failure to

rescue the homozygous *Vangl2* mutant phenotype demonstrates that a functional allele of *Vangl2* is required for this reciprocal genetic interaction.

Dact1 and Vangl2 are binding partners

One mechanism whereby Dact1 could regulate Vangl2 is through physical interaction. We tested this hypothesis through a series of co-immunoprecipitation (coIP) and pull-down assays, results of which are schematically summarized in **Figure 4.5a-c**.

When co-expressed in human embryonic kidney (HEK 293) cells, the Vangl2 protein coIPs with Dact1 (**Fig 4.5d**). We determined the region of Dact1 responsible for this interaction through a panel of Dact1 deletion constructs. Loss of the C-terminal 88 amino acids (aa) of Dact1 almost completely eliminates association with Vangl2, and the residual interaction is abolished by deletion of an additional 62 aa (**Fig 4.5d**). Under identical conditions, the same panel of Dact1 constructs shows a different coIP pattern with Dvl2: Progressive C-terminal deletions of Dact1 reduce but do not eliminate association with Dvl2 until elimination of aa 311-778 (**Fig 4.5e**). The Dact1 PDZb caps a longer stretch of 28 highly conserved aa (Fisher et al. 2006), and so we made specific deletions to probe how this region compares to the immediately upstream 60 aa in coIPs with Vangl2 versus Dvl2. Deletion of the Dact1 C-terminal 28 aa has no effect on association with Vangl2 (**Fig 4.5f**), but reduces association with Dvl2 at least as much as larger deletions (**Fig 4.5g**). Conversely, internal deletion of the adjacent 60 aa has no effect on Dact1 association with Dvl2 (**Fig 4.5g**), but reduces association with Vangl2 similar to larger deletions (**Fig 4.5f**). Taken together these data strongly suggest that separate domains of Dact1 contribute to complex formation with Vangl2 versus Dvl2.

We similarly used a series of Dvl2 deletion constructs to probe whether different conserved regions of Dvl are responsible for associations with Dact1 versus Vangl2. Consistent with prior reports (Park and Moon 2002; Torban et al. 2004), we found that the Dvl PDZ domain is the main contributor to the Dvl-Vangl2 interaction (**Fig 4.5h**). We also found that a “Dishevelled Specific” (DS) domain (**Methods**) contributes modestly to this interaction (**Fig 4.5h**). In contrast, using the same panel of Dvl2 constructs under identical conditions we found that deletion of the PDZ and DS domains reduces but does not eliminate the Dvl-Dact1 interaction (**Fig 4.5i**). Taken together, these coIP data strongly suggest that besides PDZ-b/PDZ binding (Cheyette et al. 2002), a middle region of Dact1 also contributes to interactions with Dvl2 outside the PDZ domain, consistent with some prior reports (Gloy et al. 2002; Zhang et al. 2006).

These experiments indicate that different domains contribute to associations between Dact1 and Dvl2 versus either of these proteins with Vangl2. In a final assay we asked whether Vangl2 can bind directly to Dact1 in the absence of Dvl proteins. Since Dvl proteins are specific to metazoans, we bacterially expressed and purified recombinant GST fusion proteins corresponding to the amino- and carboxy-terminal regions of Dact1 and asked whether they bind to full-length Vangl2 protein synthesized in a wheat germ extract. The C-terminal half of Dact1 binds specifically to Vangl2 in this Dvl-free system, supporting the conclusion that the Dact1-Vangl2 interaction is direct (**Fig 4.5j**).

Dact1 regulates Vangl2 at the PS

By prior report, *Vangl2* is expressed at low levels in the posterior endoderm and at higher levels in the neuroectoderm, which is contiguous with ectoderm in the PS region

(Le Douarin et al. 1998; Kibar et al. 2001b). Dact1 is expressed in a potentially overlapping domain in the posterior ectoderm and mesoderm (Hunter et al. 2006). This suggests that Dact1 and Vangl2 might functionally interact in these tissues, particularly in the PS ectoderm.

Using WISH we confirmed that the mRNA distributions of Dact1 (**Fig 4.6a-b**) and Vangl2 (**Fig 4.6c-d**) overlap in PS ectoderm. As expected for a transmembrane protein and consistent with prior reports (Kibar et al. 2001b), an affinity-purified antibody detects Vangl2 protein primarily on surfaces of epithelial cells in the PS ectoderm and endoderm, as well as more weakly on scattered surface subdomains of adjacent mesenchymal cells (**Fig 4.6e** inset; arrowheads). The adhesion protein E-cadherin shows a partially overlapping distribution with Vangl2 in all germ layers, but is concentrated at the apical and basal surfaces and is generally less apparent on the lateral membranes of ectoderm cells (**Fig 4.6f-g** inset).

In the PS ectoderm of *Dact1* mutants, Vangl2 cell surface signal is significantly increased (**Fig 4.6h**; **Fig 4.S5 b**; **e**). Moreover, cell surface E-cadherin is also significantly increased and colocalizes with the Vangl2 signal, no longer displaying enrichment on the apical-basal vs. lateral cell surfaces (**Fig 4.6i-j**; **Fig 4.S5 b**; **f**). This is a post-translational effect, as levels of both the Vangl2 and E-cadherin mRNAs are not altered (**Fig 4.S6a-b**). In these mutants, cells with high Vangl2 and E-cadherin form a bulge at the position of the PS where EMT normally occurs (**Fig 4.6j** dotted lines).

Prior reports suggest that the *Vangl2*^{Lp} mutation alters the ability of mutant Vangl2 protein to stably accumulate at the membrane, especially asymmetrically or at points of cell contact (Montcouquiol et al. 2006; Torban et al. 2007; Devenport and Fuchs 2008).

Consistent with this, we find that in *Vangl2*^{Lp/+} embryos, Vangl2 protein remains detectable in cells where the wild type protein is typically expressed, but the membrane signal is significantly reduced compared to wild type (**Fig 4.6k**; **Fig 4.S5 c**; **e**). Interestingly, E-cadherin is also mislocalized in these cells: a diffuse cytoplasmic signal appears that is absent from wild type controls (**Fig 4.6l**). Nevertheless, some apical-basal enrichment of E-cadherin remains evident (**Fig 4.6l** inset), and levels on the lateral edges of PS ectoderm cells are as low as in wild type (**Fig 4.S5 c**; **f**).

The PS ectoderm in *Dact1*^{-/-}; *Vangl2*^{Lp/+} combination mutants has Vangl2 cell surface staining intermediate between the high signal detected in *Dact1* mutants and the low signal detected in *Vangl2*^{Lp/+} embryos, such that levels are not significantly different from wild type controls (**Fig 4.6n** inset; **Fig 4.S5 d**; **e**). In contrast to *Dact1* single mutants, *Dact1*^{-/-}; *Vangl2*^{Lp/+} combination mutants also have normal surface levels and a more normal apical-basal distribution of E-cadherin in PS ectoderm cells (**Fig 4.S5 f**; **Fig 4.6o** inset). Finally, the bulge of cells with high Vangl2 and E-cadherin found at the PS in *Dact1* single mutants is absent from combination mutants (**Fig 4.6p** dotted lines).

To summarize, loss of *Dact1* leads to increased Vangl2 and E-cadherin in the PS ectoderm where cells normally undergo EMT. In *Vangl2*^{Lp} heterozygotes, there is partial loss of membrane Vangl2 signal; this most likely reflects the absence of surface-destabilized mutant protein made from the *Loop-tail* allele (Torban et al. 2007). Compared to *Dact1* mutants, *Dact1*^{-/-}; *Vangl2*^{Lp/+} combination mutant embryos have partially restored cell surface Vangl2 levels, E-cadherin distribution, and PS morphology.

DISCUSSION

The phenotypic spectrum in *Dact1* mutant mice is reminiscent of a similar spectrum of posterior malformations in humans (Pauli 1994). Etiologies previously proposed to explain all or part of this spectrum include vascular-steal (Stevenson et al. 1986), persistence of the embryonic cloaca (Manzoni et al. 1987), and defects in posterior mesoderm formation (Duesterhoeft et al. 2007). Our findings suggest that this malformation spectrum may first originate in disturbed morphogenetic movements at the PS in the early embryo.

Several morphogenetic processes take place in close spatial and temporal proximity in the posterior embryo, each of which is likely to require dynamic regulation and polarized activities of Vangl2, the PCP pathway, and adhesive proteins. The first of these to occur is EMT at the PS, where both *Dact1* and Vangl2 are expressed but where neither protein has a prior established role. Our data suggest that defective EMT is the primary defect in *Dact1* mutants. Perhaps all other disrupted morphogenesis in these mutants occurs secondarily, for example because of decreased generation of mesoderm and endoderm precursors via EMT. Nonetheless we cannot rule out additional requirements for *Dact1* alongside Vangl2 in spatially and temporally adjacent morphogenetic events, including CE movements that elongate and narrow axial mesoderm, mesenchymal-epithelial transition of endoderm precursors, or polarity and cell movements that fold and extend the hindgut.

Wnt/ β -catenin signaling and E-cadherin negatively regulate each other at the PS, such that high E-cadherin reduces Wnt/ β -catenin signal transduction in cells undergoing EMT (Ciruna and Rossant 2001), and Wnt/ β -catenin signaling reciprocally negatively regulates

E-cadherin transcription (Nelson and Nusse 2004). We have observed no statistically significant alterations in Wnt/ β -catenin signaling or in levels of E-cadherin mRNA in early *Dact1* mutant embryos. Instead the E-cadherin protein is abnormally redistributed at early stages, whereas Wnt/ β -catenin signaling reductions occur only much later in morphologically disrupted tail buds where they might contribute to somitogenesis failure specific to late-forming posterior segments (**Fig 4.S6 c-h**) (Suriben et al. 2006). In any case, the rescue of all embryonic *Dact1* mutant phenotypes by concurrent mutation of *Vangl2* powerfully demonstrates that any E-cadherin or Wnt/ β -catenin effects contributing to these phenotypes must occur downstream of *Vangl2*-dependent events.

We have discovered that a developmentally crucial function of *Dact1* is regulation of *Vangl2* at the PS. Morphogenetic abnormalities in the PS region of *Dact1* mutant embryos, while partly resembling those caused by PCP pathway reduction (Ybot-Gonzalez et al. 2007), are unique in that they are associated with decreased phosphorylation of the myosin binding subunit of myosin phosphatase (*Mypt1*), but increased JNK activity. This agrees with evidence that modulations in Rho- and Jun-kinase activities reflect separate pathways downstream of PCP (Ybot-Gonzalez et al. 2007), and that either abnormal gain or loss of upstream PCP components can cause similar disruptions in cell polarity, cytoskeletal dynamics, and CE movements (Yan et al. 2001; Takeuchi et al. 2003; Veeman et al. 2003b; Park et al. 2006a). Interestingly, other PCP phenotypes, such as inner ear and cardiac malformations (Montcouquiol et al. 2006; Phillips et al. 2007), are not evident in *Dact1* mutants (M. Montcouquiol, D.A.F., B.N.R.C., data not shown).

We propose that complex formation between the Dact1 and Vangl2 proteins is a crucial step in a novel Vangl2 regulatory pathway operating during EMT at the PS. Candidate cellular processes that might be involved include trafficking of Vangl2 to the membrane, endocytosis, subcellular sequestration, or degradation. This will be clarified by identifying additional components of this pathway through further biochemical, cellular, embryonic, and genetic experimentation.

METHODS

Targeting Construct

Approximately 7 kb of *Dact1* genomic DNA from the 129/Sv mouse strain was inserted into pGKneoF2L2DTA2 (Hoch and Soriano 2006) to create the *Dact1* targeting vector (**Fig 4.S1**). Correct targeting through homologous recombination in ES cells was confirmed by Southern blot and PCR. Mice carrying the targeted allele were created using standard embryo manipulation and chimera breeding techniques. An allelic series at the *Dact1* locus was created by crossing to the *EIIa::Cre* (The Jackson Laboratory, Bar Harbor, ME) and FLPe transgenic mouse strains in order to excise loxP-flanked and FRT-flanked sequences respectively. Genotyping was performed by genomic PCR using allele-specific primers: The primers Dact1intron1 and Dact1intron2 (See **Table 4.S4** for this and all other primer sequences) are separated by 689 bases of genomic sequence in wild type, but only 190 bases in the excised (mutant) allele; amplifying a mutant-specific PCR product of 243 bases. The primers Dact1exon2 (near start exon 2) and Dact1intron2 (near the start of intron 2) are both within the floxed region; amplifying a wild type-specific PCR product of 330 bases. Amplification parameters for wild type: 30

cycles X (95°C 30 seconds, 52°C 30 seconds, 72°C 30 seconds); for mutant: 38 cycles X (95°C 30 seconds, 57°C 30 seconds, 72°C 30 seconds).

Antibody generation

The Dact1 antibody was created by injecting rabbits with a peptide corresponding to aa 373-386 (coded within exon 4), followed by affinity purification. It is available from AbD Serotec.

General Microscopy and Imaging

As described (Fisher et al. 2006; Suriben et al. 2006).

Skeleton Preparation

As described (Zhang and Gridley 1998).

Whole Mount mRNA in situ Hybridization

As described (Suriben et al. 2006) using LacZ probe to nucleotides 576-939 and previously established probes (Echelard et al. 1993; Zhang and Gridley 1998; Kibar et al. 2001b; Fisher et al. 2006).

LWR measurements

Whole Embryo Length to Width Ratio (LWR): Whole embryo length (L) was the average distance along a straight line to the posterior tip of the embryo from the anterior tips of the right and left head folds. Whole embryo width (W) was the distance between

the lateral edges of the left and right somites positioned in the middle of the anterior-posterior axis ($L/2$). LWR was calculated as L/W .

Posterior Length to Width Ratio (LWR): Posterior length (L) was the average distance along a straight line to the posterior tip of the embryo from the posterior edges of the most posterior (last formed) left and right somites. Posterior embryo width (W) was the widest lateral distance across the embryo (perpendicular to L) in the region corresponding to L (posterior to the last formed somite). LWR was calculated as L/W .

Proliferation and Apoptosis measurements

To measure proliferation and apoptosis, embryos were sectioned and stained for phalloidin, Hoescht 33258, and phospho-histone-H3 (Millipore) or active caspase-3 (BD Biosciences), respectively. Staining was visualized on a Nikon C1si Spectral Confocal microscope. A single confocal plane from each 20 μ m section was used to avoid double counting of cells. Graphs show the average percent proliferative or apoptotic cells across all sections ($n = 2$ embryos for each genotype, 5 sections per embryo) from the same genotype. There were no significant differences between mutants and controls for all these measures.

Quantitative RT-PCR

As described (Fisher et al. 2006) with the following modifications: Samples were embryonic tissues posterior to the last-formed somite. 0.5-1 μ g of total RNA was used for

cDNA synthesis. Primers: QAxin2F, QAxin2R, QD111F, QD111R, QVangl2F, QVangl2R, QLacZF, QLacZR and for E-cadherin as described (Hyenne et al. 2005).

JNK assay

Embryonic tissues posterior to the last-formed somite were homogenized in 100ul buffer and assayed as described (Hibi et al. 1993).

Western blots, CoIPs, GST pull-downs, expression and deletion constructs

Association assays were performed essentially as described (Angers et al. 2006). GST pull downs were in PBS + 0.1% Triton-X-100 (Roche), 0.1% insulin. Binding was at 4°C for 30 minutes, followed by 3 X 5 minute washes in binding buffer at 4°C. ³⁵S-labelled in vitro translated proteins were synthesized in the TNT coupled wheat germ extract system (Promega). cDNAs were obtained commercially or by RT-PCR from wild type mouse total RNA. Expression and deletion plasmids were constructed using standard restriction digest and/or PCR techniques, and confirmed by sequencing. For Dvl2 the DS (pfam02377; aa 160-232), PDZ (cd00992; aa 265-352) and combined deletions are precise inverse PCR-mediated deletions of these domains as defined on the NCBI Uniprot website. The b (basic) domain is a conserved Arginine/Lysine-rich stretch located just upstream of the PDZ (Klingensmith et al. 1996), corresponds to aa 231-249 of mouse Dvl2, and is therefore distinct from the DS domain. Commercial antibodies (sources): Activated β -Catenin “ABC” (Millipore) (Staal et al. 2002), Vangl2, Dvl1, Dvl3, HA, FLAG (Santa Cruz Biotech), Dvl2 (Cell Signaling Technology), p120catenin

(BD Biosciences), α -tubulin (Sigma-Aldrich), Phospho-Mypt (T696) (Millipore), Total Mypt1 (BD Biosciences).

Genotyping of Vangl2 and Wnt3a alleles

Vangl2^{Lp}: Genotyping for crosses was performed by *Crp* microsatellite PCR (Copp et al. 1994). Genotypes of all combination mutant (experimental) and control littermates was verified by genomic PCR amplification and sequencing of alleles. Primers for PCR: Vangl2LpF and Vangl2LpR; for sequencing: Vangl2Lpseq.

Vangl2^{Lp-m1Jus}: Genotyping was performed by allele-specific PCR using primers homologous to the wild type versus the point mutant allele (**Fig 4.S7**). We used the primer pair Lp-m1JusWTF and Lp-m1JusWTR to amplify a 402 base pair wild type allele product using the following parameters: 30 cycles X (95°C 30 seconds, 68°C 30 seconds, 72°C 1 minute). We used the primer pair Lp-m1JusWT F and Lpm1JusMutR to amplify a 402 base pair mutant allele product using the following parameters: 30 cycles X (95°C 30 seconds, 62°C 30seconds, 72°C 1 minute).

Wnt3a⁻ (*Wnt3a^{neo}*): Genotyping was performed by genomic PCR with allele-specific primers. Primers and parameters for the wild type allele were as recommended by the supplier (The Jackson Laboratory). We used primer pair Wnt3ane0 and Wnt3aintron2 to amplify a *Wnt3a^{neo}*-specific 386 base pair product using parameters: 35 cycles X (95°C 30 seconds, 65°C 30 seconds, 72°C 1 minute).

IHC (Vangl2, E-cadherin)

Embryos were dissected in PBS, fixed in 4% paraformaldehyde for 1 hour at room temperature (RT), and washed in PBS. For embedding, embryos were incubated in 30% glucose in PBS at 4°C overnight, equilibrated with equal parts 30% glucose and O.C.T. compound (Tissue-Tek) for 2 hours on ice, then embedded in 30% glucose and O.C.T. compound. Embryos were cryosectioned (20µm) at -16°C. Sections were dried at RT, washed 2x in PBS for 5 minutes, blocked for 1.5 hour at RT using 10% heat inactivated goat serum, 1% BSA in PBS, then incubated in primary antibody overnight at 4°C. Rabbit Vangl2 antibody (Montcouquiol et al. 2006) and Mouse E-cadherin antibody (BD Biosciences) were diluted 1:500 in 1% heat inactivated goat serum, 1% BSA in PBS. Sections were washed 5x 10 min in PBS, blocked, and incubated in anti-rabbit alexa fluor 488 and anti-mouse alexa fluor 568 (Molecular Probes) diluted 1:250 overnight at 4°C. Sections were washed 5x10 min in PBS, mounted in Mowiol and imaged via confocal microscopy under identical non-saturating illumination conditions.

IHC Quantitation

Signal intensity (grey scale) was measured using *ImageJ* software (NIH), across a straight line drawn parallel to the apical surface of the PS ectoderm and bisecting 5 adjacent cells. Pixel intensity was normalized to the lowest value along the entire line, which was set to 0 (background). For comparisons of cell surface intensity between cells, the 3 highest adjacent values corresponding to the two lateral cell surfaces (6 values total/cell) were averaged and plotted.

Statistical Analyses

All quantitative data were analyzed using Prism software (Graphpad). Significance was determined by parametric unpaired two-tailed t tests. In all cluster graphs, mean values are plotted as a horizontal line; numerical values for the mean, standard error, and p-value are reported in the corresponding **Results** text.

References

- Angers, S., Thorpe, C.J., Biechele, T.L., Goldenberg, S.J., Zheng, N., MacCoss, M.J., and Moon, R.T. 2006. The KLHL12-Cullin-3 ubiquitin ligase negatively regulates the Wnt-beta-catenin pathway by targeting Dishevelled for degradation. *Nat Cell Biol* **8**(4): 348-357.
- Aulehla, A., Wehrle, C., Brand-Saberi, B., Kemler, R., Gossler, A., Kanzler, B., and Herrmann, B.G. 2003. Wnt3a plays a major role in the segmentation clock controlling somitogenesis. *Dev Cell* **4**(3): 395-406.
- Cheyette, B.N.R., Waxman, J.S., Miller, J.R., Takemaru, K., Sheldahl, L.C., Khlebtsova, N., Fox, E.P., Earnest, T., and Moon, R.T. 2002. Dapper, a Dishevelled-associated antagonist of beta-catenin and JNK signaling, is required for notochord formation. *DevCell* **2**(4): 449-461.
- Ciruna, B. and Rossant, J. 2001. FGF signaling regulates mesoderm cell fate specification and morphogenetic movement at the primitive streak. *Dev Cell* **1**(1): 37-49.
- Copp, A.J., Checiu, I., and Henson, J.N. 1994. Developmental basis of severe neural tube defects in the loop-tail (Lp) mutant mouse: use of microsatellite DNA markers to identify embryonic genotype. *Dev Biol* **165**(1): 20-29.
- Devenport, D. and Fuchs, E. 2008. Planar polarization in embryonic epidermis orchestrates global asymmetric morphogenesis of hair follicles. *Nat Cell Biol* **10**(11): 1257-1268.
- Duesterhoeft, S.M., Ernst, L.M., Siebert, J.R., and Kapur, R.P. 2007. Five cases of caudal regression with an aberrant abdominal umbilical artery: Further support for a caudal regression-sirenomelia spectrum. *Am J Med Genet A* **143**(24): 3175-3184.
- Echelard, Y., Epstein, D.J., St Jacques, B., Shen, L., Mohler, J., McMahon, J.A., and McMahon, A.P. 1993. Sonic hedgehog, a member of a family of putative signaling molecules, is implicated in the regulation of CNS polarity. *Cell* **75**(7): 1417-1430.
- Etheridge, S.L., Ray, S., Li, S., Hamblet, N.S., Lijam, N., Tsang, M., Greer, J., Kardos, N., Wang, J., Sussman, D.J. et al. 2008. Murine dishevelled 3 functions in redundant pathways with dishevelled 1 and 2 in normal cardiac outflow tract, cochlea, and neural tube development. *PLoS Genet* **4**(11): e1000259.
- Feng, J., Ito, M., Ichikawa, K., Isaka, N., Nishikawa, M., Hartshorne, D.J., and Nakano, T. 1999. Inhibitory phosphorylation site for Rho-associated kinase on smooth muscle myosin phosphatase. *J Biol Chem* **274**(52): 37385-37390.
- Fisher, D.A., Kivimae, S., Hoshino, J., Suriben, R., Martin, P.M., Baxter, N., and Cheyette, B.N.R. 2006. Three Dact Gene Family Members are Expressed During Embryonic Development and in the Adult Brains of Mice. *DevDyn* **235**: 2620-2630.
- Gloy, J., Hikasa, H., and Sokol, S.Y. 2002. Frodo interacts with Dishevelled to transduce Wnt signals. *Nat Cell Biol* **4**(5): 351-357.
- Hibi, M., Lin, A., Smeal, T., Minden, A., and Karin, M. 1993. Identification of an oncoprotein- and UV-responsive protein kinase that binds and potentiates the c-Jun activation domain. *Genes Dev* **7**(11): 2135-2148.
- Hoch, R.V. and Soriano, P. 2006. Context-specific requirements for Fgfr1 signaling through Frs2 and Frs3 during mouse development. *Development* **133**(4): 663-673.

- Huang, H. and He, X. 2008. Wnt/beta-catenin signaling: new (and old) players and new insights. *Curr Opin Cell Biol*.
- Hunter, N., Hikasa, H., Dymecki, S., and Sokol, S. 2006. Vertebrate homologues of Frodo are dynamically expressed during embryonic development in tissues undergoing extensive morphogenetic movements. *Dev Dyn* **235**(1): 279-284.
- Hyenne, V., Louvet-Vallee, S., El-Amraoui, A., Petit, C., Maro, B., and Simmler, M.C. 2005. Vezatin, a protein associated to adherens junctions, is required for mouse blastocyst morphogenesis. *Dev Biol* **287**(1): 180-191.
- Ikeya, M. and Takada, S. 2001. Wnt-3a is required for somite specification along the anteroposterior axis of the mouse embryo and for regulation of cdx-1 expression. *Mech Dev* **103**(1-2): 27-33.
- Jiang, X., Tan, J., Li, J., Kivimae, S., Yang, X., Zhuang, L., Lee, P.L., Chan, M.T., Stanton, L.W., Liu, E.T. et al. 2008. DACT3 is an epigenetic regulator of Wnt/beta-catenin signaling in colorectal cancer and is a therapeutic target of histone modifications. *Cancer Cell* **13**(6): 529-541.
- Kibar, Z., Underhill, D.A., Canonne-Hergaux, F., Gauthier, S., Justice, M.J., and Gros, P. 2001a. Identification of a new chemically induced allele (Lp(m1Jus)) at the loop-tail locus: morphology, histology, and genetic mapping. *Genomics* **72**(3): 331-337.
- Kibar, Z., Vogan, K.J., Groulx, N., Justice, M.J., Underhill, D.A., and Gros, P. 2001b. Ltap, a mammalian homolog of Drosophila Strabismus/Van Gogh, is altered in the mouse neural tube mutant Loop-tail. *Nat Genet* **28**(3): 251-255.
- Klingensmith, J., Yang, Y., Axelrod, J.D., Beier, D.R., Perrimon, N., and Sussman, D.J. 1996. Conservation of dishevelled structure and function between flies and mice: isolation and characterization of Dvl2. *Mechanisms of Development* **58**(1996): 15-26.
- Lagathu, C., Christodoulides, C., Virtue, S., Cawthorn, W.P., Franzin, C., Kimber, W.A., Dalla Nora, E., Campbell, M., Medina-Gomez, G., Cheyette, B.N. et al. 2009. Dact1, a nutritionally regulated preadipocyte gene controls adipogenesis by coordinating the Wnt/{beta}-catenin signalling network. *Diabetes* **58**: 609-619.
- Le Douarin, N.M., Teillet, M.A., and Catala, M. 1998. Neurulation in amniote vertebrates: a novel view deduced from the use of quail-chick chimeras. *Int J Dev Biol* **42**(7): 909-916.
- Lickert, H., Cox, B., Wehrle, C., Taketo, M.M., Kemler, R., and Rossant, J. 2005. Dissecting Wnt/beta-catenin signaling during gastrulation using RNA interference in mouse embryos. *Development* **132**(11): 2599-2609.
- Manzoni, G.A., Ransley, P.G., and Hurwitz, R.S. 1987. Cloacal exstrophy and cloacal exstrophy variants: a proposed system of classification. *J Urol* **138**(4 Pt 2): 1065-1068.
- Montcouquiol, M., Sans, N., Huss, D., Kach, J., Dickman, J.D., Forge, A., Rachel, R.A., Copeland, N.G., Jenkins, N.A., Bogani, D. et al. 2006. Asymmetric localization of Vangl2 and Fz3 indicate novel mechanisms for planar cell polarity in mammals. *J Neurosci* **26**(19): 5265-5275.
- Nelson, W.J. and Nusse, R. 2004. Convergence of Wnt, beta-catenin, and cadherin pathways. *Science* **303**(5663): 1483-1487.

- Park, E., Kim, G.H., Choi, S.C., and Han, J.K. 2006a. Role of PKA as a negative regulator of PCP signaling pathway during *Xenopus* gastrulation movements. *Dev Biol* **292**(2): 344-357.
- Park, J.I., Ji, H., Jun, S., Gu, D., Hikasa, H., Li, L., Sokol, S.Y., and McCrea, P.D. 2006b. Fronds Links Dishevelled to the p120-Catenin/Kaiso Pathway: Distinct Catenin Subfamilies Promote Wnt Signals. *DevCell* **11**(5): 683-695.
- Park, M. and Moon, R.T. 2002. The planar cell-polarity gene *stbm* regulates cell behaviour and cell fate in vertebrate embryos. *Nat Cell Biol* **4**(1): 20-25.
- Pauli, R.M. 1994. Lower mesodermal defects: a common cause of fetal and early neonatal death. *Am J Med Genet* **50**(2): 154-172.
- Phillips, H.M., Rhee, H.J., Murdoch, J.N., Hildreth, V., Peat, J.D., Anderson, R.H., Copp, A.J., Chaudhry, B., and Henderson, D.J. 2007. Disruption of planar cell polarity signaling results in congenital heart defects and cardiomyopathy attributable to early cardiomyocyte disorganization. *Circ Res* **101**(2): 137-145.
- Staal, F.J., Noort Mv, M., Strous, G.J., and Clevers, H.C. 2002. Wnt signals are transmitted through N-terminally dephosphorylated beta-catenin. *EMBO Rep* **3**(1): 63-68.
- Stevenson, R.E., Jones, K.L., Phelan, M.C., Jones, M.C., Barr, M., Jr., Clericuzio, C., Harley, R.A., and Benirschke, K. 1986. Vascular steal: the pathogenetic mechanism producing sirenomelia and associated defects of the viscera and soft tissues. *Pediatrics* **78**(3): 451-457.
- Suriben, R., Fisher, D.A., and Cheyette, B.N. 2006. Dact1 presomitic mesoderm expression oscillates in phase with Axin2 in the somitogenesis clock of mice. *Dev Dyn* **235**(11): 3177-3183.
- Takeuchi, M., Nakabayashi, J., Sakaguchi, T., Yamamoto, T.S., Takahashi, H., Takeda, H., and Ueno, N. 2003. The prickle-related gene in vertebrates is essential for gastrulation cell movements. *Curr Biol* **13**(8): 674-679.
- Tam, P.P. 1986. A study of the pattern of prospective somites in the presomitic mesoderm of mouse embryos. *J Embryol Exp Morphol* **92**: 269-285.
- Torban, E., Patenaude, A.M., Leclerc, S., Rakowiecki, S., Gauthier, S., Andelfinger, G., Epstein, D.J., and Gros, P. 2008. Genetic interaction between members of the Vangl family causes neural tube defects in mice. *Proc Natl Acad Sci U S A* **105**(9): 3449-3454.
- Torban, E., Wang, H.J., Groulx, N., and Gros, P. 2004. Independent mutations in mouse Vangl2 that cause neural tube defects in looptail mice impair interaction with members of the Dishevelled family. *J Biol Chem* **279**(50): 52703-52713.
- Torban, E., Wang, H.J., Patenaude, A.M., Riccomagno, M., Daniels, E., Epstein, D., and Gros, P. 2007. Tissue, cellular and sub-cellular localization of the Vangl2 protein during embryonic development: effect of the Lp mutation. *Gene Expr Patterns* **7**(3): 346-354.
- Vandenberg, A.L. and Sassoon, D.A. 2009. Non-canonical Wnt signaling regulates cell polarity in female reproductive tract development via van gogh-like 2. *Development* **136**(9): 1559-1570.
- Veeman, M.T., Axelrod, J.D., and Moon, R.T. 2003a. A second canon: Functions and mechanisms of beta-catenin-independent wnt signaling. *Developmental Cell* **5**(3): 367-377.

- Veeman, M.T., Slusarski, D.C., Kaykas, A., Louie, S.H., and Moon, R.T. 2003b. Zebrafish prickle, a modulator of noncanonical Wnt/Fz signaling, regulates gastrulation movements. *Curr Biol* **13**(8): 680-685.
- Wang, J., Hamblet, N.S., Mark, S., Dickinson, M.E., Brinkman, B.C., Segil, N., Fraser, S.E., Chen, P., Wallingford, J.B., and Wynshaw-Boris, A. 2006. Dishevelled genes mediate a conserved mammalian PCP pathway to regulate convergent extension during neurulation. *Development* **133**(9): 1767-1778.
- Yan, D., Wallingford, J.B., Sun, T.Q., Nelson, A.M., Sakanaka, C., Reinhard, C., Harland, R.M., Fantl, W.J., and Williams, L.T. 2001. Cell autonomous regulation of multiple Dishevelled-dependent pathways by mammalian Nkd. *Proc Natl Acad Sci U S A* **98**(7): 3802-3807.
- Ybot-Gonzalez, P., Savery, D., Gerrelli, D., Signore, M., Mitchell, C.E., Faux, C.H., Greene, N.D., and Copp, A.J. 2007. Convergent extension, planar-cell-polarity signalling and initiation of mouse neural tube closure. *Development* **134**(4): 789-799.
- Yoshikawa, Y., Fujimori, T., McMahon, A.P., and Takada, S. 1997. Evidence that absence of Wnt-3a signaling promotes neuralization instead of paraxial mesoderm development in the mouse. *Dev Biol* **183**(2): 234-242.
- Zhang, L., Gao, X., Wen, J., Ning, Y., and Chen, Y.G. 2006. Dapper 1 antagonizes Wnt signaling by promoting dishevelled degradation. *JBiolChem* **281**: 8607-8612.
- Zhang, N. and Gridley, T. 1998. Defects in somite formation in lunatic fringe-deficient mice. *Nature* **394**(6691): 374-377.

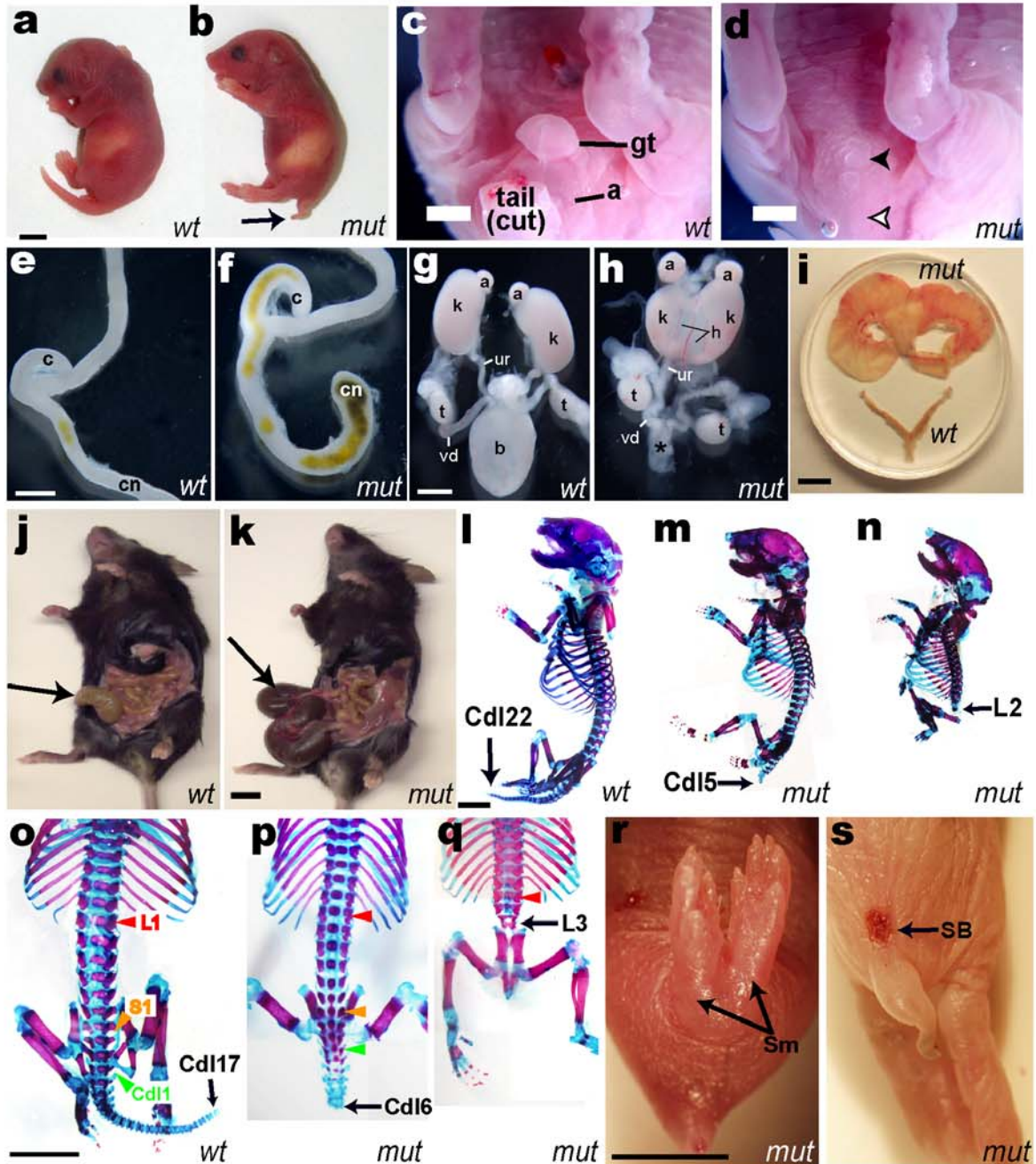


Figure 4.1 Birth phenotypes in *Dact1* mutants (*mut*) compared to *wild type* (*wt*)

a, b Outward appearance; arrow, short tail. **c, d** Genital tubercle (gt) and anus (a) are missing in mutants (filled arrowhead, empty arrowhead), along with the tail. **e, f** Mutants have a blind-ended colon (cn). **g, h** Mutants lack bladder (b vs. *), have malformed hydronephrotic (h) kidneys (k, fused in the mutant specimen), and misconnected ureters (ur, connected to the vas deferens (vd) in this mutant male). **i-k**, Phenotypes of rare surviving adult *Dact1* mutants consistent with impaired uterine outflow resulting in hydrometrocolpos (top vs. bottom in **i**), and impaired digestive tract evacuation resulting in megacolon (arrow in mutant **k** vs. wild type **j**). **l-q** Skeletons; black arrows indicate identity of the terminal ossified vertebra, colored arrowheads in **o-q** indicate segmental levels: red, lumbar-1 (L1); yellow, sacral-1 (S1); green, caudal-1 (Cd11). **r** Sirenomyelia (Sm). **s** Spina bifida (SB). Other abbreviations: (a) adrenal, (c) cecum, (t) testis. Scale bars: 0.5 mm, except **i-k** 5 mm.

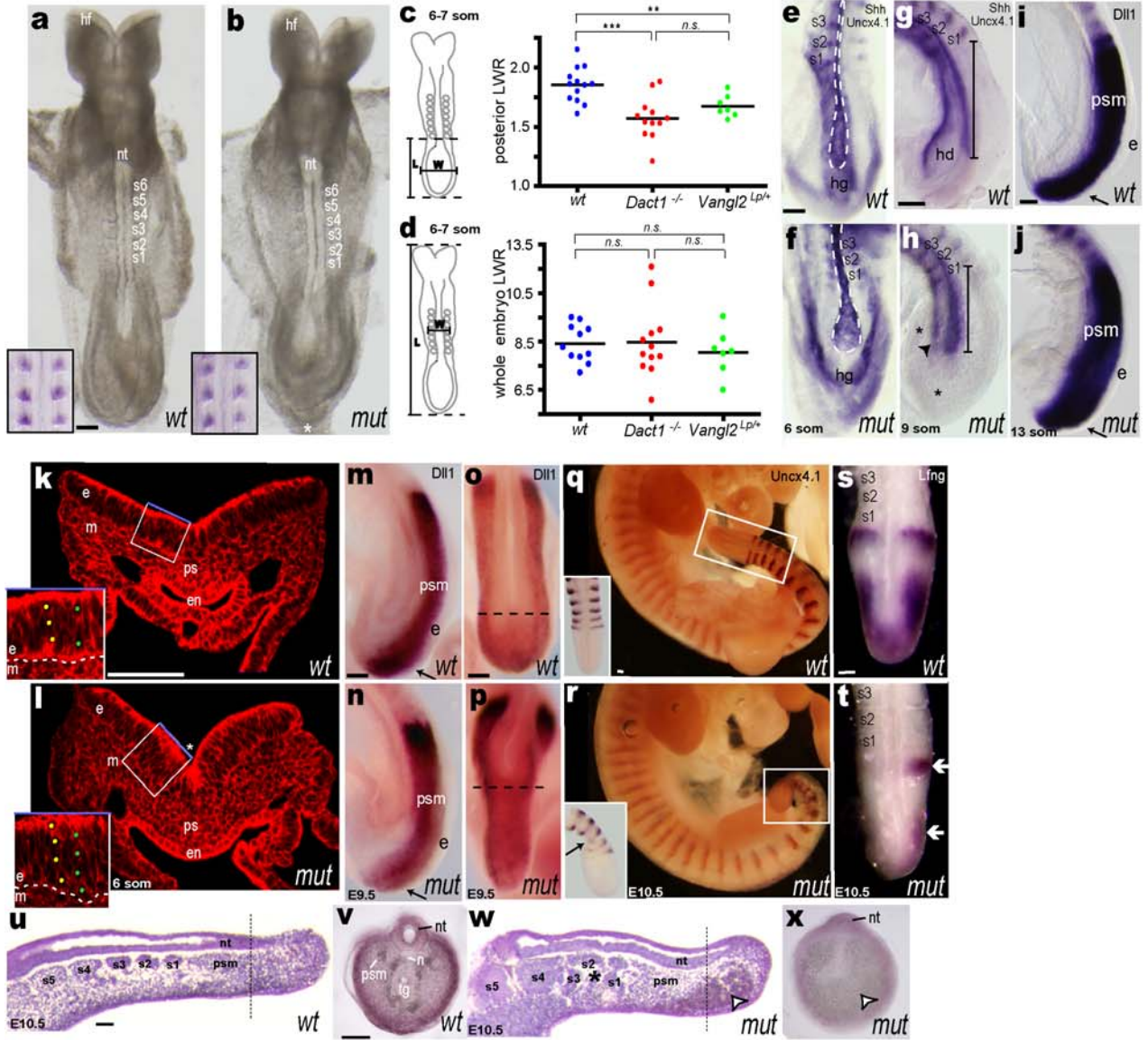


Figure 4.2 *Dact1* mutant embryonic phenotypes

a, b Early *Dact1* mutant (*mut*) embryos appear normal except for their posterior contour (*); insets: *Uncx4.1* WISH (somites). **c, d** Length-Width-Ratio (LWR) measurements in wild type (blue), *Dact1* mutants (red) and *Vangl2*^{L^{pt}/+} heterozygotes (green) posterior (**c**) or whole (**d**) embryo. **e-h** *Shh/Uncx4.1* WISH. **e, f** ventral aspect; **g, h** lateral aspect. Notochord (outline in **e, f**; bracket in **g, h**) is shorter and broader in *Dact1* mutants compared to wild type. Hindgut diverticulum (**hd** in **g**) has not formed in mutant (arrowhead in **h**). Mesenchymal tissue (*) surrounds foreshortened axial structures. **i, j** *Dll1* WISH: presomitic mesoderm (**psm**) and ectoderm (**e**, arrow) length are normal. **k, l** Phalloidin-stained transverse section at the primitive streak (**ps**). In mutant (**l**) endoderm (**en**) has not closed ventrally and is thinner, whereas ectoderm (**e**) is thicker (insets) and more sharply folded (*). **m-p** At later stages, *Dll1* WISH (**m, n** lateral aspect; **o, p** dorsal aspect) reveals presomitic mesoderm and ectoderm of normal length (arrows), but less extended axial tissues (dotted lines). **q, r** Segmental abnormalities confined to the newest somites in the tail bud (insets) can be detected by *Uncx4.1* WISH at later stages (insets: close-up and dorsal view). **s, t** Somitogenic clock abnormalities in *Dact1* mutant tail buds revealed by abnormal asymmetric *Lfng* WISH (arrows). **u-x** Representative parasagittal (**u, w**); and transverse (**v, x**) sections through wild type (**u, v**) and *Dact1* mutant (**w, x**) tail buds at E10.5. *Dact1* mutants with abnormal somites (asterisk in **w**) also have severely disrupted posterior tissues and pooled blood at their ventral posterior tip (arrowhead in **w, x**); the neural tube (**nt**) nonetheless extends toward the tail bud tip. Dotted lines in **u, w** indicate approximate position of transverse sections from different embryos in **v, x**. Other abbreviations: (**hf**) head-folds, (**s1-s8**) somites, (**hg**) hindgut, (**m**) mesoderm, (**n**) notochord, (**tg**) tail gut. Scale bars = 0.1 mm. Statistical analysis (**c, d**): parametric unpaired two-tailed t test, horizontal line = mean; n.s. $p > 0.05$, ** $p < 0.01$, *** $p < 0.001$

Wnt/ β -catenin signaling

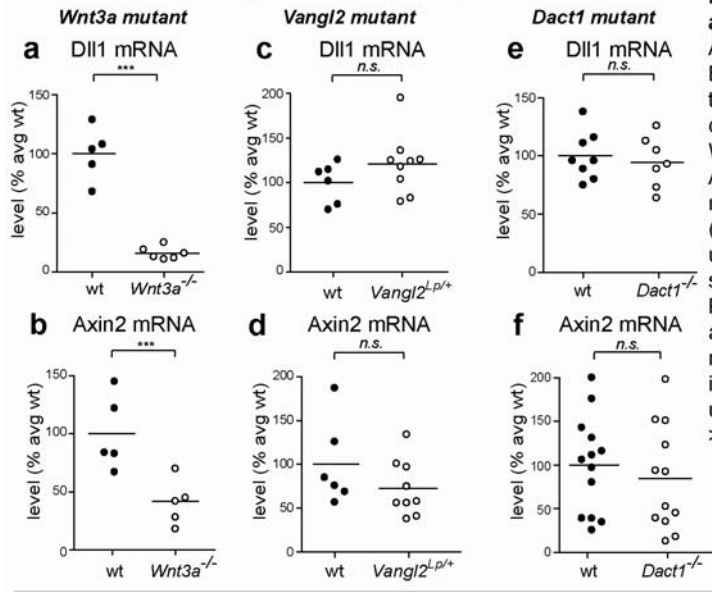
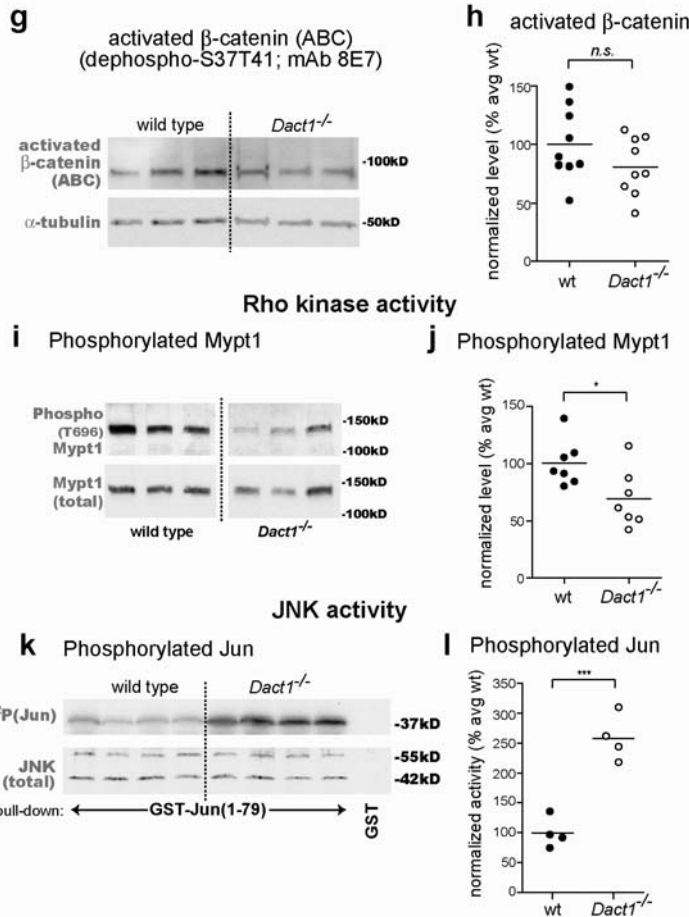


Figure 4.3 Biochemical correlates of PCP signaling are specifically affected at early phenotypic stages

Assays were conducted on posterior tissue lysates from E8 and E9 embryos. All graphs: closed circles, wild type (+/+); open circles, mutant littermates. **a-h** Wnt/ β -catenin assays. QPCR for endogenous targets of Wnt/ β -catenin signaling at E8 reveals that Dll1 and Axin2 mRNA levels are significantly reduced in *Wnt3a* null embryos (**a, b**), but not in *Vangl2^{Lp}* heterozygotes (**c, d**), nor in *Dact1* mutants (**e, f**). Similarly, levels of unphosphorylated (activated) β -catenin protein are not significantly reduced in *Dact1* mutants at E9 (**g, h**). **i-l** PCP pathway biochemistry. Phosphorylation of Mypt1, a target of Rho kinase, is significantly reduced in *Dact1* mutants at E8 (**i, j**), whereas JNK activity is robustly increased at E9 (**k, l**). Statistical analyses: parametric unpaired two-tailed t tests, horizontal line = mean; n.s. $p > 0.05$, * $p < 0.05$, *** $p < 0.001$



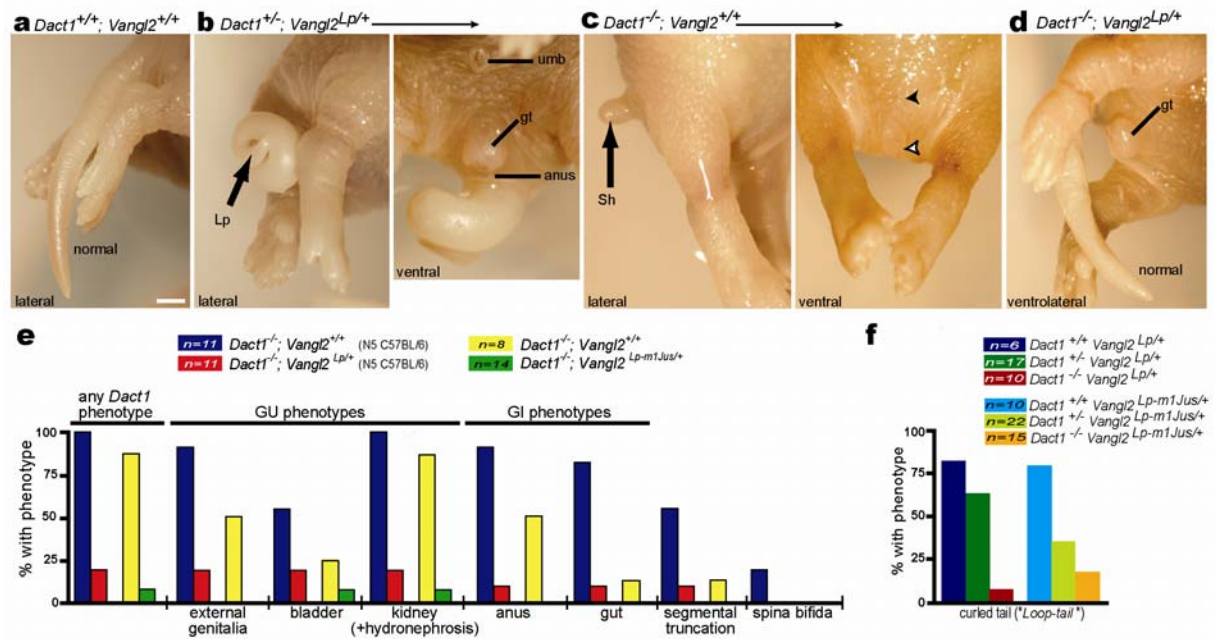


Figure 4.4 Mutations in *Dact1* and *Vangl2* mutually rescue

a-d Posterior phenotypes of littermates from a *Dact1* x *Vangl2* mutant intercross. **a** $Dact1^{+/+}; Vangl2^{+/+}$ neonate (wild type) has a normal tail. **b** $Dact1^{+/-}; Vangl2^{Lp/+}$ neonate (trans-heterozygous) has a curly tail (Lp, left panel) typical of the semidominant *Loop-tail* phenotype, while the genital tubercle (gt) and anus (a) are normal (as expected for a *Dact1* heterozygote, right panel). **c** $Dact1^{-/-}; Vangl2^{+/+}$ neonate has the shortened tail (Sh; left panel), absent genital tubercle and anus (filled and empty arrowheads, right panel) typical of *Dact1* mutants. **d** $Dact1^{-/-}; Vangl2^{Lp/+}$ combination mutant neonate (genetically rescued mutant) has a normal genital tubercle (gt), anus (not shown), and tail. **e** Quantitation of phenotypes and affected organs in *Dact1* mutant littermates that either carry (red) or don't carry (blue) the *Vangl2*^{Lp} allele, or that either carry (green) or don't carry (yellow) the *Vangl2*^{Lp-m1Jus} allele (see also Supplementary Table 3a). **f** The *Dact1* mutant allele reciprocally rescues, in a dose-dependent manner, *Loop-tail* phenotypes produced by heterozygosity for either *Vangl2*^{Lp} (left, darker bars) or *Vangl2*^{Lp-m1Jus} (right, lighter bars) (see also Table 4.3b). Other abbreviations: (umb) umbilicus. Scale bar: 1 mm.

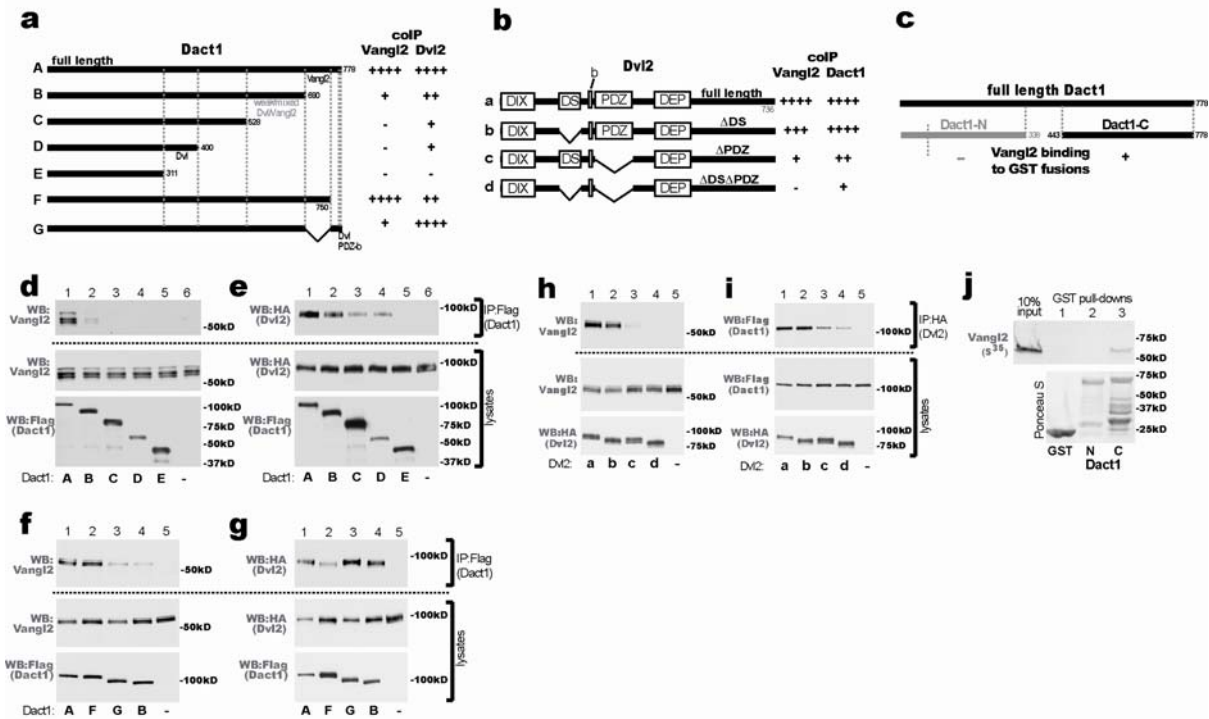


Figure 4.5 The Dact1 and Vangl2 proteins associate independently of Dvl

a-c Schematic summaries of colIP and GST pull-down data. **d-i** colIPs of proteins recombinantly expressed in human embryonic kidney cells. **d** Vangl2 colIPs with full-length Dact1, but loses affinity as the Dact1 C-terminus is progressively deleted. **e** Dvl2 colIPs with Dact1 unless both the C-terminus and middle region are deleted. **f, g** Separate C-terminal subregions of Dact1 mediate colIP with Vangl2 (**f**) versus Dvl2 (**g**). **h** Vangl2 colIPs with full-length Dvl2 unless the Dvl2 PDZ domain is deleted; there is also a slight contribution from the Dvl2 DS domain. **i** Dact1 colIPs with Dvl2 even in the absence of both these domains. **j** A GST-fusion protein incorporating the Dact1 C-terminus binds to Vangl2 protein synthesized in a wheat germ extract with no Dvl proteins

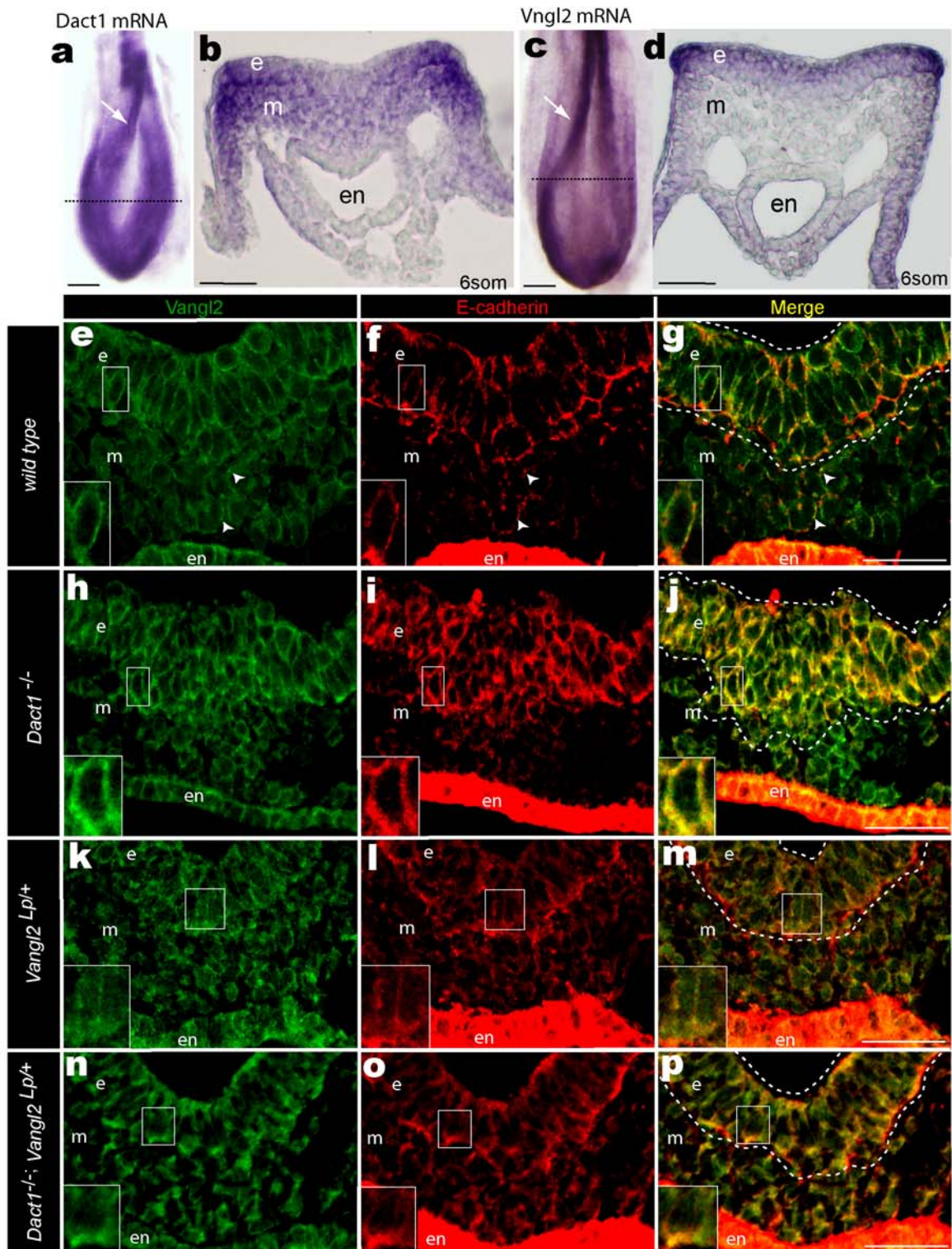


Figure 4.6 Dact1 and Vangl2 functionally interact at the PS

a, b WISH Dact1 **c, d** WISH Vangl2 **a, c** Dorsal aspect showing neural fold (arrow) and approximate level of sections in **b** & **d** (dotted lines) **b, d** Transverse section at PS level. **e-p** Confocal fluorescent immunohistological localization of Vangl2 (green) and E-cadherin proteins (red) at the PS in *Dact1*^{+/+}; *Vangl2*^{+/+} (wild type; **e-g**), *Dact1*^{-/-}; *Vangl2*^{+/+} (*Dact1* mutant; **h-j**), *Dact1*^{+/+}; *Vangl2*^{Lp/+} (*Loop-tail*; **k-m**), and *Dact1*^{-/-}; *Vangl2*^{Lp/+} (genetically rescued mutant; **n-p**). Abbreviations as in **Figure 4.2**. Scale bars in **a-d** 0.1 mm, in **e-p** 0.05mm.

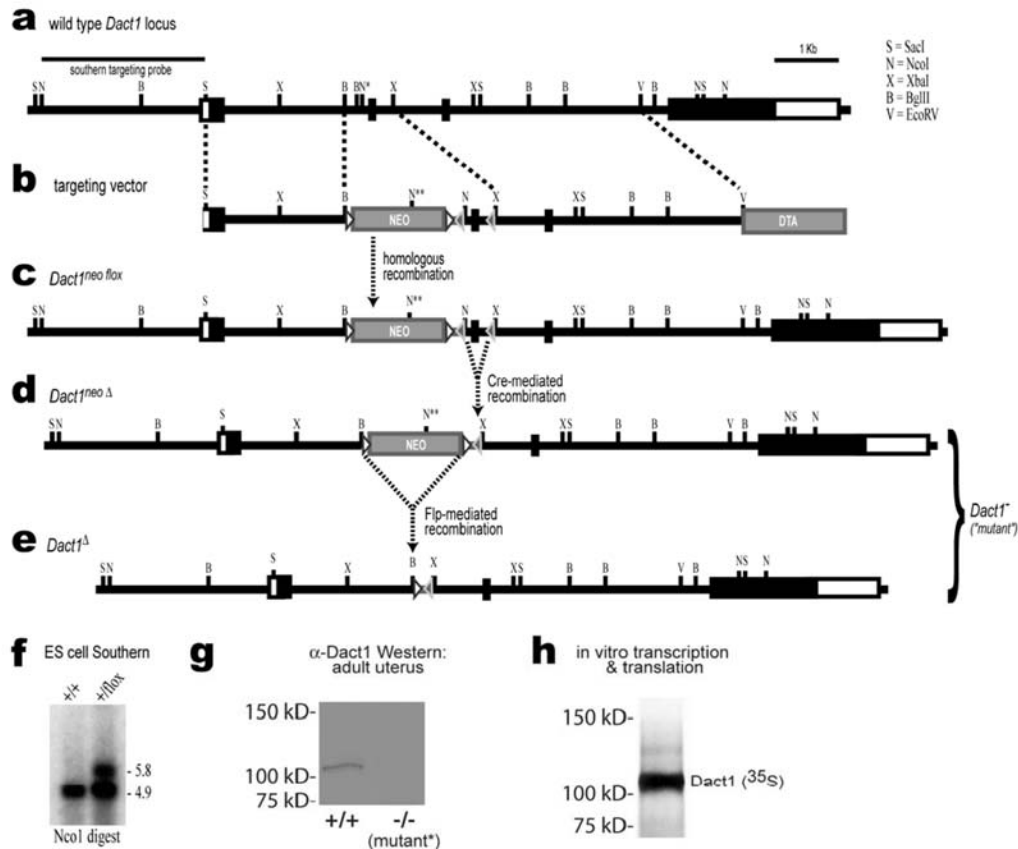


Figure 4.S1 Gene targeting of the *Dact1* locus in mice

a-c. Schema of *Dact1* wild type locus and targeting intermediates. **a**, wild type. **b**, targeting vector. **c**, *Dact1^{neo/lox}* homologously recombined allele. Boxes represent exons: filled are coding; open, non-coding. Dashed lines denote regions where homologous recombination occurred. Filled triangles represent *loxP* sites; open triangles, *FRT* sites. Exon 2 encodes a functionally important and conserved coiled-coil domain and does not contain an integral number of codons, so once it is excised any residual splicing yields a transcript lacking key sequence followed by a frame-shift. **d, e**, The phenotypically equally severe *Dact1^Δ* ("mutant") alleles *Dact1^{neo}* and *Dact1^Δ*, following excision of exon 2 and neo by the Cre and Flp recombinases, respectively. **f**, Southern blot genotyping of targeted ES cells. Positions of probe and relevant restriction sites are indicated in **a-e**. **g**, Western blot of adult uterine tissue lysate using an antibody generated against mouse Dact1 (**Methods**). Uterus was chosen as it expresses high levels of *Dact1* relative to other tissues (Fisher et al, 2006, and NCBI Unigene website). A band at ~110 kD, the same as recombinantly-expressed Dact1, disappears in the homozygous mutant (*this adult *Dact1* mutant was heterozygous for *Vangl2^{L^P}* - see text). **h**, Sizing of the mouse Dact1 protein by in vitro transcription and radioactive labelling of a full-length *Dact1* cDNA; full length Dact1 expressed recombinantly in tissue culture cells also consistently runs at this size (*cf.* **Fig. 4.5d-g i**).

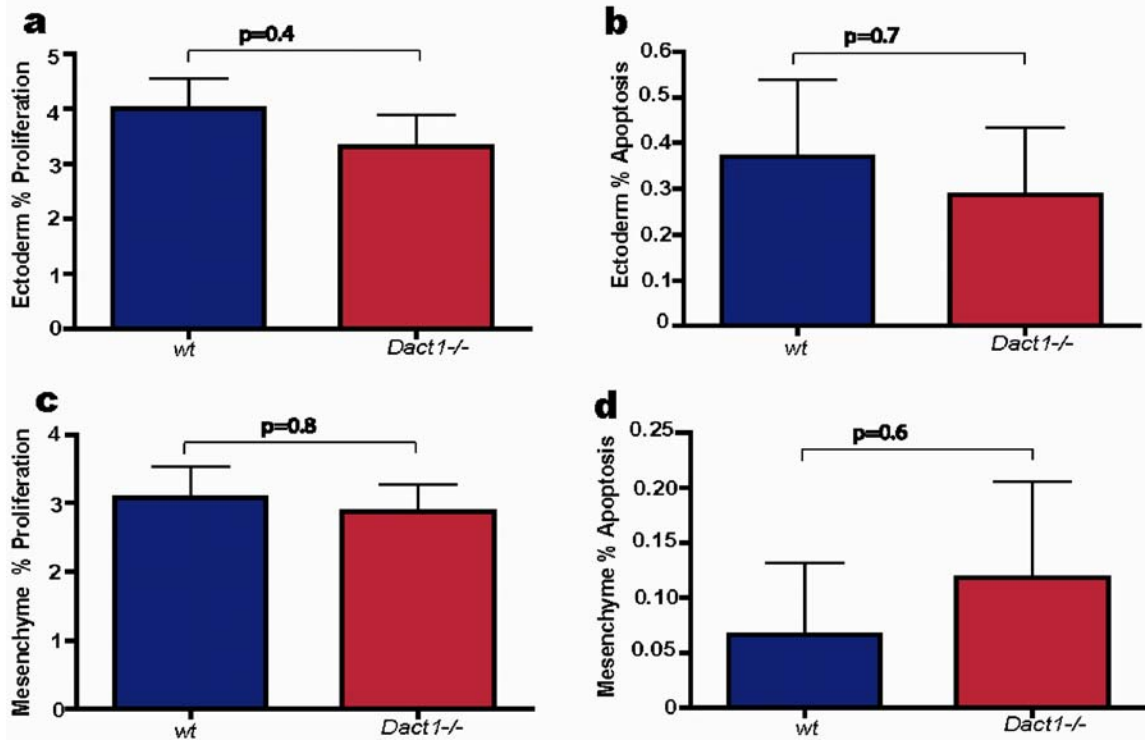


Figure 4.S2 Cell proliferation and apoptosis in the primitive streak region are not significantly different in *Dact1* mutants compared to wild type. Ectoderm measurements for percent of cells undergoing proliferation (a) and apoptosis (b). Mesenchyme measurements for percent of cells undergoing proliferation (c) and apoptosis (d). Measurements are from wild type (blue) and *Dact1*^{-/-} (red) embryos at embryonic day 8.25 (6-7 somites).

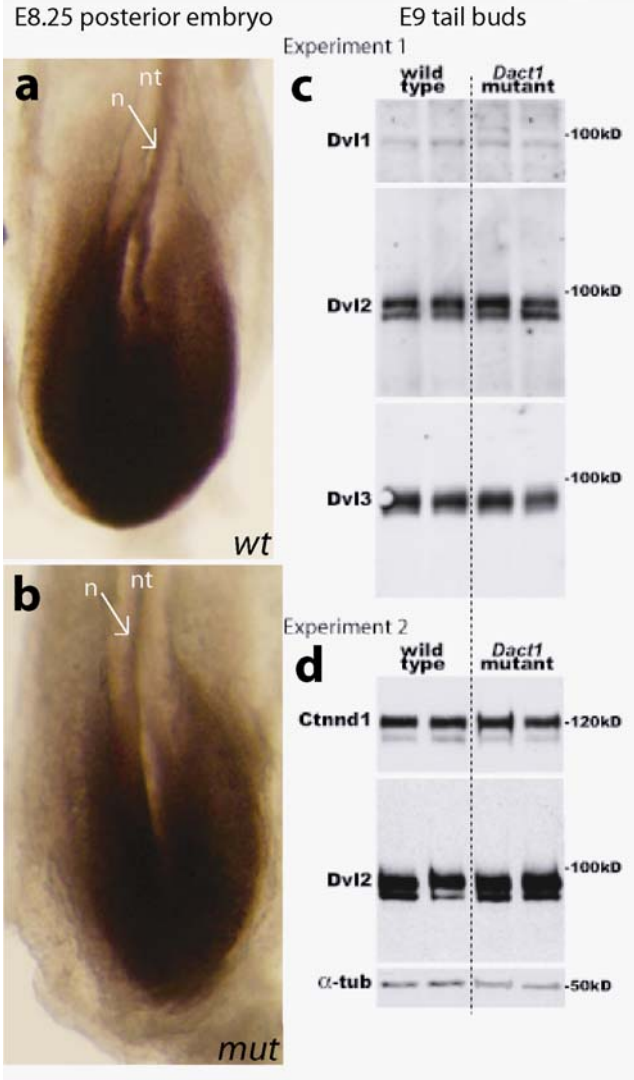


Figure 4.S3 Brachyury expression and Dvl and Ctnnd1 (p120catenin) levels are not altered in *Dact1*^{-/-} embryos

a-b Whole mount in situ hybridization for the Wnt/ β -catenin target *Brachyury* (*T*) in E8.25 embryos shows expression in the notochord (n) and posterior mesoderm and ectoderm. Levels and localization of Brachyury mRNA is comparable in wild type (**a**) and *Dact1*^{-/-} mutant (**b**) embryos despite differences in posterior tissue morphology. **c-d** Immunoblots of E9 tail bud lysates. left 2 lanes: wild type right 2 lanes: *Dact1* mutant. 4 samples of each genotype were tested in 2 different experiments. Experiment 1 (**c**): Dvl1, Dvl2, and Dvl3. Experiment 2 (**d**): Ctnnd1, Dvl2, and α tubulin loading control. There is no evidence of changes in levels of these endogenous proteins in *Dact1* mutant samples from the posterior embryo, even at this stage when the mutant phenotype is advanced. Other abbreviations: neural tube= nt

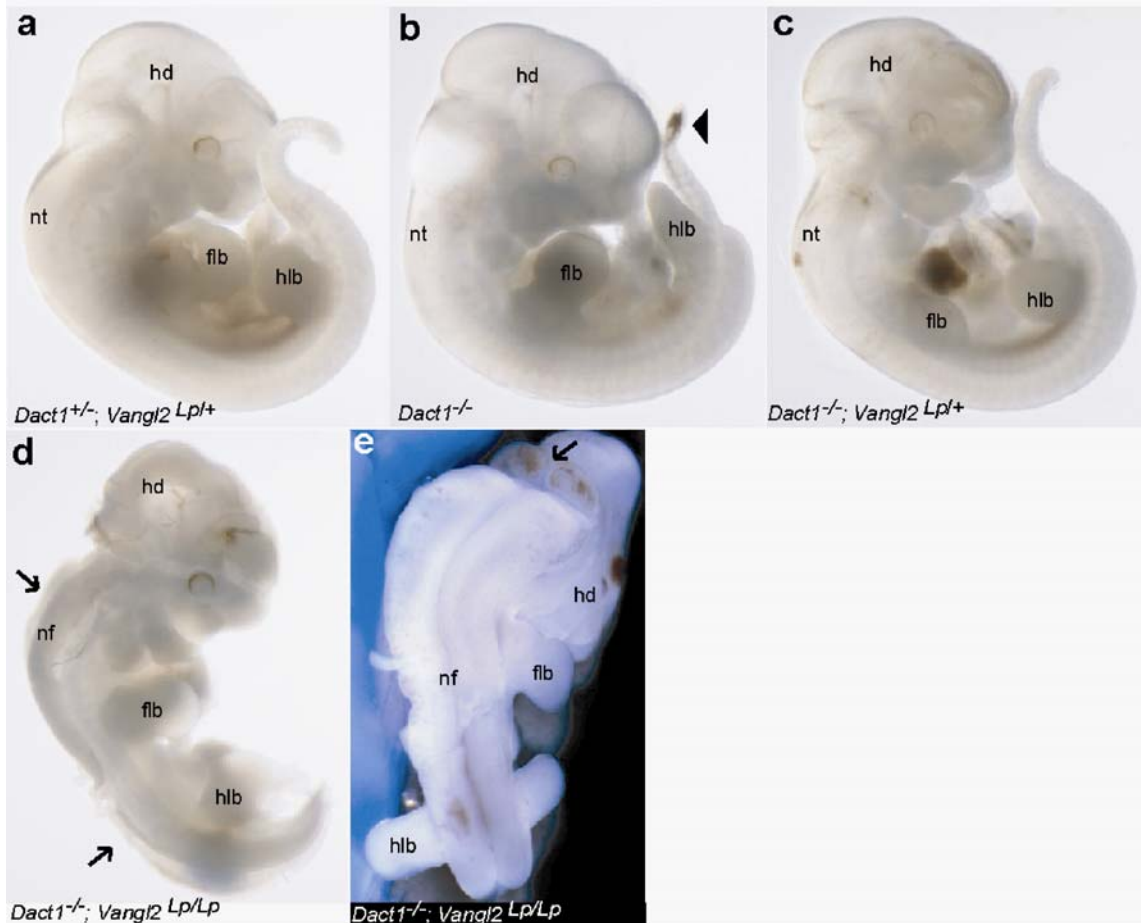


Figure 4.S4 *Dact1*^{-/-} does not rescue the *Vangl2*^{Lp/Lp} homozygous phenotype. Embryos dissected at E10.5 from a cross between a *Dact1*^{+/-} *Vangl2*^{Lp/+} male and a *Dact1*^{+/-} *Vangl2*^{Lp/+} female. **a** *Dact1*^{+/-} *Vangl2*^{Lp/+} embryo shows curling of the posterior tail bud, as seen in *Vangl2*^{Lp/+} alone. **b** *Dact1*^{-/-} embryo has pooled blood (arrowhead) in an internally disorganized tail bud. **c** *Dact1*^{-/-} *Vangl2*^{Lp/+} embryo does not have blood in the tail bud and is less curled than *Vangl2*^{Lp/+} alone; it closely resembles a genotypically wild type embryo of this stage. **d-e** *Dact1*^{-/-} *Vangl2*^{Lp/Lp} embryos show the characteristic recessive *Vangl2* mutant craniorachischesis phenotype (arrows): *i.e.* an open neural tube extending from the midbrain-hindbrain boundary (arrow in **e**) caudally, and are otherwise indistinguishable from *Vangl2*^{Lp/Lp} embryos. Thus, *Dact1* loss and partial loss of *Vangl2* reciprocally rescue, but homozygosity for mutation of *Vangl2* is epistatic to *Dact1*. This is fully consistent with other data showing that the *Dact1* mutant phenotype is mediated by post-translational upregulation of the Vangl2 protein and therefore requires a wild type *Vangl2* allele; Conversely, since *Dact1* acts on Vangl2 post-translationally, when no wild type Vangl2 protein is present (*i.e.* in homozygous *Vangl2* mutants) resultant phenotypes are not modified by loss of *Dact1*. Abbreviations: hd = head, nt = neural tube, nf = neural fold, flb = forelimb bud, hlb = hind limb bud.

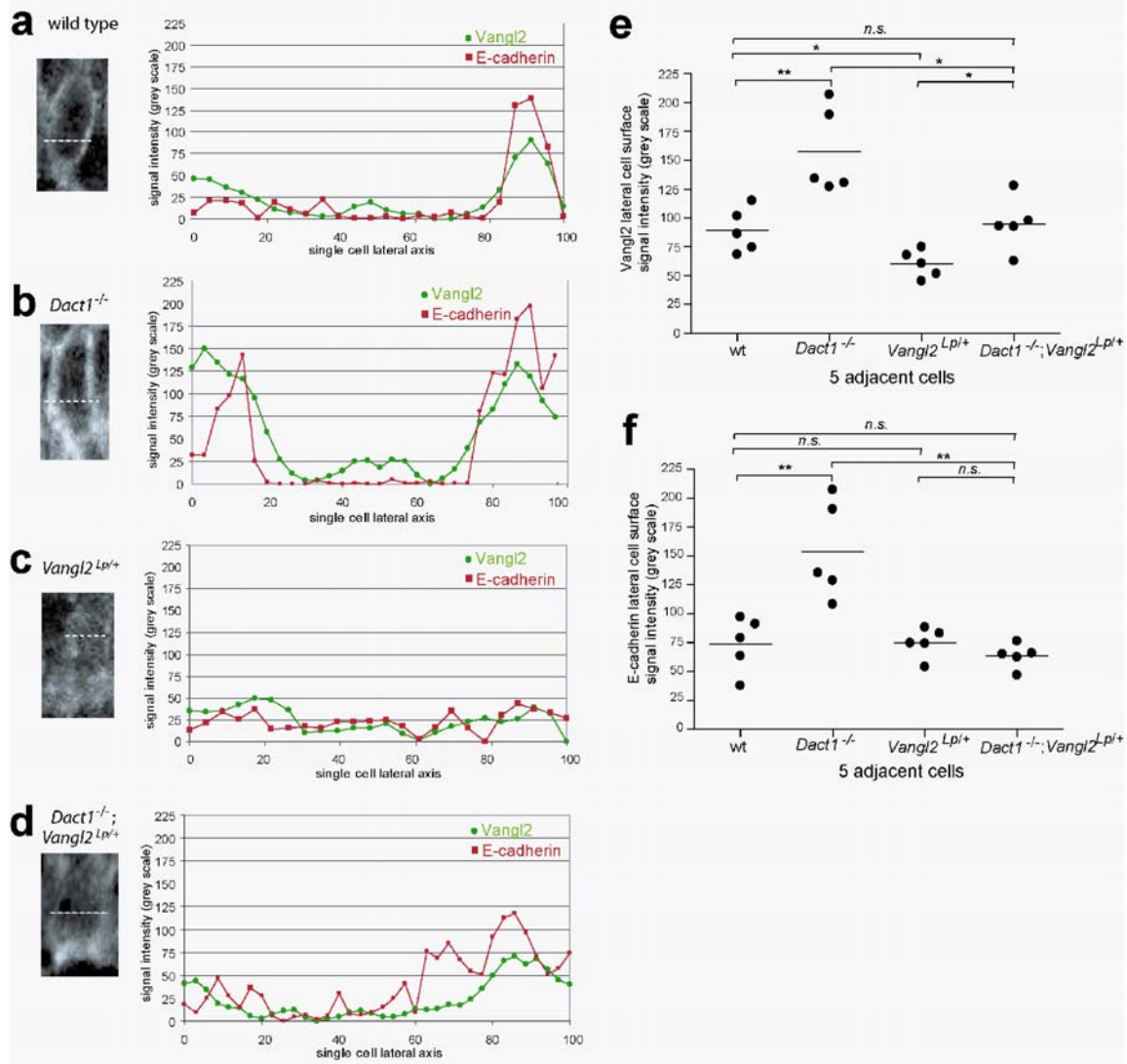


Figure 4.S5 Quantitation of cell surface Vangl2 and E-cadherin protein signals in the PS ectoderm. a-d, Vangl2 (green) and E-cadherin (red) fluorescent signal intensity (grey scale) in a representative single PS ectoderm cell bisected along the lateral axis (dotted line in inset cell images). a, wild type. b, *Dact1*^{-/-}. c, *Vangl2*^{Lp/+}. d, *Dact1*^{-/-}; *Vangl2*^{Lp/+}. e-f, Vangl2 (e) and E-cadherin (f) average lateral cell surface signal intensity as measured in 5 adjacent cells of the PS ectoderm in wild type (wt); *Dact1*^{-/-}; *Vangl2*^{Lp/+}; and *Dact1*^{-/-}; *Vangl2*^{Lp/+} embryos (see **Methods**). Statistical analysis: parametric unpaired two-tailed t-test, horizontal line = mean; *n.s.* *p* > 0.05, **p* < 0.05, ***p* < 0.01.

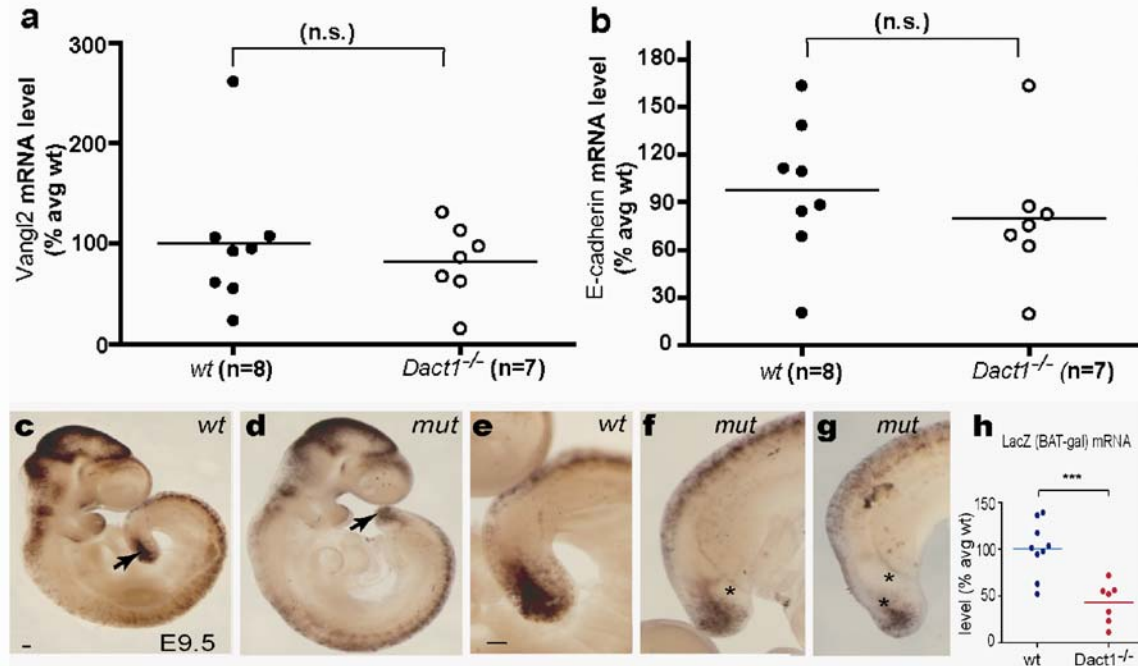


Figure 4.S6 Vangl2, E-cadherin, and Wnt/ β -catenin levels in *Dact1* mutants.

a-b Levels of Vangl2 and E-cadherin mRNA relative to cyclophilin mRNA were measured using Quantitative RT-PCR. Vangl2 (**a**) and E-cadherin (**b**) mRNA levels are similar in wild type and *Dact1*^{-/-} caudal embryo tissue at E8.25. Specimens were collected as in Figure 3. **c-h** Embryonic day 9.5 wild type (**c, e**) and littermate *Dact1*^{-/-} (**d, f, g**) embryos carrying a single copy of the transgenic Wnt/ β -catenin reporter BAT-gal, stained by WISH for LacZ. Overall Wnt/ β -catenin signaling distribution is not distinguishable between wild type and mutant embryos, except in the tail bud (arrows), where the reporter mRNA appears modestly reduced. This change is validated quantitatively (**h**) using Q-RT-PCR for relative LacZ levels. Upon closer inspection (**f, g**) the reduction of reporter mRNA in mutant tail buds corresponds to a subset of tissue that does not stain at all (*). Other histology shows that the internal anatomy of mutant tail buds is highly disrupted by this stage, with missing axial tissues and disorganized mesenchyme. At slightly later stages (E10+) many mutant tail buds have grossly apparent pooled blood and histolysis at their posterior tip (cf. Fig 4.2w, x). Scale bars = 0.1 mm. Statistical analysis: Two-tailed unpaired parametric t test; p values: (**a**) p=0.6 (**b**) p=0.5 (**h**) p=0.0007

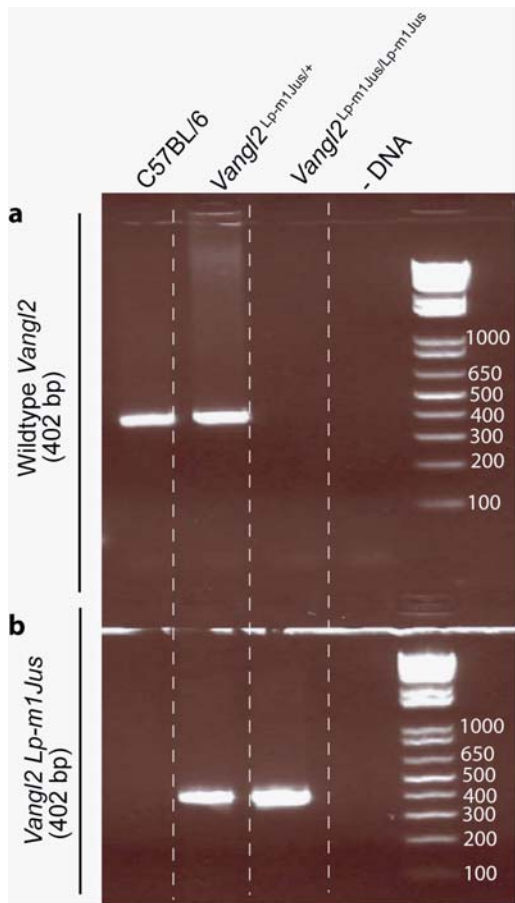


Figure 4.S7 Allele specific genotyping of the *Vangl2*^{Lp-m1Jus} point mutation

Allele specific genotyping was performed by genomic PCR using sequence specific primers at the point mutation²⁹. **a** Genotyping for the wild type allele results in a 402 base pair product from C57BL/6 (lane 1) and from the heterozygote *Vangl2*^{Lp-m1Jus/+} (lane 2), but not from the homozygote *Vangl2*^{Lp-m1Jus/Lp-m1Jus} (lane 3). **b** Genotyping for the mutant allele results in a 402 base pair product from the heterozygote *Vangl2*^{Lp-m1Jus/+} (lane 2) and from the homozygote *Vangl2*^{Lp-m1Jus/Lp-m1Jus} (lane 3), but not from wild type C57BL/6 (lane 1).

Supplementary Tables 4.1a-d Breakdown of *Dact1* mutant phenotypes at birth

Supplementary Table 1a Mutants are born at near Mendelian ratios

Neonates (N10 backcross to C57Bl/6; n=9 litters)

Genotype	<i>Dact1</i> ^{+/+}	<i>Dact1</i> ^{+/-}	<i>Dact1</i> ^{-/-}
Expected	25%	50%	25%
Observed	25% (n=23)	54% (n=50)	21% (n=19)

Supplementary Table 1b Mutant urogenital/digestive tract phenotypes (n = 18)

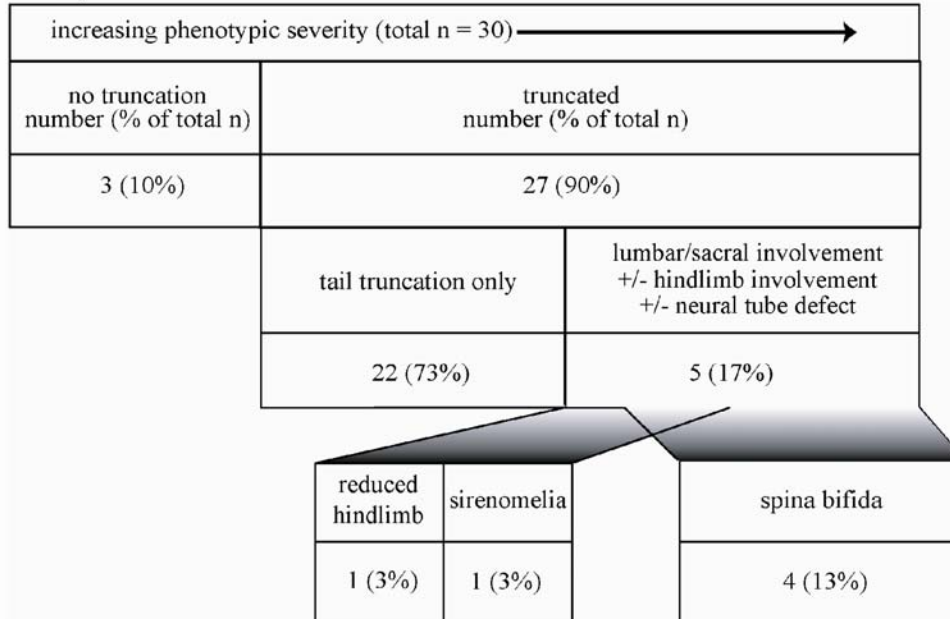
Phenotype	Genital tubercle missing (no external genitalia)	Colon ends at bladder	Bladder missing; colon ends blindly	Total with genital/bladder/hindgut phenotype
number (%)	18 (100%)	3 (17%)	15 (83%)	18 (100%)

Supplementary Table 1c Mutant kidney malformations (n = 23)

Phenotype*	“horseshoe” kidney (fused at midline)	unilateral (single) kidney	No kidneys	Total with gross kidney malformation or absence
number (%)	16 (70%)	3 (13%)	2 (9%)	21 (91%)

*100% of kidneys are hydronephrotic, presumed secondary to impaired urinary outflow (see also Supplementary Table 2)

Supplementary Table 1d Posterior truncation phenotypic spectrum (C57Bl/6 isogenic strain)



Supplementary Table 4.2 Somitogenesis cycling abnormalities in *Dact1* mutants at E10.5 (non-isogenic background)

WISH probe	n (<i>Dact1</i> ^{-/-} embryos)	Normal expression pattern in PSM	Reduced or asymmetric expression pattern in PSM (%)	Abnormal tail bud axial mesoderm, endoderm, unpatterned mesenchyme, and/or histolysis (%)	Correlation between abnormal posterior tissue morphogenesis and abnormal somitogenesis cycle gene expression in <i>Dact1</i> ^{-/-} embryos
Axin2	37	16	21 (57%)	21 (57%)	100%
Lfng	31	11	20 (65%)	20 (65%)	100%

Supplementary Tables 4.3a-b *Dact1* and *Vangl2* mutations mutually rescue

a

genotype (# of neonates)	GU phenotypes			GI phenotypes		segmental truncation	spina bifida
	external genitalia	bladder	kidney	anus	gut		
<i>Dact1</i> ^{-/-} ; <i>Vangl2</i> ^{+/+} (n=11)	10	6	11	10	3	6	2
<i>Dact1</i> ^{-/-} ; <i>Vangl2</i> ^{Lp/+} (n=11)	2	2	2	1	1	1	0
<i>Dact1</i> ^{-/-} ; <i>Vangl2</i> ^{+/+} (n=8)	4	2	7	4	1	1*	0
<i>Dact1</i> ^{-/-} ; <i>Vangl2</i> ^{Lp-M1Jus/+} (n=14)	0	1	1	0	0	0	0

* in addition, 1 animal had a crooked tail

b

genotype (# of neonates)	curled (<i>Loop-</i>) tail
<i>Dact1</i> ^{+/+} ; <i>Vangl2</i> ^{Lp/+} (n=6)	5
<i>Dact1</i> ^{+/-} ; <i>Vangl2</i> ^{Lp/+} (n=17)	11
<i>Dact1</i> ^{-/-} ; <i>Vangl2</i> ^{Lp/+} (n=10)	1
<i>Dact1</i> ^{+/+} ; <i>Vangl2</i> ^{Lp-m1Jus/+} (n=10)	8
<i>Dact1</i> ^{+/-} ; <i>Vangl2</i> ^{Lp-m1Jus/+} (n=22)	9
<i>Dact1</i> ^{-/-} ; <i>Vangl2</i> ^{Lp-m1Jus/+} (n=15)	3

Neonates born from a cross between *Dact1*^{+/-} and *Dact1*^{+/-}; *Vangl2*^{Lp/+} (n=81) or *Dact1*^{+/-}; *Vangl2*^{Lp-m1Jus/+} (n=80) mice were genotyped, counted, dissected and scored for *Dact1* mutant phenotypes (**a**) and a *Loop-tail* phenotype (**b**). **a** *Dact1* mutant neonates carrying a heterozygous mutation in *Vangl2* (*Vangl2*^{Lp/+} or *Vangl2*^{Lp-m1Jus/+}) exhibited a lower percentage of *Dact1* associated phenotypes, including defects in the development of the genitourinary (GU), gastrointestinal (GI), caudal segments and neural tube (spina bifida), compared to *Dact1* mutants alone. **b** *Vangl2*^{Lp/+} and *Vangl2*^{Lp-m1Jus/+} neonates carrying heterozygous or homozygous mutations in *Dact1* exhibited lower percentages of the *Vangl2* associated *Loop-tail* phenotype compared to *Vangl2*^{Lp/+} and *Vangl2*^{Lp-m1Jus/+} neonates alone.

Supplementary Table 4.4 Primer sequences

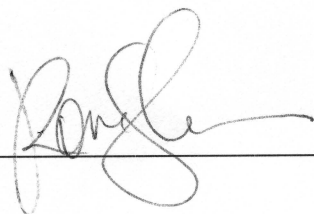
Primer name	Primer sequence
Dact1intron1	5'gga ata gga act tcg ttc tag agt c3'
Dact1intron2	5'aaa cca ctc aag taa ata gta agt ata ag3'
Dact1exon2	5'gaa ttg ttt gag gag aag aga t'3
Dact1intron2	5'ggt ctg ttt gtg ctt tca gaa3'
QAxin2F	5'cgc act gac cga cga ttc3'
QAxin2R	5'gat gtc tgg cag tgg atg tta ga3'
QDII1F	5'ccc tcc cgg ctt cta tgg3'
QDII1R	5'gcc tcc gtc agg gtt atc tg3'
QVangl2F	5'acc cct gct gga caa tga gt3'
QVangl2R	5'tgg gag ata ctg tgc tca gaa gtg3'
Vangl2LpF	5'gcc ttc ctg gag cga tat ttg gcg g'3
Vangl2LpR	5'tca cac aga ggt ctc cga ctg ca'3
Vangl2Lpseq	5'gca tga cga act tat gtg act tgg ga'3
Lp-m1JusWTF	5'gct gct gcc tcc act gct g3'
Lp-m1JusWTR	5'tag aag cgg ctg gcc cca3'
Lp-m1JusMutR	5'tag aag cgg ctg gcc cct3'
Wnt3aneo	5'agc gca tcg cct tct atc gcc ttc3'
Wnt3aintron2	5'cct cct cac ctg gcc tcc ata acc c3'
QLacZF	5'gct gga gtg cga tct tcc t3'
QLacZR	5'cgt gca tct gcc agt ttg a3'

Publishing Agreement

It is the policy of the University to encourage the distribution of all theses, dissertations, and manuscripts. Copies of all UCSF theses, dissertations, and manuscripts will be routed to the library via the Graduate Division. The library will make all these theses, dissertations, and manuscripts accessible to the public and will preserve these to the best of their abilities, in perpetuity.

Please sign the following statement:

I hereby grant permission to the Graduate Division of the University of California, San Francisco to release copies of my thesis, dissertation, or manuscript to the Campus Library to provide access and preservation, in whole or in part, in perpetuity.

A handwritten signature in black ink, appearing to be "Rongle", written over a horizontal line.

1/7/2010